MODELING OF DEPRESSURIZATION AND THERMAL RESERVOIR SIMULATION TO PREDICT GAS PRODUCTION FROM METHANE-HYDRATE FORMATIONS

A

THESIS

Presented to the Faculty
of the University of Alaska Fairbanks

in Partial Fulfillment of the Requirements
for the Degree of

DOCTOR OF PHILOSOPHY

By

Shirish L. Patil, B.E., M.S.

Fairbanks, Alaska
May 2007

MODELING OF DEPRESSURIZATION AND THERMAL RESERVOIR SIMULATION TO PREDICT GAS PRODUCTION FROM METHANE-HYDRATE FORMATIONS

By

Shirish L. Patil

RECOMMENDED:

Dr. Douglas B. Reynolds

Dr. Vikas S. Sonwalkar

Dr. Scott L. Huang

Dr. Gang Chen, Advisory Committee Chair

Chair, Mining & Geological Engineering Department

APPROVED:

Dean, College of Engineering and Mines

Dean of the Graduate School

April 9, 2007

Date

ABSTRACT

Gas hydrates represent a huge potential future resource of natural gas. However, significant technical issues need to be resolved before this enormous resource can be considered to be an economically producible reserve. Developments in numerical reservoir simulations give useful information in predicting the technical and economic analysis of the hydrate-dissociation process. For this reason, a commercial reservoir simulator, CMG (Computer Modeling Group) STARS (Steam, Thermal, and Advanced Processes Reservoir Simulator) has been adapted in this study to model gas hydrate dissociation caused by several production mechanisms (depressurization, hot water injection and steam injection). Even though CMG is a commercially available simulator capable of handling thermal oil recovery processes, the novel approach of this work is the way by which the simulator was modified by formulating a kinetic and thermodynamic model to describe the hydrate decomposition.

The simulator can calculate gas and water production rates from a well, and the profiles of pressure, temperature and saturation distributions in the formation for various operating conditions. Results indicate that a significant amount of gas can be produced from a hypothetical hydrate formation overlying a free gas accumulation by several different production scenarios. However, steam injection remarkably improves gas production over depressurization and hot water injection.

A revised axisymmetric model for simulating gas production from hydrate decomposition in porous media by a depressurization method is also presented. Self-similar solutions are obtained for constant well pressure and fixed natural gas output. A comparison of these two boundary conditions at the well showed that a higher gas flow rate can be achieved in the long run in the case of constant well pressure over that of fixed gas output in spite of slower movement of the dissociation front. For different reservoir temperatures and various well boundary conditions, distributions of temperature and pressure profiles, as well as the gas flow rate in the hydrate zone and the gas zone, are evaluated.

DISCLAIMER

This thesis was prepared as an account of work sponsored by an agency of the United States Government. Neither the United States Government nor an agency thereof, nor any of their employees, makes any warranty, expressed or implied, or assumes any legal liability or responsibility for the accuracy, completeness, of usefulness of any information, apparatus, product, or process disclosed, or represents that its use would not infringe privately owned rights. References herein to any specific commercial product, process, or service by trade name, trademark, manufacture, or otherwise does not necessary constitute or imply its endorsement, recommendation, or favoring by the United States Government or any agency thereof. The views and opinions of the author expressed herein do not necessarily state or reflect those of the United States Government or any agency thereof.

TABLE OF CONTENTS

	Page
SIGNATURE PAGE	i
TITLE PAGE	ii
ABSTRACT	iii
DISCLAIMER	iv
TABLE OF CONTENTS	v
LIST OF FIGURES	viii
LIST OF TABLES	xiii
ACKNOWLEDGEMENTS	xiv
NOMENCLATURE	xv
CHAPTER	
1 INTRODUCTION	1
1.1 CMG STARS – Numerical Model	2
1.2 Analytical Model	4
2 LITERATURE REVIEW	7
2.1 Methods for Production of Gas from Gas Hydrates	7
2.2 Thermal Simulation Techniques	10
2.2.1 Hot Fluid Injection	11
2.2.1.1 Hot Water Injection	11
2.2.1.2 Hot Brine Injection	13
2.2.1.3 Steam Injection	16
2.2.2 Downhole In-situ Heating	17
2.2.2.1 In-situ Combustion	17
2.2.2.2 Electrical/ Radio Frequency/ Electromagnetic Heating	19
2.2.2.3 Microwave Heating	21
2.3 Depressurization	23

	2.4	Hydrate Inhibitor Injection Method	26
	2.5	Fracturing	27
	2.6	Sea-Floor Mining	29
3	**MODEL FORMULATION**		31
	3.1	Numerical Simulation of Hydrate Dissociation	31
		3.1.1 Hydrate Dissociation Kinetics	33
		3.1.2 Flow Equations	34
		3.1.3 Permeabilities	35
	3.2	Governing Equations Used in the STARS Model	36
		3.2.1 Conservation Equations	36
		3.2.2 Flow Terms	37
		3.2.3 Chemical Reaction, Interface Mass Transfer, Source/Sink Terms	37
		3.2.4 Heat Loss Source/Sink Terms	38
		3.2.5 Phase Equilibrium Relationships	38
	3.3	Gas Production due to Hydrate Dissociation- Analytical Model	39
	3.4	Assumptions of the Analytical Model	40
	3.5	Mathematical Model	41
	3.6	Derivation of Analytical Solution	42
4	**PHYSICAL PROPERTIES OF THE MODEL**		47
	4.1	Model 1: Hydrate Layer and Free Gas Zone	47
	4.2	Model 2: Hydrate Layer and Aquifer	50
	4.3	Description of Scenario- Steam Injection	52
5	**RESULTS AND DISSCUSSION**		55
	5.1	Model 1: Depressurization (with free gas zone)	55

5.2 Model 2: Depressurization (with free gas zone and aquifer) 79
5.3 Model 2: Heated Well 89
5.4 Model 2: Hot Water Injection 95
5.5 Energy Efficiency Calculations 106
5.6 Sensitivity Analysis- Axisymmetric Model 112
5.6.1 Pressure, Temperature and Total Mass Flow Profile Distributions: For Well Pressure of 2 MPa 112
5.7 Simulation Results- Steam Injection 129
5.8 Comparison of Results from CMG STARS and Analytical Model 139

6 CONCLUSIONS AND RECOMMENDATIONS FOR FUTURE WORK 142

6.1 Conclusions 142
6.2 Recommendations for Future Work 146

7 REFERENCES 147

LIST OF FIGURES

Figure		Page
3.1	Schematic Representation of the Hydrate Reservoir for the Axisymmetric Model	40
4.1	Simulation Grid	48
4.2	Hypothetical Model of Formation	52
4.3	Hypothetical Model of Hydrate Formation (Steam)	54
5.1	Components of the Reservoir Voidage	56
5.2	Cumulative Gas Production vs. Time	57
5.3	Cumulative Water Production vs. Time	57
5.4	Well Bottom Hole Pressure vs. Time	58
5.5	Well Block Pressure vs. Time	58
5.6	Pressure at the Start of the Simulation	59
5.7	Pressure after Three Years of Simulation	60
5.8	Pressure after Ten Years of Simulation	60
5.9	Pressure at the End of Simulation	61
5.10	Temperature at the Start of the Simulation	62
5.11	Temperature after Three Years of Simulation	63
5.12	Temperature after Ten years of Simulation	63
5.13	Temperature at the End of Simulation	64
5.14	Hydrate Saturation at the Start of Simulation	65
5.15	Hydrate Saturation after Three Years of Simulation	66
5.16	Hydrate Saturation after Ten Years of Simulation	66
5.17	Hydrate Saturation at the End of Simulation	67
5.18	Water Saturation at the Start of Simulation	67
5.19	Water Saturation after Three Years of Simulation	68
5.20	Water Saturation after Ten Years of Simulation	69
5.21	Water Saturation at the End of Simulation	69

5.22	Production Rate, 30-Year Simulation	70
5.23	Temperature Profile Before and After 30 Years	71
5.24	Hydrate Saturation Profile at 30 Years	72
5.25	Production Rate, Reduced Hydrate Saturation	73
5.26	Water Saturation at the End of 30 Years	74
5.27	Production Rate, Reduced Permeability	75
5.28	Effect of Thermal Conductivity on Production Rate	76
5.29	Effect of Kinetic Rate Constant on Cumulative Gas Production	76
5.30	Effect of Porosity on Cumulative Gas Production	77
5.31	Effect of Rock-Fluid Data on Cumulative Gas Production	78
5.32	Effect of Rock-Fluid Data on Gas Production Rate	78
5.33	Gas Production Rate vs. Time	79
5.34	Cumulative Gas Production vs. Time	80
5.35	Hydrate Saturation Contours after One Year of Production	81
5.36	Hydrate Saturation Contours after Two Years of Production	81
5.37	Hydrate Saturation Contours after Three Years of Production	82
5.38	Pressure Contours after One Year of Production	83
5.39	Pressure Contours after Two Years of Production	83
5.40	Pressure Contours after Three Years of Production	84
5.41	Water Saturation Contours after One Year of Production	85
5.42	Water Saturation Contours after Two Years of Production	85
5.43	Water Saturation Contours after Three Years of Production	86
5.44	Cumulative Gas Production for Loose Hydrate vs. Time	87
5.45	Cumulative Gas Production for Tight Hydrate vs. Time	88
5.46	Temperature Contours after Two Years of Production, Heated Well Method	89
5.47	Temperature Contours after Three Years of Production, Heated Well Method	90
5.48	Water Saturation Contours after One Year of Production, Heated	91

Well Method
5.49 Water Saturation Contours after Two Years of Production, Heated Well Method 91
5.50 Water Saturation Contours after Three Years of Production, Heated Well Method 92
5.51 Pressure Contours after One Year of Production, Heated Well Method 93
5.52 Pressure Contours after Two Years of Production, Heated Well Method 93
5.53 Pressure Contours after Three Years of Production, Heated Well Method 94
5.54 Location of Injection and Production Wells Completed in Hypothetical Formation Model 95
5.55 Cumulative Gas Production vs. Time 96
5.56 Temperature Contours at the Start of Production, Hot Water Injection Method 97
5.57 Temperature Contours after One Year of Production, Hot Water Injection Method 97
5.58 Temperature Contours after Two Years of Production, Hot Water Injection Method 98
5.59 Temperature Contours after Three Years of Production, Hot Water Injection Method 98
5.60 Pressure Contours at the Start of Production, Hot Water Injection Method 99
5.61 Pressure Contours after One Year of Production, Hot Water Injection Method 100
5.62 Pressure Contours after Two Years of Production, Hot Water Injection Method 100
5.63 Pressure Contours after Three Years of Production, Hot Water 101

Injection Method
5.64 Hydrate Saturation Contours at the Start of Production, Hot Water Injection Method 102
5.65 Hydrate Saturation Contours after One Year of Production, Hot Water Injection Method 102
5.66 Hydrate Saturation Contours after Two Years of Production, Hot Water Injection Method 103
5.67 Hydrate Saturation Contours after Three Years of Production, Hot Water Injection Method 103
5.68 Water Saturation Contours at the Start of Production, Hot Water Injection Method 104
5.69 Water Saturation Contours after One Year of Production, Hot Water Injection Method 105
5.70 Water Saturation Contours after Two Years of Production, Hot Water Injection Method 105
5.71 Water Saturation Contours after Three Years of Production, Hot Water Injection Method 106
5.72 Energy Efficiency Ratios vs. Time 108
5.73 Temperature Contours during Hot Water Injection at Maximum Production Rate 109
5.74 Temperature Contours during Hot Water Injection at Maximum Energy Efficiency 109
5.75 Hydrate Saturation Contours during Hot Water Injection at Maximum Production Rate 110
5.76 Hydrate Saturation Contours during Hot Water Injection at Maximum Energy Efficiency 111
5.77 Temperature and Pressure Profiles in an Extended Field (a), (b) And In Near-Well Zone (c), (d). 115

5.78	Mass Flux and Total Mass Flow Profiles	116
5.79	Comparison of Temperature, Pressure and Natural Gas Flow for Different Well Pressures and Reservoir Temperatures	118
5.80	Comparison of Location of Dissociation Front for Different Well Pressures and Reservoir Temperatures	119
5.81	Comparison of Temperature, Pressure, Gas Flux Profiles and Location of Dissociation Front for Different Permeabilities	122
5.82	Comparisons of Temperature, Pressure, Gas Flux Profiles and Displacement of Dissociation Front for Different Porosities	124
5.83	Comparisons of Temperature, Pressure, and Gas Flow Profiles and Displacement of Dissociation Front for Different Boundary Conditions	128
5.84	Gas and Water Production Rate vs. Time of Base Case	130
5.85	Components of Reservoir Voidage	131
5.86	Temperature and Hydrate Saturation Distributions vs. Time	132
5.87	Cumulative Gas and Water Production vs. Time	134
5.88	Cumulative Gas Production Vs. Time for Various Production Schemes	135
5.89	Temperature Profiles During Steam Injection After Three and Eight Years Respectively	136
5.90	Effect of Cumulative Gas Production to the Rock Thermal Conductivity	137
5.91	Effect of Cumulative Gas Production to the Rock Permeability	138
5.92	Effect of Cumulative Gas Production to the Reaction Frequency Factor	139
5.93	Cumulative Gas Production vs. Time Comparison of CMG STARS and Analytical Model	140

LIST OF TABLES

Table		Page
4.1	Component Thermal Properties	49
4.2	Base Case Parameters	50
4.3	Base Case Parameters (Steam Case)	54
5.1	Values of Dissociating Temperature and Pressure and Parameter γ for Given Reservoir and Well Conditions	114
5.2	Values of Dissociating Temperature and Pressure and Parameter γ for Different Zone Permeabilities	121
5.3	Values of Dissociating Temperature and Pressure and Parameter γ for Different Reservoir Porosities	123
5.4	Values of Dissociating Temperature and Pressure and Parameter γ for Given Reservoir and Well Conditions (*Constant Gas Output*)	126
5.5	Values of Dissociating Temperature and Pressure and Parameter γ for Different Zone Permeabilities (*Constant Gas Output*)	127

ACKNOWLEDGEMENTS

I would like to take this opportunity to thank Dr. Gang Chen, Chair of my graduate academic advisory committee for his guidance, encouragement, and support throughout this work. Also, I am very thankful to members of my graduate academic advisory committee, Drs. Scott Huang, Douglas Reynolds and Vikas Sonwalkar, for their collective wisdom, constructive and critical comments on my work through the past three years. I am grateful to them for their flexibility and willingness to meet with me, whenever it was needed.

This research was not an easy task to accomplish while continuing my job at the University of Alaska Fairbanks. Thanks are due to many individuals for their help, patience with me, providing me the encouragement needed at any time to stay focused and the technical discussions that have helped me not only in this work but also throughout my career. I am certain I will miss some names here. However, I would like to express my sincere thanks to Drs. Abhijit Dandekar, Santanu Khataniar, Godwin Chukwu, and Sukumar Bandopadhyay, and Mr. Narendar Nanchary.

I would also like to acknowledge the support of my family, my wife Anjali and children, Samir and Mitali, who have provided me all the support needed and stayed behind me through many weeknights and weekends without me. This research would not have been possible without their sacrifice.

Finally, I would like to dedicate this dissertation to my late father, Liladhar Patil, who would have been very happy to see this day.

NOMENCLATURE

°C	degrees Celsius
c(i)	concentration of component i, gmol/m^3
C_{ks}	concentration of component k in solid phase, gmol/m^3
D	direction r, z
D_{ji}	dispersibilities
E	activation energy, J/mol
enrr(i)	order of reaction with respect to component i
$\dot{g}_g$	reaction rate, gmol/m^3day
$\dot{g}_l$	generation rate of phase l unit volume, kg/m^3
$\dot{g}_{ml}$	sink due to production, kg/m^3
h_l	specific enthalpy of phase l, K/kg
HL_c	constant heat transfer model
HL_k	heat transfer to region of interest through block face k
H_{rk}	enthalpy of reaction, J/kg
HL_v	rate of heat transfer calculated from convective model
μ_l	viscosity of phase l, Pa.s
Φ_l	potential of phase l, kPa
$\vec{u}_l$	velocity of phase l, m/s
hr	hour
k	absolute permeability, m^2
k_c	thermal conductivity, w/mK
K	thermal transmissibility at the interface between two regions
K_i	equilibrium constant for component i
k_{rl}	relative permeability to phase l
m	meter
md	millidarcies

M_l	molecular weight of phase *l*, kg/kmol
mmscfd	million standard cubic feet per day
mmscmd	million standard cubic meters per day
N_H	hydrate Number (5.75)
n_r	number of reactions
p	pressure
p_c	capillary pressure, kPa
p_e	H-V-L_w equilibrium pressure, kPa
p_l	pressure of phase *l*, kPa
p_{cow}	water oil capillary pressure, kPa
p_{cog}	gas oil capillary pressure, kPa
ϕ	porosity
ϕ_f	fluid porosity
ϕ_v	void porosity
$\dot{Q}_H$	heat of hydrate decomposition unit volume, J/m^{3}s
$\dot{Q}_{in}$	direct heat input unit volume, J/m^{3}s
$\dot{q}_{ml}$	mass production rate of phase *l* unit volume, kg/m^{3}s
R	gas constant (8.314 J/mol K)
rrf	reaction frequency factor, 1/day
r_{rk}	volumetric rate of reaction, gmol/m^3
rxk1-5	coefficient for Antoine's co-relation
ρ_l	density of phase *l*, kg/m^3
ρ_i	density of phase *l*, kg/m^3
$\bar{S}_l$	normalized saturation of phase *l*
S_{gr}	residual gas saturation
S_{ki}	product stoichiometric coefficient of component i in reaction k
S_l	saturation of phase *l*
S_{wr}	irreducible water saturation

T	temperature, K/C
t	time, s
U_l	specific internal energy of phase l, J/kg
U_r	energy per rock volume, J/m^3
V_l	volume of phase l, m^3
x_i	liquid phase mole fraction of component i
y_i	vapor phase mole fraction of component i

a,b,c	empirical constants; a= 0.0342 K^{-1}, b= 0.0005 K^{-2}, c= 6.4804
a_n	thermal diffusivity of zones, m^2/s
c_v	volume heat capacity of gas, ($3000\,J/K.Kg$)
c_1, c_2	heat capacity of zone I and II ; c_1=2400.2 $J/K.Kg$, c_2=1030.2 $J/K.Kg$
k_1, k_2	phase permeability of gas in zone I and II ; k_1= 5.2md, k_2= 0.4md
p_e	initial reservoir pressure, 15 MPa
p_0	atmospheric pressure, 0.1 MPa
p_D	dissociation pressure, Pa
p_n	pressure in zone I and II , Pa
p_G	well pressure, Pa
Q	gas production rate per unit length of well, m/s
r	spatial position, m
r_0	radius of well, m
R	radius of decomposition front, m
S_G, S_H	saturation of gas, hydrate respectively (fraction)
t	time, s
T_D	dissociation temperature, K

T_e	initial temperature of hydrate, K
T_n	temperature in zone I and II , K
T_0	$273.15\,K$
v_1, v_2	velocity of natural gas in zone I and II , m/s
z	compressibility of gas; (0.88)
Φ	porosity of rock (0.2)
Φ_1, Φ_2	content of free gas at zone I and II
γ	constant related to movement of dissociation front, m^2/s
ε	mass fraction of gas in methane hydrate (0.129)
δ	throttling coefficient of gas, $(8*10^{-7}\,K/Pa)$
η	adiabatic coefficient of gas, $(3.2*10^{-6}\,K/Pa)$
ρ_0	Density of methane gas at STP, $(0.706\,Kg/m^3)$
ρ_3	Density of hydrate, $(910\,Kg/m^3)$
ρ_W	Density of water, $(1000\,Kg/m^3)$
μ	viscosity of gas, $(1.5*10^{-5}\ Pa.s)$

Subscripts

g	*Gas Phase*
w	*Water Phase*
o	*Oil Phase*
H	*Hydrate Phase*
R	*Rock*

Acronyms

EOSHYDR	Equation of State Hydrate
TOUGH2	Transport Of Unsaturated Groundwater and Heat

CHAPTER ONE

INTRODUCTION

The estimated amount of gas in the hydrate accumulations of the world greatly exceeds the volume of known conventional gas reserves. However, the role that gas hydrates will play in contributing to the world's energy requirements will depend ultimately on the availability of sufficient gas hydrate resources and the "cost" to extract them. Yet considerable uncertainty and disagreement prevails concerning the world's gas hydrate resources.

Gas hydrate is an ice-like material consisting of a structure of water molecules like ice, but having an expanded crystal lattice that encages a gas molecule, generally methane. Gas hydrates occur in sedimentary deposits under conditions of pressure and temperature present in permafrost regions and beneath the sea in outer continental margins. The combined information from Arctic gas-hydrate studies shows that, in permafrost regions, gas hydrates may exist at subsurface depths ranging from about 130 to 2,000 m. The presence of gas hydrates in offshore continental margins has been inferred mainly from anomalous seismic reflectors known as bottom-simulating reflectors, which have been mapped at depths below the sea floor ranging from about 100 to 1,100 m. The most critical and fundamental question in gas hydrate study is: how much gas hydrate is stored in marine sediments? Variable estimates have been reported (McIver, 1981; Kvenvolden, 1988; Dillon et al., 1995), but the global inventory of gas hydrate is believed to be 10^4 Gt (10^{19} g) as carbon (Kvenvolden, 1988). Current estimates of the amount of gas in the world's marine and permafrost gas hydrate accumulations are in rough accord at about 20,000 trillion cubic meters.

Proposed methods of gas recovery from hydrates usually deal with dissociating or "melting" in-situ gas hydrates by either, (1) heating the reservoir beyond hydrate formation temperatures, (2) decreasing the reservoir pressure below hydrate equilibrium, or (3) injecting an inhibitor, such as methanol or glycol, into the reservoir to decrease

hydrate stability conditions. First order thermal stimulation computer models have shown that gas can be produced from hydrates at sufficient rates to make gas hydrates a technically recoverable resource. However, the economic cost associated with these types of enhanced gas recovery techniques would be prohibitive. Among the possible techniques for production of natural gas from in-situ gas hydrates, the most economically promising method is considered to be the depressurization technique.

There have been numerous studies on hydrate decomposition in the past few years (Tsypkin, 1991; Ji et al., 2001; Moridis, 2002). Ullerich et al. (1987) described the decomposition of a synthetic core of methane hydrate as a moving boundary heat transfer problem. Most of the models assume equilibrium decomposition (Ji et al., 2001; Tsypkin, 1991). In the equilibrium models, the three-phase hydrate-gas-water interface is at equilibrium. Kim et al. (1987) developed a model for the intrinsic rate of gas hydrate decomposition and determined the rate constant for methane from experimental data. Yousif et al. (1991) discussed a two-phase fluid flow and kinetics of dissociation for the performance prediction of gas production from hydrate reservoirs, but under isothermal conditions. Ji et al., (2001, 2003) have studied the natural gas production from hydrate decomposition by depressurization using a one-dimensional analytical model and a Cartesian 1-D numerical model. Ji et al. (2001) developed an axisymmetric model for production of natural gas at a constant rate from hydrate reservoirs. Moridis (2002) developed EOSHYDR, a new module for the TOUGH2 general purpose simulator that can model the non-isothermal methane (CH_4) release, phase behavior and flow under the conditions of the common methane hydrate deposits.

1.1 CMG STARS - Numerical Model

Numerical simulations give useful information in assessing the technical and economic analysis of the hydrate-dissociation process. For this reason this study has adapted a commercial simulator, CMG STARS, to model gas hydrate dissociation caused by

several production mechanisms (depressurization, hot water injection and steam injection). Even though CMG is a commercially available simulator capable of handling thermal oil recovery processes, the novel approach of this work was the way in which the simulator was modified by formulating a kinetic and thermodynamic model to describe the hydrate decomposition. This work introduces the theoretical background of this simulator and presents the assessment of several gas production schemes using this simulator.

The simulator can calculate gas and water production rates from a well, and the profiles of pressure, temperature and saturation distributions in the formation for various operating conditions. Results indicate that a significant amount of gas can be produced from a hypothetical hydrate formation overlying a free gas accumulation by different production scenarios. However, steam injection remarkably improved gas productivity over depressurization and hot water injection. The effect on gas production due to the presence of an aquifer in the formation is also studied. Various cases were run with variations in absolute permeability, rock thermal conductivity and kinetic rate constant.

Models of the behavior of hydrate-capped gas and hydrate reservoirs have been studied by various authors in the past. Several analytical and numerical models have been developed to model the hydrate dissociation. Simplifying assumptions of analytical models, numerical solutions to the analytical models and simple material and energy balance approaches are not sufficient any longer for developing production concepts for natural gas hydrate formations. For this reason, this work has applied a modified commercial simulator, CMG STARS, to model the hydrate-dissociation process. A black oil simulator was modified by formulating kinetic and thermodynamic models to predict the production from natural gas hydrates.

Most of the researchers have come to the conclusion that under favorable operating conditions, simple depressurization appears to be an effective production strategy when

the hydrate interval is capped by free gas accumulation. However, the low operating pressures at the production wells result in lower temperatures because of the endothermic nature of the hydrate reaction. Many analytical and numerical models published so far in the literature do not incorporate hydrate behavior below 0 °C. A novel approach is presented here that makes use of a thermal compositional reservoir simulator which is capable of handling temperatures much below 0 °C.

This study was undertaken to determine the feasibility of modeling production behavior of a hypothetical hydrate reservoir by using STARS. The objectives of this work include:

- To adapt a conventional reservoir simulator for describing the process of hydrate decomposition.
- To make the thermal compositional reservoir simulator work for temperatures below 0°C.
- To understand the reservoir behavior of natural gas hydrates by using various decomposition scenarios.
- To study the inclusion of an aquifer in the formation.
- To find out the relative importance of various operating conditions on the gas cumulative volumes.
- To investigate the effect of sensitivity parameters on gas production behavior.

1.2 Analytical Model

Production of natural gas from hydrates by depressurization and with constant well output is also studied in this work. For case 1 considered in this study, a well is drilled into a methane hydrate-bearing layer, and maintained at a constant pressure below the hydrate dissociation pressure. In case 2, a well is drilled into hydrate sediment, and maintained at a fixed production rate. Also included in this work is the study of gas

production from an unbounded axisymmetric hydrate reservoir that is partially saturated with solid hydrate and contains pressurized natural gas. For describing the decomposition model of case 1, the governing equations can be written in a linearized form similar to Makogon's (1997) equations for the process of hydrate decomposition. The linearized form of the governing equations as reported by Makogon is used in the analysis of case 2. For various conditions at the well, a set of self-similar solutions for the temperature and pressure distributions in the reservoir are obtained. The outcome leads to a system of coupled algebraic equations for the location of the decomposition front and the temperature and pressure at the front. Numerical solution of the resulting system has been obtained by the Newton method of iteration. The calculations have been made for the available data of the parameters listed in the nomenclature. On comparison with the simulation results of Ji et al. (2003), significant differences were observed in the position of the decomposition front, and the dissociation temperature and pressure for different values of well output. Inconsistencies in the values of the dissociation temperature and pressure, and the position of the front have been noticed with the figures displayed in Ji et al. (2003). The errors observed in Ji et al. (2003) have been fixed in the model and the results obtained by depressurization are presented in this study. A comparison of the effect of boundary conditions on temperature and pressure distribution and production rate is studied. Effects of variations in the reservoir porosity and zone permeability are also considered.

A completely rigorous reservoir model without assumptions and limitations would be extremely complex and difficult to solve numerically. Normally, idealizations can be made without compromising the integrity of the model for the purposes intended. Limitations arise in the developed model from the assumptions made in order to obtain the model solutions. First, the model assumes the presence of a large natural gas hydrate reservoir with pressurized gas, which is unbounded. Second, the model assumes a single-phase fluid flow where the water produced from the hydrate dissociation is stationary and does not affect the flow of natural gas. In a reservoir, however, the presence of water will

reduce gas permeability and decrease gas production from the reservoir. Third, the adiabatic effect is taken into account in modifying the energy balance equation, because of which the heat transferred from the surroundings is neglected. Finally, thermo-physical properties are assumed to be constant. Viscous dissipation, inertial effects, and the possibility of mutual or external energy transmission are neglected. Some of these assumptions will affect the actual rate of hydrate dissociation. However, the primary objective of this study is to determine if it is feasible to produce natural gas from hydrate dissociation by depressurization. Estimation of dissociation rates are not a high priority.

CHAPTER TWO

LITERATURE REVIEW

In this section various questions related to gas hydrate production technology are addressed. Some of these questions are as follows:

- What are the different techniques available for production of natural gas from gas hydrate reservoirs in onshore and offshore environments?
- What are the principles, concepts, pros and cons associated with each of the techniques?
- What are the technological advances in these techniques?
- What are the anticipated field problems associated with these techniques?
- Which are the past studies that addressed gas hydrate production techniques?

2.1 Methods for Production of Gas from Gas Hydrates

Gas hydrate deposits principally have been found in three types of environments. These types include: a) Arctic onshore environments where they occur in shallow sediments within and underneath permafrost; b) Arctic oceanic environments where they occur in shallow as well as deep oceanic sediments; and c) Deep offshore temperate and tropical environments where they occur in oceanic sediments underneath deep offshore waters. The examples of the Type-a environment are the North Slope of Alaska, the McKenzie Delta belt of Canada and the Messoyakha field in Russian Siberia. The examples of the Type-b environment are the Bering Sea, the Arctic Ocean and the Aleutian Trench. The

third type of environment includes offshore Japan, the Middle America Trench and others.

The estimates of the amount gas within the naturally occurring gas hydrate deposits are so huge, that they represent an unconventional resource of natural gas for the 21st century. The potential of gas hydrate resources is particularly attractive when one considers hydrates as a concentrated form of natural gas. Various methods have been suggested for production of gas from gas hydrate reservoirs. These techniques utilize one and/or all of the three principal mechanisms of decomposition of hydrates. These three principal mechanisms are categorized as follows:

1. Depressurization - Pressure reduction below that for hydrate equilibrium, causing a pressure drop as a driving force for decomposition.
2. Thermal Stimulation - Providing heat of dissociation to hydrates, causing a temperature difference as a driving force for hydrate decomposition.
3. Hydrate Thermodynamic Equilibrium Shift by use of Inhibitors - Inhibitors shift the hydrate thermodynamic equilibrium P-T conditions, causing a driving force for decomposition.

The various methods for production of gas from gas hydrates include:

(a) Thermal Stimulation Techniques

- Steam/Hot Water/Hot Brine Injection
- Down-Hole Heater
- In-Situ Combustion
- Electromagnetic Heating
- Microwave Heating
- Electrical Wave Heating

(b) Depressurization Method

(c) Hydrate Inhibitor Injection Method

(d) Fracturing

(e) Sea Floor Mining and Water Jet Drilling

None of the above techniques have been tested in the field except for depressurization. The only field proof of gas production from hydrates comes from the Messoyakha gas/gas hydrate field in Russia. This provides some clue that gas hydrates are technically producible via the depressurization method, even though no heat is supplied from the surface. However, a large number of technical, geo-political, economical, and environmental and safety concerns and issues remain to be addressed before commercial production from gas hydrates becomes a reality. Some of these are discussed in this chapter.

Since gas hydrates are solids and since they exist in reservoirs as relatively immobile and impermeable phase, the first step in the production is to decompose gas hydrates into gas and water by various means. The process of hydrate decomposition requires that heat be provided to the decomposing hydrate surface that is sufficient to shift the equilibrium between hydrates, gas and water. The heat of decomposition includes the heat needed to raise the temperature of the region to a level where the hydrate is not stable, and a latent heat of vaporization. Thermodynamically, through energy balance calculations, it can be shown that the energy required for decomposition of gas hydrates into gas and water is approximately one tenth of the energy value of the produced gas (Kamath and Godbole, 1985). This heat of decomposition is dependent upon the pressure, temperature, gas composition and the concentration of the inhibitor used in decomposition, if any. Thus, the energy efficiency ratio (EER) in the range of 10 to 13 represents the highest that can be achieved in the most thermodynamically efficient process without inhibitors. Higher energy efficiency ratios are only possible with the use of inhibitors, which reduce the decomposition energy. Thus, some of the recent literature (Islam, 1994; Isuex, 1990) that

has indicated energy efficiency ratios greater than 20 violates the basic energy-balance considerations.

The type of hydrate system encountered will influence the method of recovery. The possibilities are:

- All hydrates;
- Hydrates in conjunction with free gas;
- Hydrates along with ice;
- Hydrates along with ice and free gas.

In addition, the nature of hydrates within the sediments will also affect the method of recovery. Hydrates can occur as,

- Dispersed within the pore space (extremely low hydrate saturation);
- Nodular (intermediate hydrate saturation);
- Laminated or layered (hydrate layers separated by impermeable shale or clays);
- Massive (extremely low sediment content).

The most promising targets for hydrate production probably include situations where hydrates occur in conjunction with free gas (onshore or offshore) and thick-layered hydrate reservoirs where sufficient hydrate volume exists to make it economically viable.

2.2 Thermal Stimulation Techniques

The thermal stimulation techniques can be further classified in two categories:

1) Methods that involve providing heat from the surface via injection of hot fluids;

2) Methods that involve down-hole or in-situ heat generation.

The examples of the first class are steam stimulation, hot water stimulation and hot saline water stimulation. The examples of the second type include down-hole heater (Radio - Frequency or electrical heater) technology, microwave heating, electromagnetic heating and in-situ combustion. First of all, in all thermal stimulation techniques, the heat must be provided to a large contact surface area of hydrates to yield significant hydrate decomposition rates. Also, means must be provided for the propagation of the heat front away from the well bore.

In the first class of methods, where large volumes of hot fluids have to be injected, there will be need for generating sufficient injectivity. This can be accomplished by fracturing techniques discussed later. The heat transfer can occur via conduction as well as convection. One concern associated with the first type of techniques is that since heating is at the surface, heat losses through the well bore will be present and can be substantial. In the second class of methods, the heat-transfer occurs mainly downhole in the formation and thus well bore heat losses can be avoided. The principal mode of heat transfer to hydrates will be via thermal conduction. However, once sufficient hydrates have decomposed and the volume of the decomposed zone has increased, heat transfer by convection will also become important. Further details about these techniques are provided in subsequent sections.

2.2.1 Hot Fluid Injection

In this section, the hot fluid injection methods such as hot water, brine and steam injection are discussed.

2.2.1.1 Hot Water Injection

There are only a limited number of published studies on the hot water injection method for decomposition of gas hydrates. The work has been conducted by four groups, which are, Holder et al. (1982), Kamath et al. (1991), Sloan (1991) and Bishnoi et al. (1989). These include laboratory decomposition studies by Kamath and Holder (1987), Sira et al. (1989) and modeling studies by Kamath and Godbole (1985), Roadifer (1988), Kamath et al. (1991), Sloan (1991) and Jamaluddin et al. (1989). The laboratory studies involved forming synthetic cores of gas hydrates followed by their decomposition via the hot water injection method. Details of these studies are provided in a report to Japan Oil Engineering (JOE) (Kamath and Patil, 1994). Among the modeling studies on gas hydrate decomposition, the only studies that address reservoir modeling are those by Kamath and co-workers (Kamath and Godbole, 1985; Roadifer, 1988, Kamath et al. 1991). No other studies on hot water injection have been reported since 1993. The only study where hot water injection into hydrate reservoirs was investigated is by Kamath and Godbole (1985).

Hot water injection has never been tested in the field. Laboratory studies have provided some useful information on the kinetics of hydrate decomposition. Kamath and Godbole (1985) have reported energy efficiency ratios in the range of 9 to 10.8 for the cyclic hot water injection method. The thermal efficiency has ranged between 70-85% for 350 °F hot water injection when fully insulated tubing is used. This indicates that the well-bore heat losses are significant. To reduce the well-bore heat losses, one would have to reduce injection water temperature and increase injection rate. In offshore situations, where an abundant supply of warm, saline ocean surface water is readily available, ocean surface water injection may be worthwhile considering. The temperature of the water to be used would depend upon individual cases where simulation studies and field tests could be performed to determine the optimum.

Cyclic hot water injection would be useful compared to continuous hot water injection as an operating procedure, at least at the start up, due to lack of communication between the

wells. Fracturing would be needed to increase the injectivity as well as the surface contact area of the dissociating hydrates. In the later part of the production life, continuous hot water injection with hot water drive may work, once the communication between the wells is developed. Some of the envisioned technical problems associated with hot water injection include: significant production of water, from both injected water and dissociated zones; potential problems with movement of the gas to the surface since the gas pressure has to overcome the water loading in the well; the possibility of reformation of ice and/or hydrates near the well-bore causing plugging of the pore throats due to the cooling effect from gas production; and water handling at the surface.

Since hydrate reservoirs will have very limited injectivity and communication between the wells, stimulation by cyclic hot water injection is preferable to continuous injection.

Simulation studies need to be done for evaluating the feasibility of hot water injection for individual cases. Different well configurations including fracture geometry need to be considered for optimization. Preliminary calculations based on previous study (Kamath and Godbole, 1985) indicate that for hydrate production to be economical, every well in arctic conditions would have to produce at least 1-3 MMSCF per day, whereas, in offshore conditions production needs to be at least 3-10 MMSCF per day.

2.2.1.2 Hot Brine Injection

Several factors make use of hot brine for dissociation of hydrates an attractive recovery scheme compared to other thermal stimulation techniques that involve fluid injection into hydrate reservoirs. First, brine acts as a hydrate inhibitor. At a given pressure, brine reduces the equilibrium dissociation temperature of hydrates, depending upon its salinity. Thus, with use of brine the reservoir temperature need not be raised to the extent needed for other hot fluid injection techniques. The higher the salinity of brine, the lesser is the requirement of reservoir heating. Secondly, at lower dissociation temperatures the heat of

hydrate dissociation itself is lower. Thus, higher energy efficiency ratios are possible with this technique compared to other hot fluid injection techniques. Kamath and Godbole (1985) provide detailed discussion on this subject. Finally, as a consequence of lower dissociation temperatures, the heat losses are lower for brine injection. Thus, the triple effect of reduction in sensible heat requirements, reduction in hydrate dissociation energy requirements, and reduction in heat losses result in better thermal efficiencies. This technique may be applicable to situations where geothermal reservoirs exist in close proximity to hydrate reservoirs. Typically, the temperature of geothermal brine ranges from 300-700°F for depths between 3,000-5,000 ft. and their salinities vary between 0.5-2% by weight (Thomas, 1982). For oceanic hydrate applications, use of saline, ocean surface water would be a natural way for hydrate stimulation.

There are only a limited number of published studies so far on the hot brine injection method for decomposition of gas hydrates. The work has been conducted by three groups, which are McGuire (1981), Kamath and co- workers, and Iseux (1990). These include laboratory decomposition studies by Sira et al (1989) and modeling studies by Kamath and Godbole (1985). The laboratory studies involved forming synthetic cores of gas hydrates followed by their decomposition via the brine injection method. Details of these studies are provided in the report to Japan Oil Engineering (JOE) (Kamath and Patil, 1994). Among the modeling studies on gas hydrate decomposition, only studies that address reservoir modeling are those by McGuire (1981); Kamath and Godbole (1985); and Isuex (1990). No other studies on brine injection have been reported since 1993. The only studies where hot brine injection in hydrate reservoirs was applied and investigated is by Kamath and Godbole (1985) and Isuex (1990).

McGuire (1981) presented single well cyclic thermal injection and multi-well continuous thermal injection models. In his models, steam injection was considered for hydrate dissociation and brine injection was considered as a means of keeping hydrates from

reforming around the well-bores and fractures once dissociated by steam. Kuuskraa et al. (1983) provide a detailed review of McGuire's model.

Isuex (1990) further extended the work by Kamath and Godbole (1985), to include modeling of flow through fractures. While this work would be useful for future modeling work, his results leave behind some ambiguity. For example, Figure 15 of his paper indicated energy efficiency ratios for the STSF method (the name for hot brine injection with fracturing, (Isuex, 1990)) greater than 20 and as high as 45. This clearly violates energy balance considerations, which dictate that the maximum EER be in the range of 13-16 for brine, depending upon the salinity.

Hot brine injection has never been tested in the field. Laboratory studies have provided some useful information on the kinetics of hydrate decomposition. Kamath and Godbole (1985) have reported energy efficiency ratios in the range of 11 to 16 for the cyclic hot brine injection method. The thermal efficiency has ranged between 70-85% for 350 °F hot brine injection when fully insulated tubes were used. This indicates that the well-bore heat losses are significant. To reduce the well-bore heat losses, one would have to reduce injection brine temperature and increase injection rate. In offshore situations, where an abundant supply of warm, saline, ocean surface water is readily available, ocean surface water injection may be worth considering. The temperature of the water to be used would depend upon individual cases, where simulation studies and field tests could be performed to determine the optimum.

Cyclic hot brine injection would be useful compared to continuous hot brine injection as an operating procedure, at least at the start up, due to lack of communication between the wells. Fracturing would be needed to increase the injectivity as well as the surface contact area of the dissociating hydrates. In the later part of the production life, continuous hot brine injection with hot brine drive may work once the communication between the wells is developed. Some of the envisioned technical problems associated

with hot brine injection are similar to those of hot water injection. These include: significant production of water, from both injected brine and dissociated zones; potential problems with movement of gas to the surface, since the gas pressure has to overcome the water loading in the well; the possibility of reformation of ice and/or hydrates near the well-bore causing plugging of the pore throats due to the cooling effect from gas production; and water handling at the surface.

Simulation studies need to be done for evaluating the feasibility of hot brine injection for individual cases. Different well configurations including fracture geometry need to be considered for optimization. It is likely that among all the thermal stimulation techniques that involve fluid injection, brine injection is most preferable, especially for offshore hydrate deposits.

2.2.1.3 Steam Injection

The studies that have been reported for steam injection as a method for producing gas from hydrates include: reservoir modeling work by McGuire (1981); modeling of cyclic steam stimulation by Bayles et al. (1986) and Kamath and Godbole (1985) and laboratory decomposition studies by Kamath et al. (1991). Since 1994, no other studies on steam injection have been reported in the literature.

Applicability of the use of steam for hydrate thermal stimulation is very limited due to several problems indicated below.

- Extremely high depths of naturally occurring hydrate reservoirs (greater than 3,000 ft.) would result in high well bore heat losses and low thermal efficiencies.
- Propagation of the steam front within the reservoir would be extremely difficult to obtain.

- Other problems are similar to those with the hot fluid injection schemes described above.
- Overall economic viability of this technique is questionable.

2.2.2 Down-Hole In-Situ Heating

In this section, in-situ combustion, electrical heating, electromagnetic heating and microwave heating techniques are discussed.

2.2.2.1 In-Situ Combustion

In-situ combustion has been used as a recovery process in the production of crude oil (mainly residual oil after waterflood) and is one of the important Enhanced Oil Recovery (EOR) methods (Chu, 1983). However, the application of this method for production of gas from gas hydrates still remains conceptual and speculative in nature. Neither laboratory nor modeling studies nor field tests have been reported in literature in regard to this technique for potential application to hydrate reservoirs.

It is advisable that laboratory experiments such as combustion tube experiments be conducted along with development of simulation tools prior to field implementation in hydrate reservoirs. The experimental and simulation results can provide valuable information such as whether the reservoir is capable of sustaining combustion, whether the technique will be feasible technically and viable economically. Due to lack of such information in literature at this time, it is difficult to determine the feasibility of this concept. Therefore, the discussion below will pertain to the principles and envisioned technical problems associated with application of this technology for decomposition of gas hydrates.

Technology exists for unconventional extraction techniques such as in-situ combustion and, as such, can be modified for implementation in hydrate reservoir production. In this technique, thermal energy is generated within the reservoir as opposed to injection of thermal energy in the form of steam, hot water or hot brine, which supplies sensible and/or latent heat to the hydrate zone. The in-situ combustion technique involves injection of air or oxygen or oxygen-rich-air, which forms a combustible mixture with the gas available in the reservoir. A down-hole ignition assembly can ignite this mixture in the hydrate zone of the reservoir. Controlling the stoichiometric ratio of oxygen and methane in the ignition mixture and injection rate can control the combustion of methane within the hydrate reservoir. The exothermic combustion reaction will thus provide the energy for the decomposition of hydrates, allowing the production of the liberated gas from hydrates. Also, like any other thermal stimulation technique, the viability of this method will depend upon the overall Energy Efficiency Ratio (EER). Even though there are no well-bore heat losses in this technique, the heat losses to the surrounding reservoir rock can be significant. The areal and vertical sweep of the burning front in the hydrate zone will play a major role in the overall economics of the project.

Like other thermal stimulation methods, a cyclic near well bore treatment is more desirable than a continuous process as in EOR projects, because the hydrate zones will have almost no injectivity and thus no areal sweep. In the permafrost regions and shallow marine hydrate deposits, other problems such as subsidence will still need to be addressed. Also, numerical simulation tools need to be developed and reservoir simulation studies need be conducted to determine the heat transfer rates, reservoir performance, energy efficiency ratio, optimum injection rate to sustain the combustion, etc. Operational problems such as injectivity and/or productivity, propagation of a sustained combustion front, corrosion of tubing, water handling, high temperature cement failures, and rig safety issues also need to be addressed. Due to these envisioned operational problems, high capital costs including air compression costs, and the complicated nature of the combustion process itself that may be difficult to control, in-

situ combustion processes for gas hydrate reservoirs have not received much attention from researchers.

2.2.2.2 Electrical / Radio Frequency / Electromagnetic Heating

Potential field application of radio frequency (RF) or electromagnetic (EM) heating techniques have thus far been restricted to heating of shallow tar sand resources. No laboratory studies or field tests have been reported in the literature to investigate the applicability of RF/EM heating of hydrates. This is so far just a concept. RF/EM stimulation deserves attention for its potential application to producing gas from gas hydrate reservoirs for three reasons:

- Hydrates, like tar sands, are nearly impermeable to injected fluids and thus make it difficult to transfer heat deeper into the reservoir for hot fluid injection methods.
- The major part of the heat generated by EM/RF heating can be directed and will be utilized in decomposing gas hydrates.
- RF/EM heating can be utilized to penetrate heat deeper into the hydrate zones away from the well bore.

RF/EM stimulation has been considered as a potential technique for heating large volumes of in-situ gas hydrates. Sresty et al. (1986) suggest that frequencies in the lower portion of the RF spectrum can permit EM wave penetration of up to 3000 ft, depending upon the electrical properties of formation to be penetrated. Efficient volumetric RF power deposition technology for heating such large volumes in-situ has been developed (Sresty et al., 1986) for EOR applications and, as such, can be utilized for gas production from gas hydrate reservoirs. In this method of reservoir heating, special tubular electrodes are inserted into the well bore. By application of RF energy to these conductors, heat can be generated in-situ to uniformly heat the large volumes of gas hydrates. There is a need to direct efforts toward matching the conductor pattern and the operating frequency to

that of the electrical characteristics of the hydrate resource to be heated, thus assuring that almost all the applied RF power is contained and does not leak out.

One possible combination worthwhile investigating might be thermal stimulation of the hydrate zone by RF/EM heating to create injectivity by melting hydrates around the well bore followed by injection of brine or hot water. The RF/EM technique is expected to provide enough injectivity in the hydrate zones for the possibility of injecting these fluids.

Careful attention must be paid in designing RF/EM, such that a uniform electric field is created within the hydrate zone. Leakage of currents into adjacent formations can induce potentials in the earth and in the metallic materials such as tubing at distances far away from the electrodes. This can cause operational and safety problems such as disrupting electrical systems, accelerating corrosion and lethal shocks to human beings. Furthermore, at high frequency, such leakage can cause radiation, which may lead to RF interference in aircraft navigational systems.

Only one modeling study has been reported in the literature on use of EM heating for producing gas from gas hydrates. This is a simulation study by Islam (1994), performed while at the University of Alaska Fairbanks, where he reported that EM heating with vertical or horizontal wells may recover as much as 70% of hydrate reserves, with energy efficiency ratios as high as 40. He also suggested that intermittent heating is superior to continuous heating. He modified an existing thermal simulator used for tar sand recovery for hydrate reservoirs by solving only conduction and electrical charge balance equations during the pre-heat period. After the pre-heating period, a constant pressure is applied at the production well. The complete energy balance equation is activated only when the temperature of the near well-bore region is high enough to dissociate hydrates. Following the pre-heat period, the complete energy balance equation is solved in the dissociated zone and the conduction equation is solved for the hydrate zone. He evaluated 25

different reservoir-heating scenarios with EER ranging from 5 to 40. Although his results are quite promising, the EER greater than 20 indicate either violation of energy balance considerations or that another natural mechanism is active for decomposition of the hydrates.

For near well-bore heating, (rather than heating away from the well-bore as in RF/EM heating), additional choices include a downhole electrical heater. A downhole steam generator can be used in oil fields that lie below permafrost. In this method, by endothermic reaction, steam and methane are reformed above ground into hydrogen and carbon monoxide. In the reactor, hydrogen and carbon dioxide react to reform into steam and methane, with a large amount of heat being emitted to generate steam of 700 °F. The applicability of such devices or any other down-hole heating tools for decomposing hydrates has not been studied in great detail or tested.

Experimental studies need to be done with laboratory hydrate samples to measure decomposition rates and to determine the energy efficiency of the RF/EM process.

2.2.2.3 Microwave Heating

When microwave heating can be used and is used properly, almost certainly more volume can be heated in less time at lower cost and in a controlled manner than for any other method. Throughout history there has been one way to heat a material: apply heat to its surface. About thirty years ago, industrial engineers began developing microwave-heating techniques that avoid some limitations of conventional heating. With microwaves, no heat is applied. Instead, radio waves (which are neither nuclear nor ionizing radiation) pass through the material. The molecules in the material then act like miniature magnets attempting to align themselves with the electrical field. Under the influence of this high frequency alternating electrical field, the particles oscillate about their axes creating intermolecular friction, which manifests itself as heat.

In conventional heating, the heat source affects the molecules from the surface toward the center so that successive layers of molecules heat in turn. The surfaces to be heated may be in danger of over-heating by the time heat penetrates the material. Microwaves, however, produce a volume heating effect. All molecules are set in motion at the same time. This heating method also evens temperature gradients and offers other important benefits.

It is well known that some solids can be heated efficiently in a microwave field as a result of the dielectric relaxation, causing the microwaves to act as a transfer agent of the electric power. As a result, rapid heating of solids is possible. Interesting aspects of the use of microwave energy are:

1. It is possible to create inverse temperature fields due to bulk heating by radiation instead of by conduction;
2. Rapid heating is feasible, in contrast to the (slow) heat transfer in the case of conduction;
3. Pulsing of the waves is possible;
4. Heating of solids is selective as gases are transparent to microwaves. This is a beneficial effect for application of this technology to heat hydrates.

Some of the problems and pitfalls of this technique may be as follows:

1. The analysis of microwave heating is complicated by the difficulty of temperature measurements and the sample-size effect. In view of the radiation wavelength of microwaves (normally 2.45 GHz is used, corresponding to a wavelength of 0.12 m) the size of the sample to be heated influences the distribution (homogeneity) of the dielectric field experienced by the particles comprising the sample.

2. The success of the application of this technique for hydrate reservoir heating will depend upon how deep and how efficiently the microwave waves can transfer or generate the heat.

Experimental studies need to be conducted with laboratory hydrate samples to measure decomposition rates and to determine the energy efficiency of the microwave heating process.

2.3 Depressurization

In the depressurization method for decomposition of gas hydrates, the reservoir pressure is reduced below the three-phase vapor-liquid-hydrate equilibrium pressure. This change in equilibrium causes hydrates to decompose. The basic mechanism involved here is that hydrates absorb energy from the surrounding formations as a temperature gradient is created in the hydrate zone by a decrease in the reservoir temperature. This decomposition will continue till the new equilibrium pressure is reached at the lower temperature.

The production of gas from hydrates in the Messoyakha free gas/gas hydrate reservoir in Siberia via the depressurization method is the only field example where gas is commercially produced from hydrate reservoirs. In the Messoyakha reservoir, hydrates exist above a free gas zone. Gas production in this field started in 1965. During conventional production from the free gas zone, hydrates in this reservoir started decomposing once the reservoir pressure declined below hydrate equilibrium pressure corresponding to formation temperature. This provided additional gas to the free gas zone, thus maintaining reservoir pressure or reducing the reservoir pressure decline. Although the Russian literature in early 1960's indicated the presence of gas hydrates in this field, only later was it discovered that hydrate decomposition in this field is the cause of maintenance of reservoir pressure (Makogon, 1988). Thus, although the

depressurization scheme in this field was not designed for hydrate production, it worked naturally as a field mechanism for production of gas from hydrates. Nonetheless, this example provides field proof that gas production from naturally occurring hydrates is technically and economically feasible. Also, in the Messoyakha wells, methanol (hydrate inhibitor) was circulated in the wells to thaw the refrozen hydrates at the well bottom that caused hydrate plugging. This methanol well treatment in 8 wells as reported in literature (Sloan, 1991) helped to thaw hydrates and increase gas production rates by a factor of 2-6.

The depressurization technique is probably the most practical among all the techniques. However, it may be applicable to only those arctic and oceanic reservoirs that contain hydrates and associated free gas. Heat required for decomposition of hydrates in this technique comes from the surrounding rocks as a result of the temperature gradient created by reduction in pressure, thus eliminating the heat losses, which can be significant in thermal stimulation methods.

McGuire (1981) was the first researcher to advocate the depressurization method to decompose gas hydrates. However, he proposed that fracturing methods need to be used in order to increase the flow capacity of the hydrate zones. Holder et al. (1982) conducted three dimensional finite difference modeling of heat and mass transfer in a reservoir containing hydrates and free natural gas to model the depressurization scheme. As opposed to fracturing, Holder et al. (1982) assumed a free gas zone immediately beneath and in communication with the hydrate zone, whereby gas can be produced from the free gas zone to lower the reservoir pressure. Burshears et al. (1986) used and extended the Holder et al. model to incorporate the composition of hydrates. This simulator is probably the most up-to-date for the depressurization method since it is designed for reservoir simulation application and includes compositional effects, 3-D and 3-phase flow. Kamath et al. (1991) reported the first experimental work in decomposition of hydrates by depressurization to study the effect of gas production rate on the contribution of hydrate

decomposition to the total gas produced. Kamath and coworkers did not report modeling of the depressurization technique. Yousif et al. (1990) proposed the depressurization model with a moving boundary to simulate a semi-infinite hydrate layer and also conducted laboratory measurements of hydrate decomposition by depressurization in Berea Sandstone Cores. Their modeling work, however, is limited to simulating laboratory decomposition experiments rather than reservoir modeling.

The depressurization technique is a thermodynamically efficient process since the energy for decomposition comes from within the reservoir. However, it may not be a practical choice for reservoirs that contain hydrates only, as it may be difficult to sustain the gas production rate for long periods of time. The energy efficiency ratio of 10-11 has been reported for this process based on the energy balance considerations (Kuuskraa et al, 1983). Furthermore, as the temperature of the hydrate zone drops upon reduction in pressure, due to the Joule-Thompson cooling effect and due to the endothermic hydrate decomposition process, it can lead to further problems of freezing of water by formation of ice and/or by reformation of hydrates. In order to use this technique successfully for reservoirs containing hydrates, the presence of free gas will be necessary, where the gas production from hydrates will be supplemented by free gas to sustain the rates and maintain production. In the absence of free gas, assuming the hydrate decomposition can be maintained for longer periods of time, the amount of water produced will be so large that there may be a danger of the well being watered out. In such cases artificial lift methods may have to be employed to lift the gas to the surface and water handling at surface must be addressed.

The depressurization method can also be combined with other thermal stimulation schemes discussed above and with fracturing for either onshore or offshore environments. Hence the productivity of hydrate reservoirs can be enhanced, thus making depressurization an economically viable and commercially feasible way to produce hydrates.

2.4 Hydrate Inhibitor Injection Method

There are only a limited number of published studies on the hydrate inhibitor injection method for decomposition of gas hydrates. Sira et al. (1989) conducted laboratory work to study the effects of methanol and glycol injection on decomposition characteristics of laboratory synthesized hydrate cores. Details of this study are given in Sira et al. (1989), and Kamath et al. (1991), and are provided in the JOE report (Kamath and Patil, 1994). No modeling studies on gas hydrate decomposition by hydrate inhibitor injection have been reported in the literature.

Although hydrate inhibitor injection has never been tested in the field before, hydrate inhibitor injection has been used as a means of stimulating hydrate wells in the Messoyakha Field in Russia. A laboratory study by Sira et al. (1989) and field experience on increase of gas production due to inhibitor injection indicate that hydrate inhibitors play a key role in enhancing the rate of decomposition of hydrates. Hydrate thermodynamic inhibitors such as methanol and glycol destabilize gas hydrates by shifting the hydrate thermodynamic equilibrium. Thus, in this regard, they behave in the same manner as brine and reduce hydrate decomposition temperature and energy, providing an increased temperature driving force. As in the case of brine injection, higher energy efficiency ratios than for water are expected depending upon the concentration of inhibitor solution. Based on the laboratory experimental data, Sira et al. (1989) provided a correlation for rate of decomposition of hydrates. These correlations indicate that methanol and ethylene glycol enhance the rate of decomposition significantly (up to a factor of 4-8).

Application of hydrate inhibitors is more suitable for small volume near well-bore treatment, rather than as a large volume injection method. This is due to the high cost of such inhibitors that may not be recoverable from the reservoirs once injected. Methanol stimulation followed by drill stem testing was carried out in the 1998 Japan National Oil

Corporation (JNOC) Hydrate Test Well in Canada. This test provided very useful information on technical feasibility and capability of methanol stimulation as a hydrate recovery mechanism.

Assuming the hydrate inhibitor injection technique is feasible, cyclic inhibitor injection would be more suitable than continuous inhibitor injection as an operating procedure, due to lack of communication between the wells. Fracturing would be needed to increase the injectivity as well as the surface contact area of the dissociating hydrates. In the later part of the production life, continuous hot water injection with hot water sweeping the reservoir may work, once the communication between the wells is developed by inhibitor injection. Some of the envisioned technical problems associated with this technique include: recovery of injected costly inhibitor, significant production of water and potential problems with lifting of gas to the surface which has to overcome the water loading in the well.

Simulation studies need to be conducted for evaluating the feasibility of inhibitor injection for individual cases. Different well configurations including fracture geometry need to be considered for optimization.

2.5 Fracturing

Hydrate reservoirs, due to the immobile and impermeable nature of gas hydrates, will have very limited or no injectivity whatsoever. Furthermore, hydrate decomposition is a surface phenomenon and the rate of decomposition of hydrates during thermal stimulation will depend upon the surface area of hydrates in contact with the dissociating fluid. Therefore, for all practical purposes, fracturing will be essential to increase injectivity of injection fluids and for enhancing the rate of hydrate decomposition.

Fracturing technology has been in existence for a very long time and significant field experience with this technology is available. Prior to fracturing hydrate reservoirs, it will

be necessary to obtain some data related to the mechanical properties of sediments containing gas hydrates, such as Young's modulus, compressive strength and shear stress relationships. Such information is very limited in regards to actual hydrate field samples, although some work has been reported on the mechanical properties of pure hydrates. Also, simulation studies need to be conducted that include flow and heat transfer through fractures in gas hydrate reservoirs. Once such information and data are available, they can be used to design fracturing jobs including the fracture size and geometry, and type and volume of proppant to be used.

Most of the past modeling work on gas production from hydrate reservoirs via thermal stimulation techniques has indicated the need for fracturing to enhance the injectivity. Only two studies have been conducted to actually model the flow and heat transfer through fractures. These include: linked vertical fracture model presented by McGuire (1981) and STSF - hot solvent stimulation after hydraulic fracturing model presented by Iseux (1990). While McGuire's study indicates the most favorable case of the parametric sensitivity analysis, only 16% of the energy input to the reservoir was recovered; the Iseux study reports three times higher gas production and energy efficiency ratios than reported by others.

Some of the technical problems associated with fracturing hydrates that need to be addressed include:

- Lack of information on mechanical properties of reservoir hydrate samples;
- Possibility of poor compressive strengths of hydrate formations;
- Possibility of poor control on obtaining desirable fracture geometry;
- Possibility of closure of the fractures due to reformation of hydrates and /or ice due to the cooling effect from hydrate decomposition.

It may be worthwhile to consider use of hot injection fluids themselves as proppants or use of electrical heating to induce thermal stresses in the hydrate reservoirs for creating "thermally induced fractures". This is mostly a concept and has not been tested in the field.

2.6 Sea-Floor Mining

This type of recovery method is applicable to development of very shallow offshore hydrate deposits located at the ocean bottom. A similar technique is used for mining of manganese oxide. This process will involve building a huge inverted cone and installing it at the ocean bottom over the potential hydrate deposit. A drill string can be inserted in the cone through the central funnel. With the bit grinding the hydrate zone and injecting warm water, the hydrates will decompose and the gas will be produced through the annulus. This is mostly a concept that is in its infancy. No serious thought has been given so far to this technique by hydrate researchers and no studies have been done to develop this concept further. Several issues that need to be addressed in regards to this method are:

- Sufficiently thick hydrate deposits with very large volume per unit surface area are needed.
- The cone can settle as hydrates decompose causing gas leaks.
- If gas leaks to the surrounding water, seawater density will decrease as significant quantities of gas can dissolve in seawater. Shell has experienced this, as one of their supply ships started sinking. This is a major concern for offshore gas hydrate production).

Another alternative for oceanic hydrates proposed in published literature is use of the high pressure, hydraulic-jet drilling technique. No published work exists in literature on application of this technique for hydrate drilling/decomposition, but rather only passing remarks are made. This technique is similar to sea floor mining, except a water jet at high

velocity is used to drill and decompose the gas hydrate zones. Significant work has been conducted in water jet drilling at Los Alamos Laboratory. A small hole of several miles in length can be drilled using extremely high-pressure water jet through composite (ceramic/graphite) pipe. Work conducted at Los Alamos Laboratory was for the defense department with different objectives. However, it can be applied for hydrate production purposes.

In a separate study funded by the Gas Research Institute, development of a downhole high-pressure pumping system for jet-assisted drilling is reported by Cohen et al. (1995). Jet-assisted drilling utilizes a high-pressure jet of water or drilling mud directed at the gauge of the hole to erode and/or weaken the rock so that faster drilling can be achieved. This is particularly useful in deep wells where the penetration rate slows with increasing depth. The reported research developed two key components of the pump system: the motor and the high-pressure pump. They were developed using existing centrifugal submersible oil-field pump parts. The results are a turbine motor capable of developing 360 horsepower and a high-pressure pump that can produce 22 gallons per minute at 10,000 pounds per square inch.

CHAPTER 3
MODEL FORMULATION

The main goal of this study was to develop a model which can predict production of methane from hydrate reservoirs by depressurization and thermal stimulation. The model development is explained in Sections 3.3-3.5. However, to determine whether the model works properly or not, it needs to be compared with either experimental or field production data. At present, no such data exists. Therefore, general consensus in the scientific community is that a model should be based on, currently available commercial reservoir simulators with demonstrated capability to predict the field performance of oil producing reservoirs. However, the commercial simulators need to be modified in order to be able to predict performance of the hydrate reservoirs. This task was performed in Sections 3.1 and 3.2. The STARS simulator was modified to predict production of methane from the hydrate reservoirs. The modification details are given in the following sections.

3.1 Numerical Simulation of Hydrate Dissociation

Swinkels and Drenth (2000) had previously modified a commercial simulator to model hydrate dissociation. This approach was used in this study, using STARS (Steam, Thermal, and Advanced Processes Reservoir Simulator). It is a three-phase multi-component thermal and steam additive simulator, developed by the Computer Modeling Group Limited (CMG). It is an off the shelf simulator widely used throughout the petroleum industry. The CMG STARS simulator was modified by formulating a kinetic and thermodynamic model to describe the hydrate decomposition. Grid systems may be Cartesian, cylindrical, or variable depth/variable thickness. One, two, and three-dimensional configurations are allowed with any of the grid systems. A variety of operating conditions and constraints may be specified for each of the multiple or horizontal wells. STARS can be used to model in-situ combustion processes that may be applied for the enhanced recovery of heavy oil reservoirs.

The CMG STARS simulator was actually developed for conventional hydrocarbon production. It consists of conservation equations, which are the material balance equations, the flow equations, the chemical reactions, the heat transfer equations and the phase equilibrium relationships. If the properties governing these equations are altered, then the same simulator can be used to describe other systems such as hydrate reservoirs, as the same flow equations govern the flow of methane produced from the hydrate reservoirs. Thus, the following properties are changed in the equations discussed above to modify the STARS simulator to describe production of gas from the hydrate reservoir.

- Conservation Equations: Instead of the oil phase, the hydrate phase was considered.
- Flow Equations: The oil phase was assigned a very high viscosity of 1000 cp to make it immobile. Also, since the gas-water relative permeability data in the presence of a hydrate phase are not available, equations published by Hong and Darvish (2003) were used to describe the gas-water relative permeability in the presence of hydrates.
- Chemical Reactions: Hydrate dissociation produces methane and water. Thus, the hydrate dissociation reaction was considered, while for the kinetics part, the activation energy of the hydrate dissociation reaction was considered.
- Heat Transfer equations: The hydrate dissociation reaction is endothermic and hence the enthalpy was negative.
- Phase Equilibrium Relationships: The hydrate dissociation equilibrium was considered as part of the phase equilibrium relationship.

Thus, by modifying these values and taking a trial and error approach, many simulations were conducted to produce acceptable data and the CMG STARS simulator was successfully modified to describe production of methane from hydrate reservoirs. The solution of all these equations is obtained by the simulator during internal execution, which is essentially a "black box".

3.1.1 Hydrate Decomposition Kinetics

STARS uses a number of mathematical equations to express all the physical phenomena that occur during the production of a hydrocarbon reservoir. The equations are an integral part of the modeling software and a user cannot change or alter them. The key equations are reproduced in this section simply to outline the calculations that are occurring during simulation. Further details are provided in the current CMG STARS user manual.

The expression for reaction rate (gmole/m^3-day) is the following series of factors

$$\dot{g}_g = rrf * \exp(-\frac{eact}{TR}) * c(i)^{enrr(i)} * ..... * c(n)^{enrr(n)} \quad (1)$$

where, *rrf* is the reaction frequency factor (1/day), *eact* is the reaction activation energy (J/gmole), T is the temperature (K), $c(i)$=concentration factor contributed by reaction component *i (gmole/m^3)* and $enrr(i)$ is the order of reaction with respect to component *i*.

The concentration factor for component i in a fluid phase is usually based on density,

$$c(i)=\frac{\phi_f \rho_i S_i X_i}{M_i} \quad (2)$$

$$\phi_f = \phi_v \left(1 - \Sigma \frac{C_{ks}}{\rho_{sk}(p,T)}\right). \quad (3)$$

Here void porosity ϕ_v is corrected for pore pressure and temperature, and fluid porosity ϕ_f is corrected for the volume of the solid phase in the pore space. Each component *k* in the solid phase has concentration C_{ks} and density $\rho_{sk}(p,T)$.

When chemical reactions deviate from equilibrium,

$$c(i) = \frac{\phi_f \rho_i S_i (X_i - X_{eq})}{M_i} \quad (4)$$

As i=1,

$$\dot{g}_g = rrf * \exp\left(-\frac{eact}{TR}\right) \frac{\phi_f \rho_H S_H (X_H - X_{eq})}{M_H} . \quad (5)$$

The equilibrium value is the inverse of the K value from the Antoine correlation

$$K(p,T) = \left(\frac{rxk1}{p} + rxk2 * p + rxk3\right) \exp\left(\frac{rxk4}{T - rxk5}\right) \quad (6)$$

$$(X_H - X_{eq}) = \frac{\exp\left(\frac{rxk4}{T - rxk5}\right)}{rxk1} (p - p_{eq}) \quad (7)$$

$$\dot{g}_g = rrf * \exp\left(-\frac{\left(\frac{eact}{R} + rxk4\right)}{(T - rxk5)}\right) \frac{\phi \rho_H S_H}{M_H A} (p - p_{eq}) . \quad (8)$$

The kinetic rates of water production and hydrate decomposition are represented as:

$$\dot{g}_w = \dot{g}_g N_h \frac{M_w}{M_g} \quad (9)$$

$$\dot{g}_H = \dot{g}_g \frac{M_H}{M_g} . \quad (10)$$

The equilibrium pressure is calculated using:

$$p_{eq} = \exp\left(a + \frac{b}{T}\right) \quad (11)$$

where a and b are constants.

3.1.2 Flow Equations

The two-phase flow of gas and water, coupled with a change in hydrate saturation is represented by:

$$-\nabla \cdot \left(\rho_l \vec{u}_{lD}\right) + \dot{g}_{ml} + \dot{g}_l = \frac{\partial}{\partial t}\left(\phi \rho_l S_l\right) \quad (12)$$

(*l* represents phases with *g, w, H representing gas, water and hydrate; D* represents direction *r, z*) where,

$$\vec{u}_{lD} = -\frac{kk_{rl}}{\mu_l}\frac{\partial \Phi_l}{\partial D} \tag{13}$$

and *l* represents *g, w, H*; *D* represents *r, z*; $\dot{g}_{ml}$ is the sink due to production, $\dot{g}_l$ is the source term due to hydrate decomposition and Φ_l is the fluid potential of phase '*l*', defined as:

$$\Phi_l = p_l - \gamma_l z \cdot \tag{14}$$

(*l* represents *g, w*)

3.1.3 Permeabilities

There are no published data for relative permeabilities for hydrate zones. Hong and Pooladi-Darvish (2003) have modified models presented by Van Genuchten (1980) and Parker et al. (1987) to account for the hydrate phase:

$$k_{rw} = k_{rwo}\bar{S}_w^{1/2}\left[1-\left(1-\bar{S}_w^{1/m}\right)^m\right]^2 \tag{15}$$

$$k_{rg} = k_{rgo}\bar{S}_g^{1/2}\left[1-\left(1-\bar{S}_{wH}^{1/m}\right)^m\right]^{2m} \tag{16}$$

$$p_c = p_{co}\left[\left(\bar{S}_w\right)^{-1/m}-1\right]^{1-m} \tag{17}$$

where,

$$\bar{S}_w = \frac{S_w - S_{wr}}{1 - S_{wr} - S_{gr}} \tag{18}$$

$$\bar{S}_{wH} = \frac{S_w + S_H - S_{wr}}{1 - S_{wr} - S_{gr}} \tag{19}$$

$$\bar{S}_g = \frac{1 - S_w - S_H - S_{gr}}{1 - S_{wr} - S_{gr}} \tag{20}$$

and where P_{co} = 1kPa, m = 0.45, S_w = 0.3, S_{gr} = 0.05, k_{rwo} = 0.5 and k_{rgo} = 1.0.

3.2 Governing Equations Used in the STARS Model

There is one conservation equation for each chemical component plus equations to describe the phase equilibrium between the different phases. A set of these calculations is computed for each grid block, while further equations describe any injection and production wells.

3.2.1 Conservation Equations

All conservation equations are based on the control volume (V) within the region of interest. That is:

Rate of change of accumulation = net rate of inflow from adjacent region + net rate of addition due to sources and sinks

The accumulation term for a flowing component 'i' is:

$$V\frac{\partial}{\partial t}\left[\phi_f\left(\rho_w S_w w_i + \rho_o S_o x_i + \rho_g S_g y_i\right) + \phi_v A d_i\right] \tag{21}$$

The accumulation term for energy is:

$$V\frac{\partial}{\partial t}\left[\phi_f\left(\rho_w S_w U_i + \rho_o S_o U_i + \rho_g S_g U_i\right) + \phi_v + \left(1 - \phi_v\right)U_r\right] \tag{22}$$

where U_j (j = w, o, g) is the internal energy as a function of temperature and phase composition and ρ are the fluid phase densities. U_r is energy per rock volume.

3.2.2 Flow Terms

The flow term of a flowing component 'i' between two regions is:

$$\rho_w V_w w_i + \rho_o V_o x_i + \rho_g V_g y_i + \phi\rho_w D_{wi}\Delta w_i + \phi\rho_g D_{gi}\Delta y_i + \phi\rho_o D_{oi}\Delta x_i \quad (23)$$

D_{ji} are the component dispersibilities in the three phases e.g. D_{wi} is the dispersibility of component i in water phase and V_j is the volumetric flow rate of various phases given by equation 25. The variables w_i, y_i and x_i are the mole fractions of component i in water, vapor and liquid phases, and ρ_j represents density of each phase. Thus, equation 23 gives the mass flow rate of component i in all the phases.

The flow of energy is represented by:

$$\rho_w V_w h_w + \rho_o V_o h_o + \rho_g V_g h_g + K\Delta T . \quad (24)$$

The volumetric flow rates are calculated by:

$$V_j = T\left(\frac{k_{rj}}{\mu_j r_j}\right)\Delta\Phi_j \quad (25)$$

where, *'T'* is the transmissibility between grid blocks, and *k* is the thermal transmissibility of the interface between the two blocks.

3.2.3 Chemical Reaction, Interface Mass Transfer Source/Sink Terms

The expression for the reaction for component 'i' source/sink is:

$$V\sum_{k=1}^{n_r}\left(s'_{ki} - s_{ki}\right)\bullet r_k \quad (26)$$

and the reaction source/sink for energy is:

$$V \sum_{k=1}^{n_r} H_{rk} r_{rk} \tag{27}$$

where: s'_{ki} is the product stoichiometry coefficient of component i in reaction k. s_{ki} is the reaction stoichiometry coefficient of component i in reaction k. H_{rk} is the enthalpy of reaction k. rk is the volumetric rate of reaction k, calculated from a model for reaction kinetics in STARS.

3.2.4 Heat Loss Source/Sink Terms

The energy source/sink is calculated by:

$$\sum_{k=1}^{n_r} HL_k + HL_v + HL_c \tag{28}$$

where, HL_k is the rate of heat transfer to the region of interest through block face number k, from the adjacent formation. If calculating heat transfer between the reservoir and overburden, the dimensions of the overburden are considered infinite. HL_v is the rate of heat transfer, calculated from a convective model. HL_c represents a constant heat transfer model. These values are calculated in STARS.

3.2.5 Phase Equilibrium Relationships

Phase mole fractions are related by the equilibrium ratios, also known as K values.

$$\begin{aligned} y_i &= K_i^{go} x_i \;;\; x_i = K_i^{og} y_i \\ x_i &= K_i^{ow} w_i \;;\; w_i = K_i^{wo} x_i \\ w_i &= K_i^{wg} y_i \;;\; y_i = K_i^{gw} w_i. \end{aligned} \tag{29}$$

For three phases, in reality, only two of the K values are independent.

Phase pressures and saturations are constrained by:

$$Sw + So + Sg = 1$$
$$pw = po - pcow(Sw) \quad (30)$$
$$pg = po + pcog(sg)$$

where, *pcow* is the water-oil (hydrate) capillary pressure and *pcog* is the gas-oil (hydrate) capillary pressure.

3.3 Gas Production due to Hydrate Dissociation - Analytical Model

Considering the Stefan model assumption, an analytical model is developed to predict the decomposition of gas hydrate in porous media. This model gives a quick estimation of hydrate reservoir analysis without using any empirical correlation.

In this study the decomposition of methane hydrate in a reservoir due to depressurization is considered. When pressure is lowered or temperature is raised, methane hydrate decomposes to give methane and water, i.e.,

$$CH_4 \,.\, 6H_2O \rightarrow CH_4 + 6H_2O. \quad (31)$$

It is assumed that there is a natural gas hydrate reservoir containing solid hydrate and excess natural gas at the initial reservoir pressure P_{in} and temperature T_{in} that occupies the semi-infinite region $r_o < r < \infty$. At this pressure and temperature hydrate is stable before drilling. After a well (of radius r_o) is drilled into the reservoir, the pressure in the well can be set to a constant well pressure, P_G, below the dissociation pressure p_D at the dissociation temperature, T_D. Hydrate dissociation commences and, as a result, there is a moving interface at some distance, $r = R(t)$, which separates the water /gas region from the non-dissociated hydrate zone. Thus at any time, $t > 0$, the water/gas phase (dissociated hydrate zone) occupies the region, $r_o < r < R(t)$ while the non-dissociated hydrate zone occupies the region, $R(t) < r < \infty$ these regions are designated as I and II, respectively.

Pressures and temperatures gradually decrease, and the natural gas moves towards the well because of the pressure gradient, while the decomposition front moves away from the well.

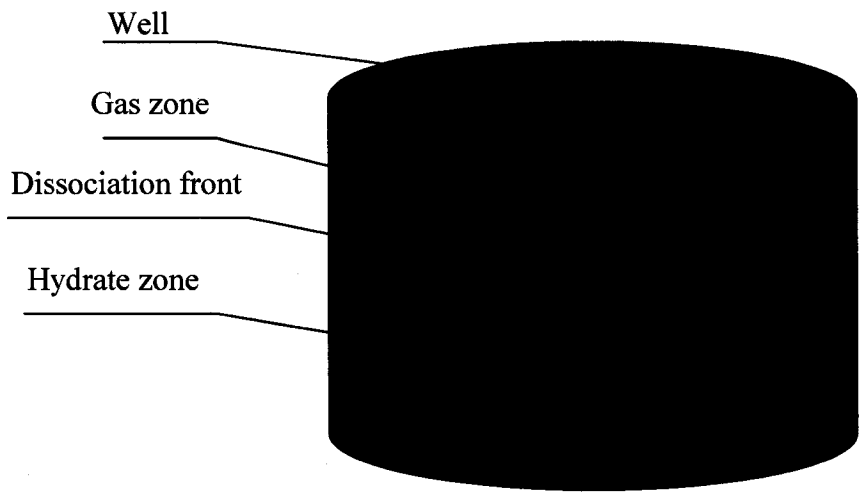

Figure 3.1 Schematic Representation of the Hydrate Reservoir for the Axisymmetric Model

3.4 Assumptions of the Analytical Model

- Darcy's law applies to flow of gas through the decomposed region. Darcy's law is widely used to describe flow through a broad range of porous media. To make the problem more tractable, we assume that the liquid, gas and methane hydrate are in chemical equilibrium. That is, kinetics of the phase transition between hydrate and water plus methane is ignored. The hydrate reservoir is homogenous and semi-infinite. Movement of water in the porous medium is negligible. Diffusion of methane gas in gas hydrate and free gas phases is negligible. Dissociation pressure, p_D and dissociation temperature, T_D, is assumed to be constant at the interface at all times for given specific conditions.
- The conductive heat transfer is neglected compared to the convective heat transfer.

- Gas is only in gaseous and hydrate states; water is only in liquid and hydrate states, i.e., ice and vapor do not form.
- Variations in potential and kinetic energy are considered negligible compared to the variation in thermal energy.

3.5 Mathematical Model

The mathematical formations suggested by Makogon (1997) are summarized in this section. For the hydrate reservoir with a single production well at the center as shown in Figure 3.1, the differential mass, momentum and energy balances describing the dissociation process may be written as follows.

$$\Phi_1 = (1 - S_W)\Phi, \tag{32}$$

$$\Phi_2 = (1 - S_H)\Phi, \tag{33}$$

$$\frac{k_n}{2\phi_n \mu}\left(\frac{\partial^2 p_n^{\,2}}{\partial r^2} + \frac{1}{r}\frac{\partial p_n^{\,2}}{\partial r}\right) = \frac{\partial p_n}{\partial t} \tag{34}$$

$$\frac{a_n}{r}\frac{\partial}{\partial r}\left(r\frac{\partial T_n}{\partial r}\right) = \frac{\partial T_n}{\partial t} - \frac{c_v k_n}{c_n \mu}\frac{\partial p_n}{\partial r}\left(\frac{\partial T_n}{\partial r} + \delta\frac{\partial p_n}{\partial r}\right) - \frac{\phi_n c_v \eta}{c_n}\frac{\partial p_n}{\partial t} \tag{35}$$

where, n=1 corresponds to region, ro < r < R(t), n =2 correspond to region, R(t) < r < ∞. The mass balance for gas at the decomposition front, R(t), is:

$$v_1(R,t) - v_2(R,t) = -[\varepsilon S_H \frac{\rho_3 p_0 T_D}{\rho_0 p_D T_0} z - (S_H - S_W)]\Phi\frac{\partial R}{\partial t}. \tag{36}$$

The relation between pressure p_D and temperature T_D on the decomposition front is

$$\log_{10} p_D = a(T_D - T_0) + b(T_D - T_0)^2 + c. \quad (37)$$

The corresponding boundary conditions are:

$p_1 (r_0,t) = p_G$ (38)

$p_2 (\infty,t) = p_2 (r,0) = p_e$ (39)

$T_2 (\infty,t) = T_2 (r,0) = T_e$ (40)

$p_1 (R(t),t) = p_2 (R(t),t) = p_D$ (41)

$T_1 (R(t),t) = T_2 (R(t),t)$. (42)

The mass balance for gas at the decomposition front, R(t), is:

$$k_1 \frac{\partial p_1(R,t)}{\partial r} - k_2 \frac{\partial p_2(R,t)}{\partial r} = (\varepsilon\beta z \frac{\rho_3 p_o T_D}{\rho_o p_D T_o} - (\beta - \alpha))\Phi\mu \frac{\partial R}{\partial t}. \quad (43)$$

The mass balance equation for water is given as

$$S_W = \frac{(1-\varepsilon)\rho_3 S_H}{\rho_W}. \quad (44)$$

3.6 Derivation of Analytical Solution

The mathematical formulation discussed in Section 3.5 is linearized and a self-similar solution is developed in this section following a procedure suggested by Ji et al. (2001). Using the approximation:

$$\frac{\partial p_1^2}{\partial t} \approx 2p_D \frac{\partial p_1}{\partial t}, \frac{\partial p_2^2}{\partial t} \approx 2p_e \frac{\partial p_2}{\partial t} \quad (45)$$

eq. (34) may be linearized as

$$\frac{\partial p_n^2}{\partial r^2}+\frac{1}{r}\frac{\partial p_n^2}{\partial r}=\frac{1}{\chi_n}\frac{\partial p_n^2}{\partial t} \tag{46}$$

where,

$$\chi_1=\frac{k_1 p_D}{\mu\Phi_1}, \chi_1=\frac{k_2 p_e}{\mu\Phi_2}. \tag{47}$$

Self-similar solutions of Eq. (46) with given boundary conditions are given as

$$p_1^2=p_D^2-(p_D^2-p_G^2)\frac{(E_i(-\lambda_1^2)-E_i(-\alpha_1^2))}{(E_i(-\lambda_1^2=0)-E_i(-\alpha_1^2))} \tag{48}$$

$$p_2{}^2=p_e{}^2+\left(p_D{}^2-p_e{}^2\right)\frac{E_i(-\lambda_2{}^2)}{E_i(-\alpha_2{}^2)}\ . \tag{49}$$

Neglecting the conductive heat transfer compared to convective heat transfer in the porous medium, Eq. (35) becomes

$$\frac{\partial T_n}{\partial t}=\frac{c_v k_n}{c_n\mu}\frac{\partial p_n}{\partial r}\left(\frac{\partial T_n}{\partial r}-\delta\frac{\partial p_n}{\partial r}\right)+\frac{\phi_n c_v\eta}{c_n}\frac{\partial p_n}{\partial t}. \tag{50}$$

Solutions to the linearized form of Eq. (50) satisfying the boundary conditions are given as:

$$T_1=T_D+A_1\delta\left(E_i(-\lambda_1{}^2)\right)-E_i(-\alpha_1{}^2)+\left(\frac{\eta B_1}{\delta}-1\right)(\psi_1(-\lambda_1{}^2)-\psi_i(-\alpha_1{}^2)) \tag{51}$$

$$T_2=T_e+A_2\delta(E_i(-\lambda_2{}^2)-\left(\frac{\eta B_2}{\delta}-1\right)\psi_2\left(-\lambda_2{}^2\right) \tag{52}$$

$$E_i(-\lambda_1^{\,2} = 0) = -\int_0^{\infty} \frac{e^{-u}}{u} du \tag{53}$$

$$\psi_1(\zeta) = \int_0^{\zeta} \frac{e^{-u}}{u + C_1 e^{-u}} du \tag{54}$$

$$\psi_2(\zeta) = \int_0^{\zeta} \frac{e^{-u}}{u + C_2 e^{-u}} du \tag{55}$$

where,

$$R(t) = \sqrt{\gamma \bullet t} \tag{56}$$

$$E_i(-\zeta) = -\int_{\zeta}^{\infty} \frac{e^{-u}}{u} du \tag{57}$$

$$A_1 = \frac{(p_G^{\,2} - p_D^{\,2})}{2p_c(E_i(-\lambda_1^{\,2} = 0) - E_i(-\alpha_1^{\,2}))} \tag{58}$$

$$A_2 = \frac{(p_e^{\,2} - p_D^{\,2})}{2p_e E_i(-\alpha_2^{\,2})} \tag{59}$$

$$B_1 = \frac{c_v \Phi_1}{c_1} \tag{60}$$

$$B_2 = \frac{c_v \Phi_2}{c_2} \tag{61}$$

$$C_1 = \frac{c_v k_1 (p_G{}^2 - p_D{}^2)}{2\mu x_1 c_1 p_G . (E_i(-\lambda_1{}^2 = 0) - E_i(-\alpha_1{}^2))} \tag{62}$$

$$C_2 = \frac{c_v k_2 (p_e{}^2 - p_D{}^2)}{2\mu x_2 c_2 p_e E_i(-\alpha_2{}^2)} \tag{63}$$

$$\lambda_n = \frac{r}{2\sqrt{x_n . t}} \tag{64}$$

$$\alpha_n = \sqrt{\frac{\gamma}{4.x_n}} . \tag{65}$$

The values of pressure p_D and temperature T_D at the interface, and the constant γ, which determines the motion of the decomposition front, are calculated for a given set of conditions. From the evaluation of Eq. (55) at the decomposition front (i.e. $\lambda_2 = \alpha_2$), it follows that:

$$\Psi_2(\xi)\ T_D = T_e + A_2 \delta (E_2(-\alpha_2^2) - (\frac{\eta B_2}{\delta} - 1)\Psi_2(-\alpha_2^2)) . \tag{66}$$

The mass balance equation at the front becomes:

$$2k_1((p_G^2 - p_D^2)\frac{e^{-\alpha_1^2}}{(E_i(-\lambda_1^2 = 0) - E_i(-\alpha_1^2))}) + 2k_2((p_e^2 - p_D^2)\frac{e^{-\alpha_2^2}}{E_i(-\alpha_2^2)}) = A\gamma \tag{67}$$

$$A = (\varepsilon\beta z \frac{\rho_3 p_o T_D}{\rho_o T_0} - (\beta - \alpha) p_D)\Phi\mu .$$

The equilibrium pressure p_D and the equilibrium temperature T_D are related through:

$$\log_{10} p_D = a(T_D - T_0) + b(T_D - T_0)^2 + c. \tag{68}$$

For the analytical solution, equations 34, 35 and 36 represent heat, momentum transfer equations and interface conditions. These equations were solved to provide the gas flux of methane, location of the dissociation front, and the temperature profiles across the reservoir. These values were used to predict total production of methane. Various boundary conditions were changed to see the effect of reservoir parameters and operating conditions. The results are given in section 5.5.

CHAPTER FOUR
PHYSICAL PROPERTIES OF THE MODEL

4.1 Model 1: Hydrate Layer and Free Gas Zone

Numerical studies were carried out for gas recovery from a hypothetical formation model containing gas hydrates. Table 4.1 outlines the basic geologic characteristics of the hydrate formations. The hydrate zone is characterized by a 4 mile length and 1 mile width, which is of variable hydrate thickness and depth. The hydrate accumulation is adjacent to a free gas zone. The hydrate layer and free gas zone are bounded by a tight and relatively thick mud/silt formation (100 m) that acts as a no-flow boundary. A constant porosity of 36% is used and the absolute permeability is set at 300 md (personal communications with USGS staff). If it is assumed that the un-dissociated hydrate is impermeable, the variation in depth of the reservoir implies that the pressures and temperatures within the formation will vary. The corresponding initial pressure and temperature for each grid block were determined by hydrostatic pressure and a given geothermal gradient. A water saturation of 20% was chosen throughout the reservoir. Gas hydrate saturation in the initial gas hydrate zone is 74% and is zero elsewhere. The gas hydrate zone has 6% methane gas saturation, while in the free gas zone there is a gas saturation of 80%. A simulation block is represented in Figure 4.1.

A grid was constructed with a grid block size of 50x50 meters. The block thicknesses were varied from 1 meter (thick portion of the reservoir) to 0.156 meters (thin portion of the reservoir). In addition, 2 degree dip was built into the model to resemble the Alaska North Slope reservoir. A grid of 128 blocks in the "I" direction, 32 in the "J" direction and 20 in the "K" direction comprising 81,920 blocks in total is used.

The total initial components in place are listed in Table 4.2. A well was drilled and completed in the free gas zone. The initial maximum flow rate used is 707921 m^3/day with a minimum bottom hole pressure (BHP) of 2068 KPa (~ 300 psi).

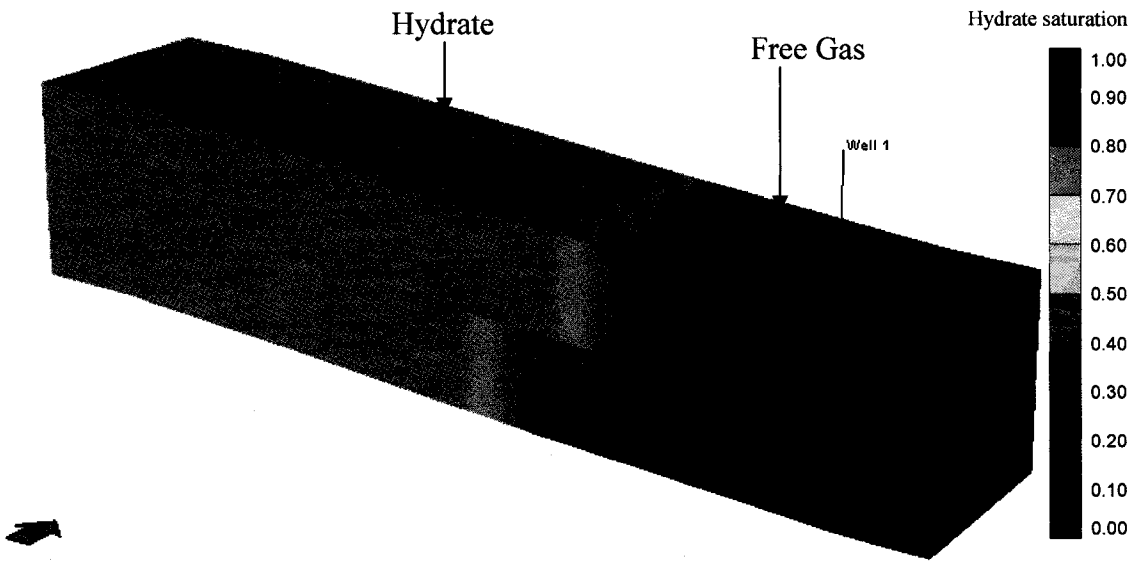

Figure 4.1: Simulation Grid

Recognizing the symmetry of the system, it was decided to simulate half the fault block, i.e. split the block vertically down the middle. A number of simulations were completed that used two wells in the fault block (a single well in the simulation). Two wells were placed immediately adjacent to the hydrate-gas interface, equally spaced along the grid block. In the split reservoir simulation, only one well was modeled, and the output was represented per well. The base case run used the values given in Table 4.2. An absolute permeability of 300 md was assigned to the reservoir rock and each well had a maximum flow rate of 25 mmscfd (707921 m^3/d) resulting in an overall peak production rate of 50 mmscfd. The time of the simulation was 15 years.

Table 4.1: Component Thermal Properties

Reservoir Rock Heat Capacity	2.347E+06 J/m^3-C
Reservoir Rock Conductivity	1.496E+05 J/m-day-C
Water Conductivity	5.35E+04 J/m-day-C
Hydrate Conductivity	1.653E+06 J/m-day-C
Gas Conductivity	7400 J/m-day-C
Surrounding Rock Heat Capacity	2.347E+06 J/m^3-C
Surrounding Rock Conductivity	1.496E+05 J/m-day-C
Hydrate density	7696 (gmole /m^3)
Heat of hydrate decomposition	51857.93 J/gmole
a for the calculation of CH_4 stability	38.98
b for the calculation of CH_4 stability	-8533.8

Table 4.2: Base Case Parameters

Porosity of hydrate layer	36%
Permeability of hydrate layer	300md
Porosity of underburden & overburden	0.01%
Permeability of underburden & overburden	0.001md
Hydrate Saturation	0.74
Gas Saturation (hydrate zone)	0.06
Gas Saturation (gas zone)	0.8
Water Saturation	0.2
Max. Well Flow Rate	$7.08*10^5$ (scmd)
Total initial components in place (methane)	$1.82*10^9$ (m^3)
Total initial components in place (hydrate)	$3.25*10^7$ (m^3)
Total initial components in place (water)	$1.33*10^7$ (m^3)

4.2 Model 2: Hydrate Layer and Aquifer

A conceptual reservoir model was used and numerical simulation studies were carried out for natural gas production from a hypothetical gas hydrate formation. Figure 4.2 shows the hypothetical model of formation. Basic geologic characteristics of the hydrate formations are listed in Patil and Nanchary (2005) and Howe et al. (2004). We assume the hydrate layer is 16 m thick, extends from –905 m to –921 m, and is underlain by a 2 m thick water saturated layer. The hydrate layer and the aquifer are bounded by a tight and relatively thick mud/silt formation that acts as a no-flow boundary. At the bottom of the hydrate layer, the pressure is 9 MPa and the temperature is 7.5 °C. The hydrate and

water saturations in the hydrate interval are 0.6 and 0.4 respectively; and they are 0 and 1 in the other formations. Table 4.1 shows the primary properties of the model. The thermal conductivity, density and compressibility of the hydrate formation are assumed to be similar to those of the mud/silt formation. The top and bottom silt formations are assumed to extend uniformly over the hydrate interval and act as a heat source for hydrate dissociation. A constant hydrate number of 5.75 is used for the hydrate property. The initial gas volume in place in the hydrate layer is about $5.7\times10^6\ m^3$ at STP. If it is assumed that the un-dissociated hydrate is impermeable, the variation in depth of the reservoir implies that the pressures and temperatures within the formation will vary. The corresponding initial pressure and temperature for each grid block were determined by the hydrostatic pressure and the known geothermal gradient. There are no published data for relative permeabilities for hydrate zones. Relative permeabilities and capillary pressures were computed from the modified models presented by Van Genuchten (1980) and Parker et al. (1987), to account for the hydrate phase. Details of the derivation and the complete set of equations describing the process of hydrate decomposition are presented in (Patil and Nanchary, 2005). Three production schemes of depressurization, heated well and hot water injection were tested. The initial base case run has a single production well drilled at the center of the hydrate formation, perforated almost the entire depth of the reservoir. The initial maximum flow rate used is 7079.21 m^3/day with a minimum bottom hole pressure (BHP) of 2068 KPa (~ 300 psi). The BHP is based on the minimum pressure required for the gas to flow through the 24" pipeline to the separation plant. In hot water injection, four injecting wells were drilled at four corners of the simulation block. The hot water was injected at low rates to avoid possible fracturing of the bounding formations and cavitation.

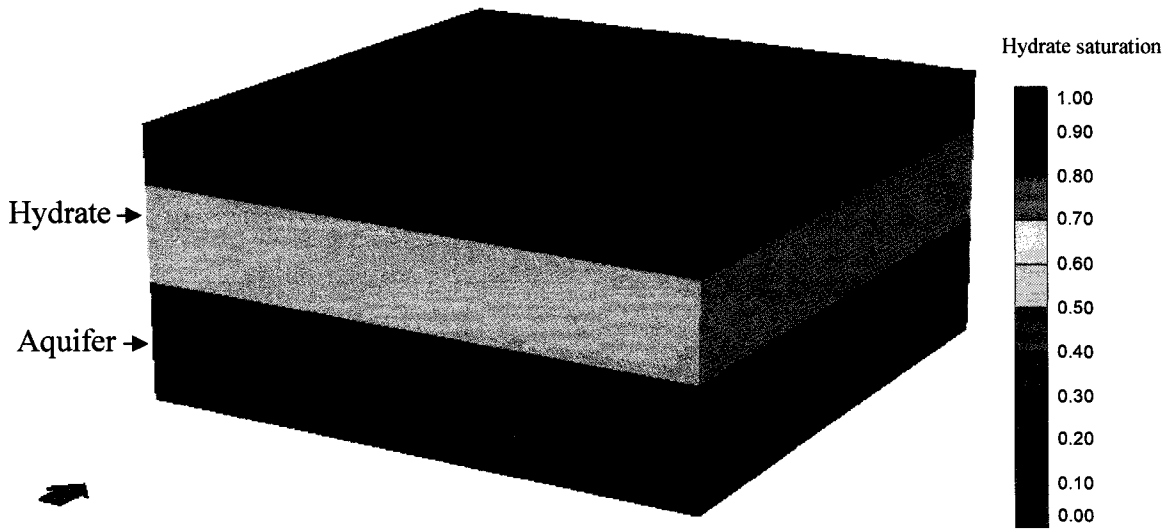

Figure 4.2: Hypothetical Model of Formation

4.3 Description of Scenario - Steam Injection

At present, a full, detailed reservoir characterization does not exist for the Alaska North Slope Hydrate reservoir. However, work has been conducted by others to analyze existing well logs. Collett (1993) outlined the basic geologic characteristics of the formations. These parameters are listed in Table 4.1. In the absence of other data, a broadly representative simulation has to be developed to capture the key parameters.

The hydrate zone is characterized by approximately 1.25 mile length and 0.8 mile width. The simulation block is of variable hydrate thickness and depth. The hydrate interval has a free gas zone and the simulation block ends with a thick water saturated zone. The depth to the center of the top face of the grid block in the top layer is 967 m and the bottom of the hydrate accumulation is marked at 1214 m. A constant porosity of 36% is used, and the absolute permeability is set at 300 md. The permeabilities in the Y and Z direction are assumed to be equal to the permeability in the X direction.

The rock thermal properties are based on default values suggested for fluid flow modeling using CMG STARS (CMG STARS User's Guide, 2003). Relative permeability calculations for hydrates have not been published to date. The values used in the model are illustrated in Section 2.1.3. If it is assumed that the un-dissociated hydrate is impermeable, the variation in depth of the reservoir implies that the pressures and temperatures within the formation will vary. A water saturation of 20% was chosen throughout the reservoir except in water-saturated zone. Gas hydrate saturation in the initial gas hydrate zone is 70% and is zero elsewhere. The gas hydrate zone has 10% methane gas saturation, while in the free gas zone there is a gas saturation of 80%. A hypothetical model for this scenario is shown in Figure 4.3.

Figure 4.3 represents a hypothetical reservoir in which representative properties of hydrate reservoirs are used with the data available in the literature. The properties used are shown in Table 4.3. Figure 4.3 represents the initial condition of the reservoir and the location of the production well. At time zero of the simulation, the block contains 2.258 million cubic meters of initial free gas in the gas zone and 99.5 million cubic meters of initial gas in hydrate zone measured at surface conditions. Total initial components in place for this case are listed in Table 4.3. A well was drilled and completed in the free gas zone. The initial maximum flow rate used is 283168.5 m^3/day (10 mmscfd), with a minimum bottom hole pressure (BHP) of 2068 kPa (~ 300 psi).

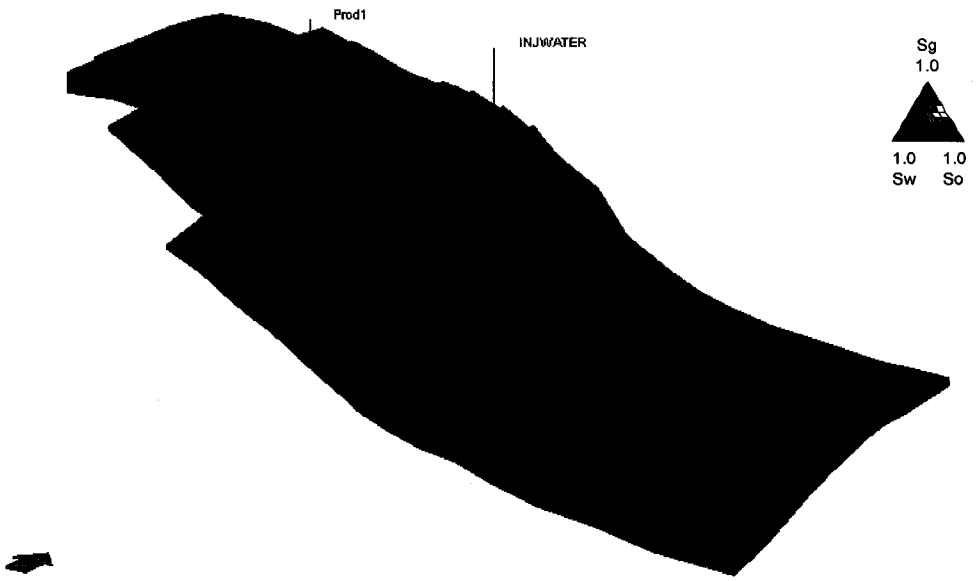

Figure 4.3: Hypothetical Model of Hydrate Formation (Steam)

Table 4.3: Base Case Parameters (Steam Case)

Reservoir Characterization	
Porosity	36%
Permeability	300md
Hydrate Saturation	0.7
Gas Saturation (hydrate zone)	0.1
Gas Saturation (gas zone)	0.8
Water Saturation	0.2
Max. Well Flow Rate	10 mmscfd
Total initial components in place (methane)	$2.77*10^8$ (m^3)
Total initial components in place (hydrate)	$5.47*10^6$ (m^3)
Total initial components in place (water)	$4.93*10^6$ (m^3)

CHAPTER FIVE
RESULTS AND DISCUSSION

This chapter presents results obtained from the modified CMG STARS simulator and the analytical model. Several scenarios of gas production from the hydrate reservoir were considered. The scenarios considered here are depressurization, depressurization with heating of wells, hot water injection, and steam injection. The chapter also discusses energy efficiency ratio, which assesses the effectiveness of thermal stimulation techniques. In addition, results from the sensitivity analysis of the axisymmetric model are presented.

Section 5.1 describes the results obtained by CMG STARS simulator for the production of methane from reservoir described in Section 4.1, by the depressurization technique. The reservoir considered in this case has a hydrate layer and a free gas zone but no aquifer. Section 5.2 presents the results obtained by the depressurization technique. However, the geometry considered here is described in Section 4.2. The simulations were performed using the CMG STARS simulator. The reservoir considered in this case has a hydrate layer, a free gas zone and an aquifer. The objective was to observe the effect of an aquifer on the gas production. Other reservoir properties were kept same as in Section 5.1.

5.1 Model 1: Depressurization (with free gas zone)

Figure 5.1 shows the gas production profile output from the simulation. The production plateaus at a rate of 50 mmscfd for over two years. The main contributor during the plateau is likely to be the free gas and when this is depleted, the rate quickly diminishes. After the initial rapid decline from the plateau rate, the production rate declines more gradually, as the dissociation of the hydrate supports production. Figure 5.2 displays the cumulative gas production with simulation time. The contribution of gas from the free

gas zone and the reservoir is illustrated. At the end of a 15-year production period, 36% of the gas initially in place has been recovered. The large quantities of water produced during hydrate dissociation will drain to the bottom of the reservoir and as such, quantities of produced water will be low. Figure 5.3, showing the produced water profile appears to indicate that this is the case.

WBHP and well block pressure are shown in Figures 5.4 and 5.5. Pressure profiles with time are shown in Figures 5.6 through 5.9. Temperature, hydrate saturation and water saturation profiles are shown in the following figures.

Recognizing that at the end of a 15-year production period only 36% (approximately) of the gas initially in place has been recovered, an extended 30-year production simulation of the base case was performed. At the end of the simulation, the total cumulative production was 54% of the initial gas potential in place.

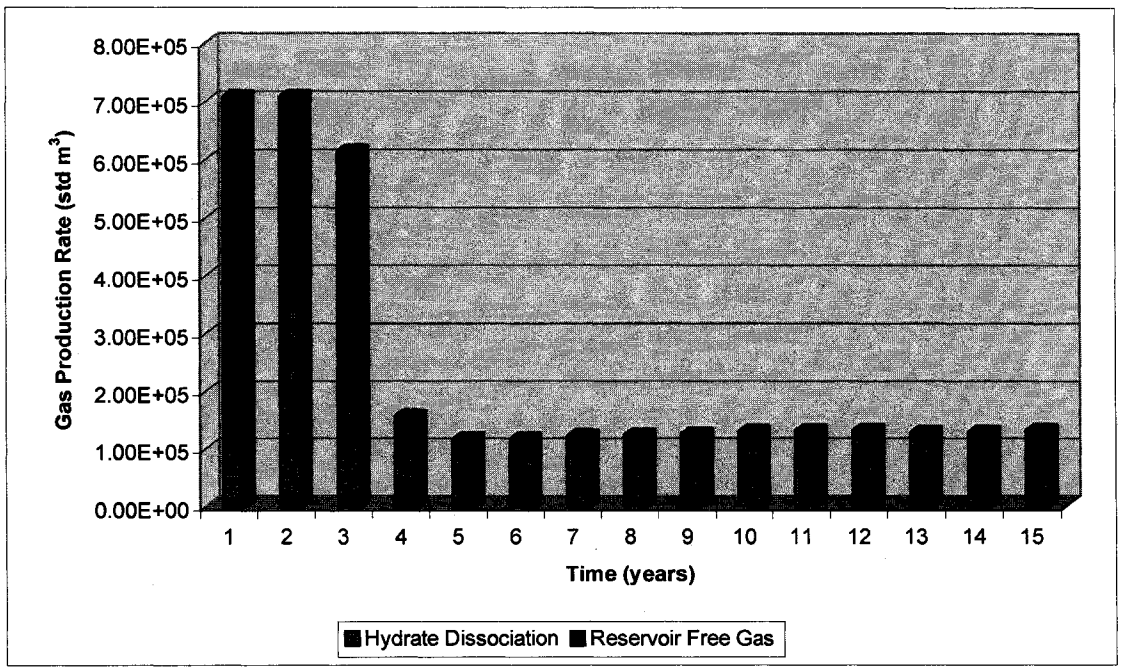

Figure 5.1: Components of Reservoir Voidage

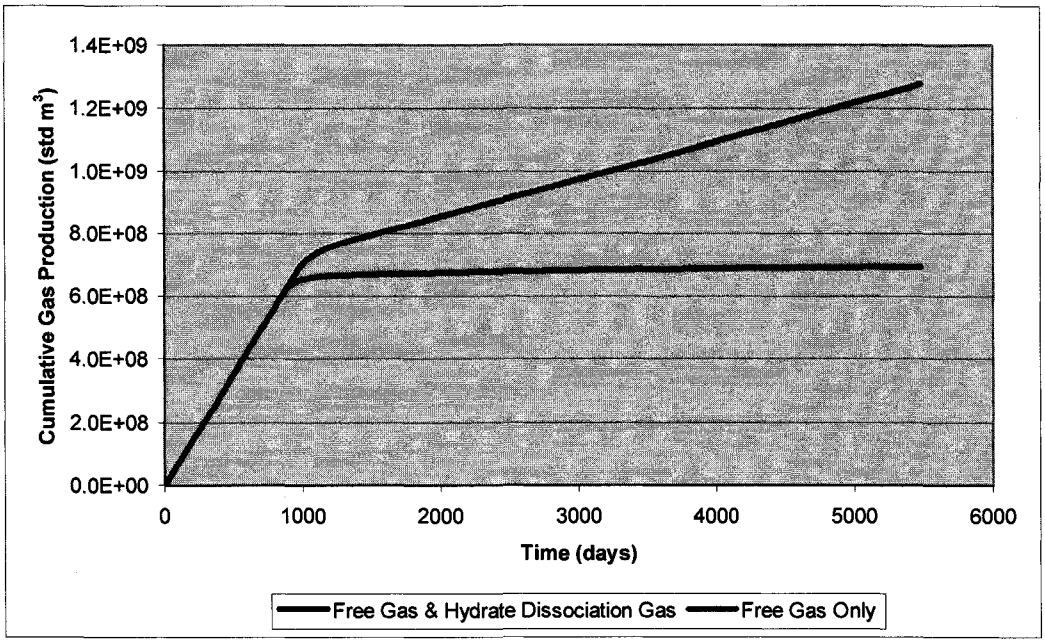

Figure 5.2: Cumulative Gas Production vs. Time

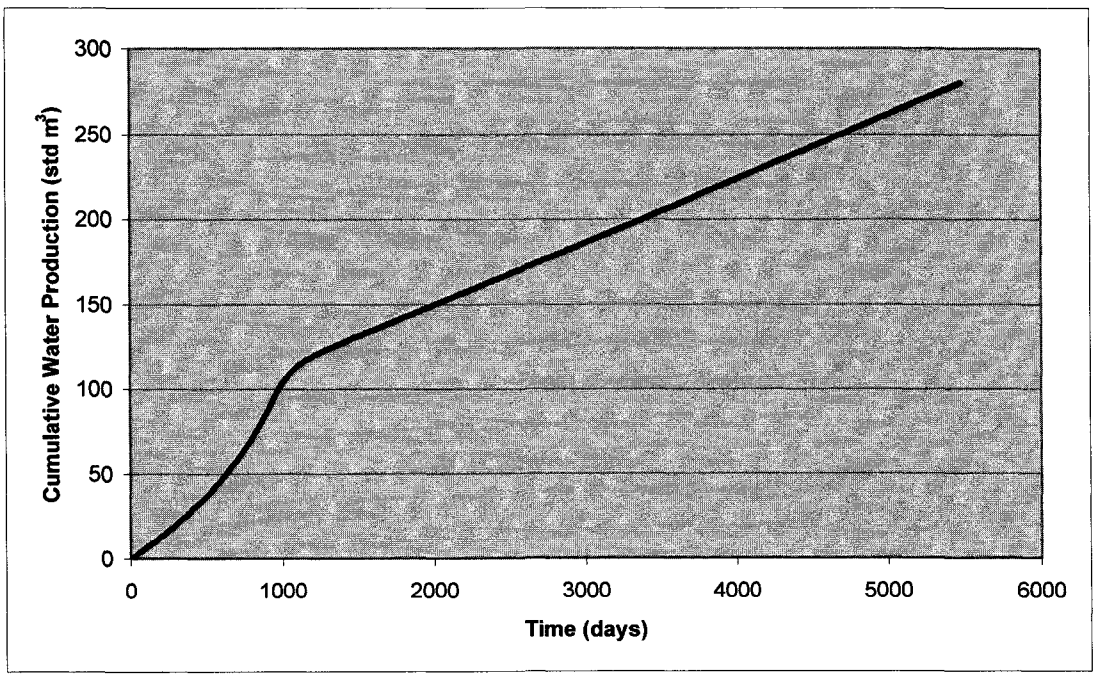

Figure 5.3: Cumulative Water Production vs. Time

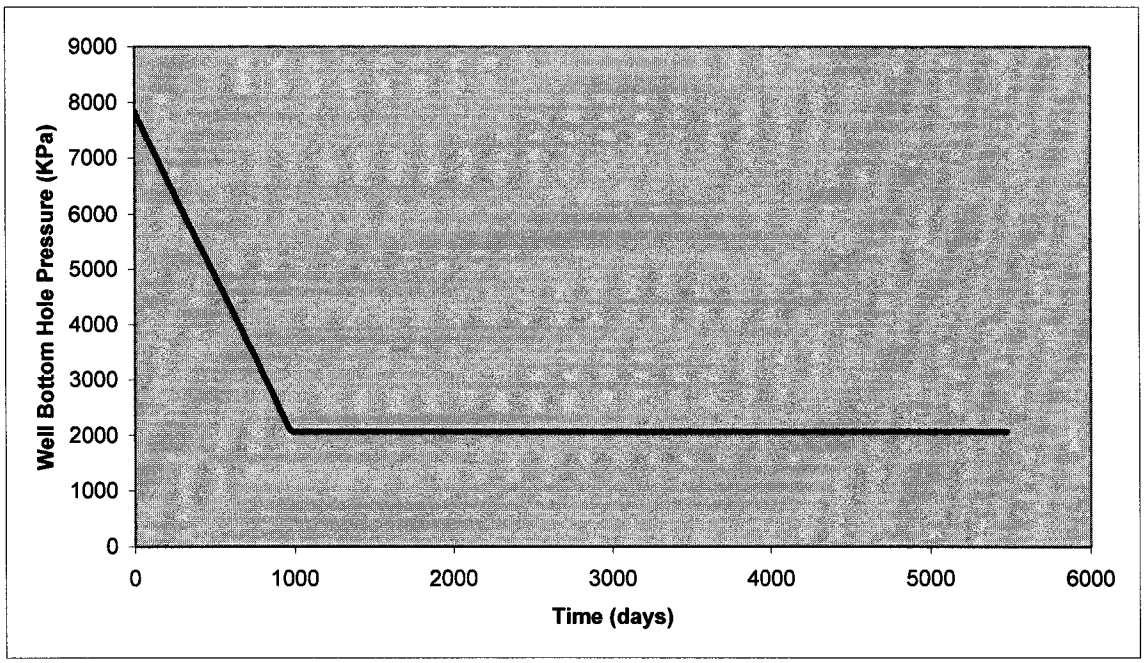

Figure 5.4: Well Bottom Hole Pressure vs. Time

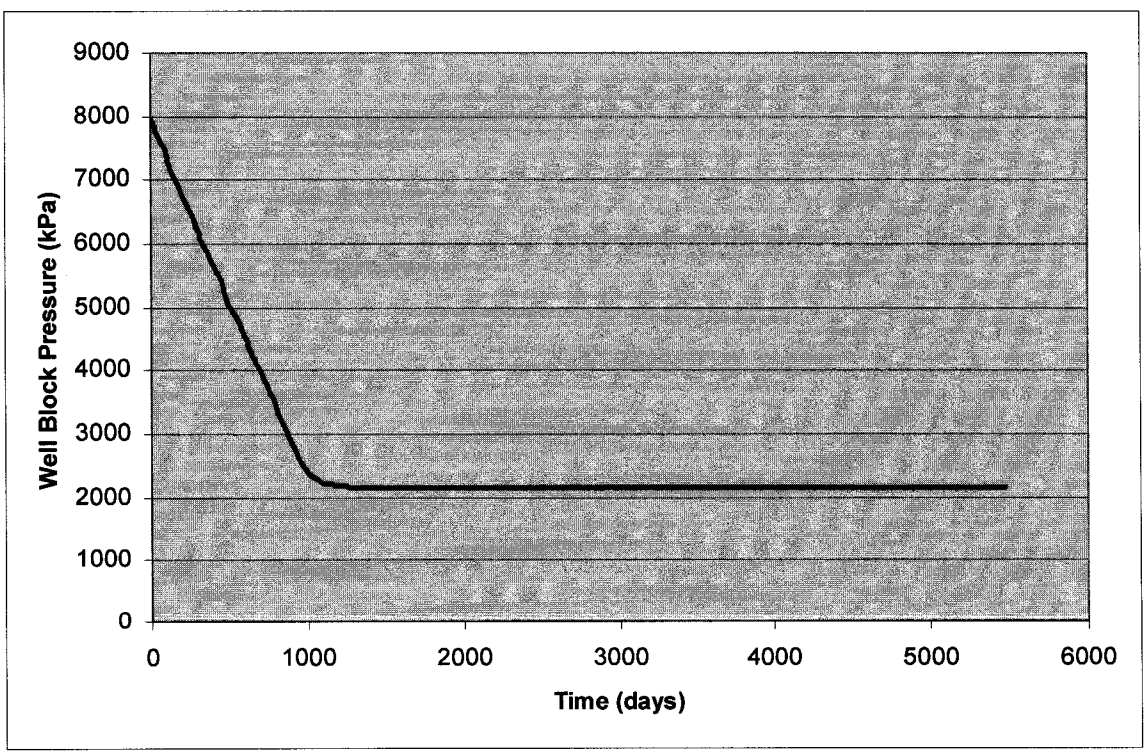

Figure 5.5: Well Block Pressure vs. Time

Effect on pressure:

Initial pressure conditions in the reservoir are shown in Figure 5.6. It can be seen that initially the pressure near the production well is close to 8000 kPa. The flowing bottom hole pressure was maintained constant at a value of 2068 kPa. It can be observed from Figure 5.5 that approximately three years into production the pressure near the production well approaches the flowing bottom hole pressure. In future years, as hydrates are dissociated and the dissociated gas is being produced, the pressure in the reservoir is fairly constant due to the recharge phenomenon. The same conclusion can be drawn from Figures 5.8 and 5.9. As expected, a significant part of the reservoir is closer to the bottom hole pressure at the end of simulation (Figure 5.9) than at 3 years (Figure 5.7) and 10 years (Figure 5.8).

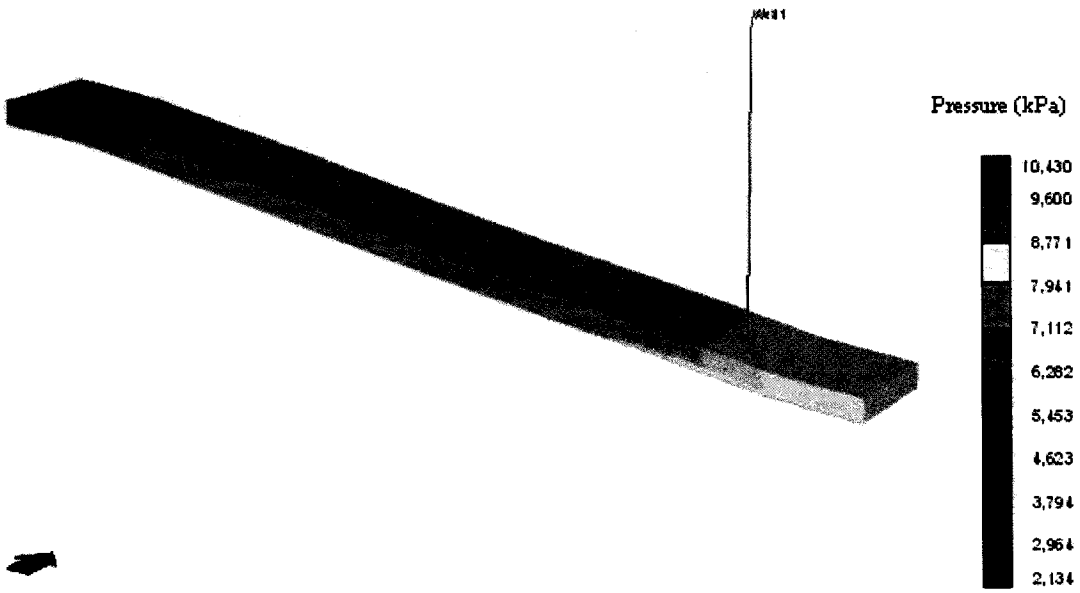

Figure 5.6: Pressure at the Start of the Simulation

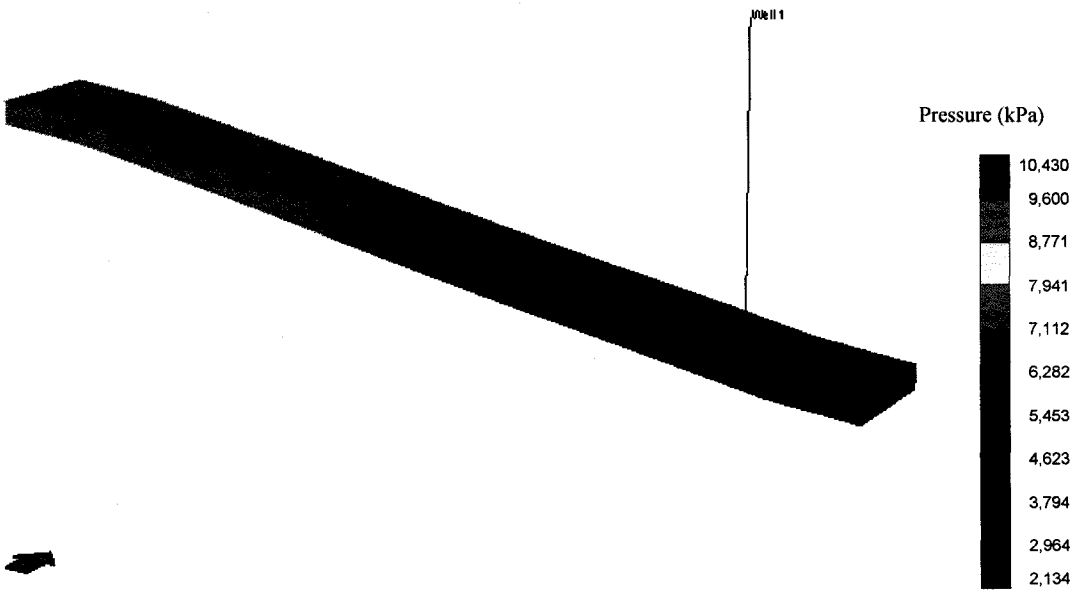

Figure 5.7: Pressure after Three Years of Simulation

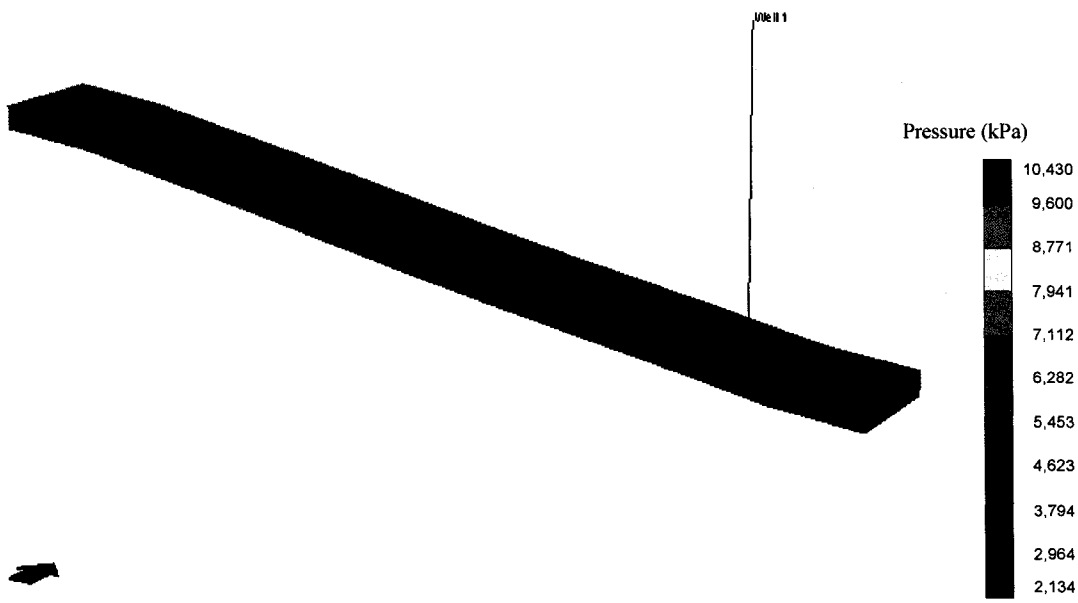

Figure 5.8: Pressure after Ten Years of Simulation

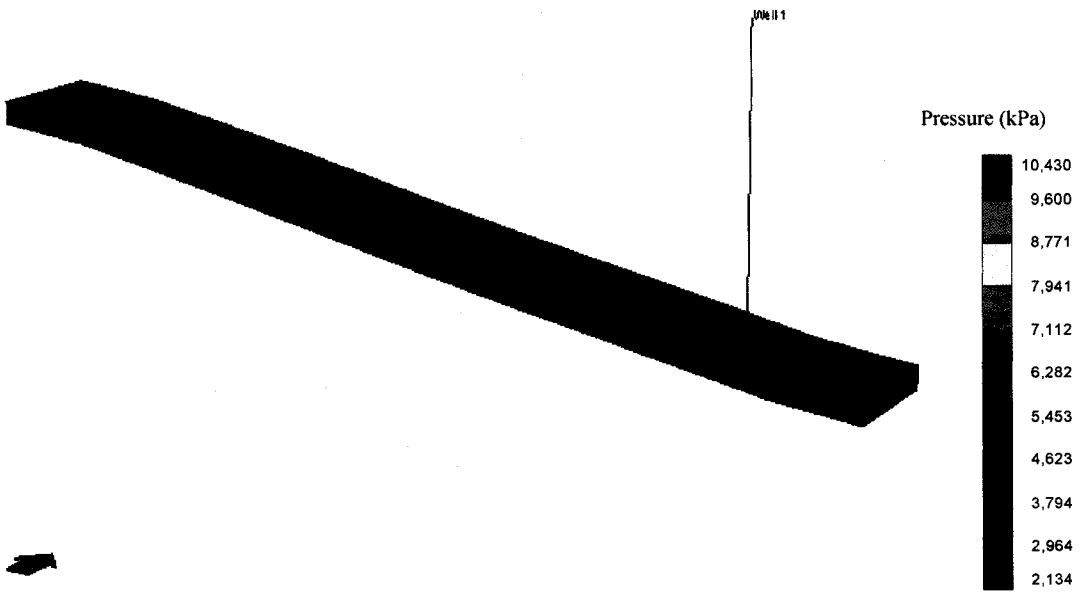

Figure 5.9: Pressure at the End of Simulation

Effect on temperature:

Initial temperature conditions in the gas hydrate reservoir are shown in Figure 5.10. It can be seen that the temperature near the production well is close to 22 °C and farther from the well; the temperature is lower and ranges from 22 °C to 17 °C.

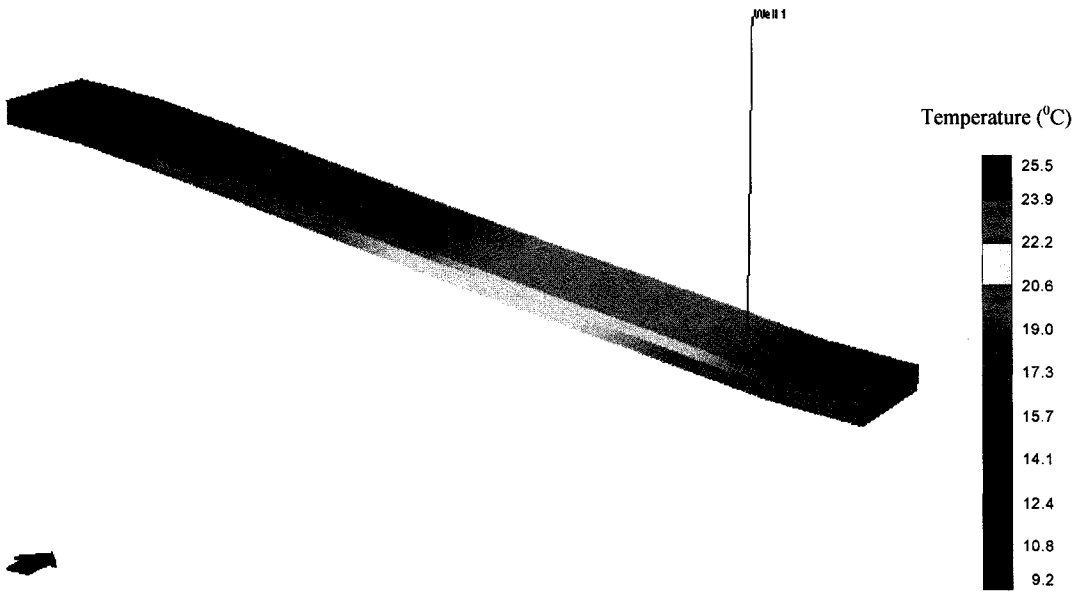

Figure 5.10: Temperature at the Start of the Simulation

As the gas starts getting produced (initially from the free gas zone), the pressure in the adjacent region is reduced and hence the gas hydrates in that region get dissociated. The hydrate dissociation is an endothermic process and needs the heat to sustain the dissociation. The heat required for this dissociation is obtained from the adjacent hydrate zone and hence the fall in temperature near the hydrate dissociation front is observed (the blue zone in Figures 5.11-5.13). It can be seen from Figures 5.11-5.13 that as time passes, more and more hydrate gets dissociated and the temperature drop in the region adjacent to hydrate dissociation front increases.

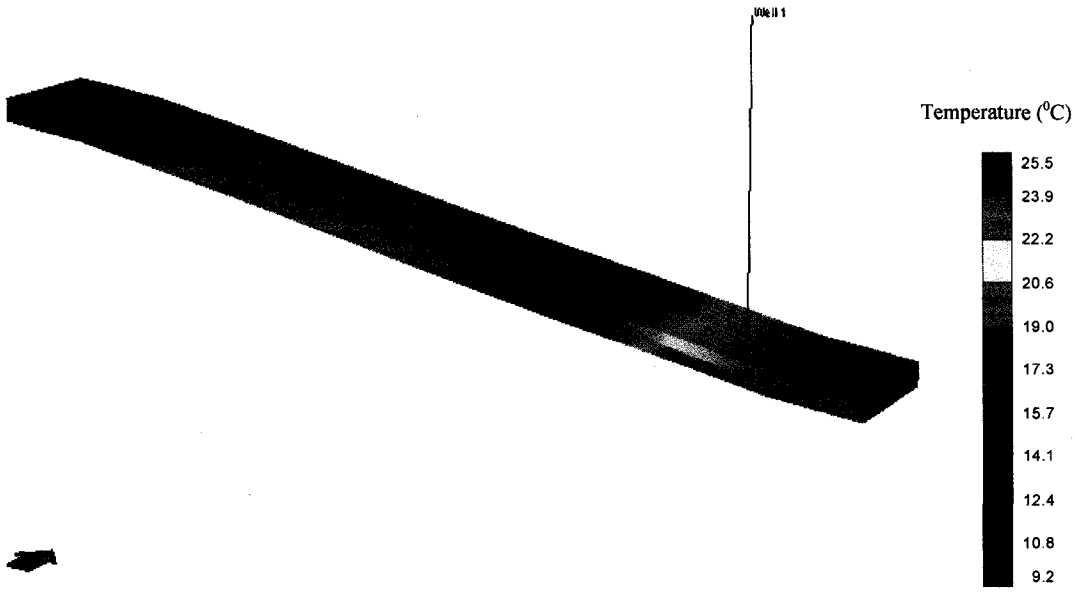

Figure 5.11: Temperature after Three Years of Simulation

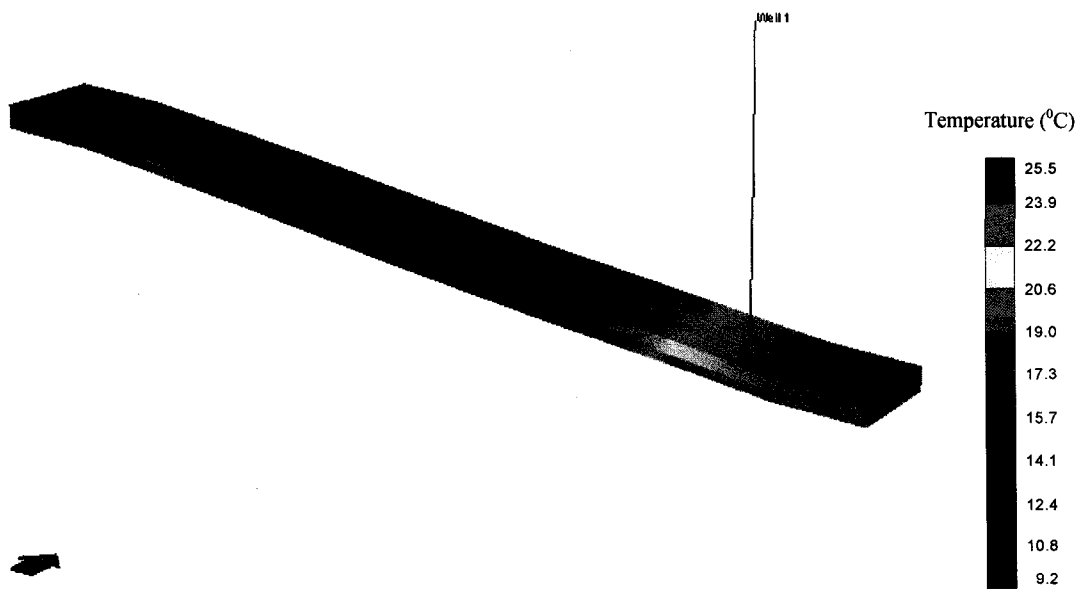

Figure 5.12: Temperature after Ten years of Simulation

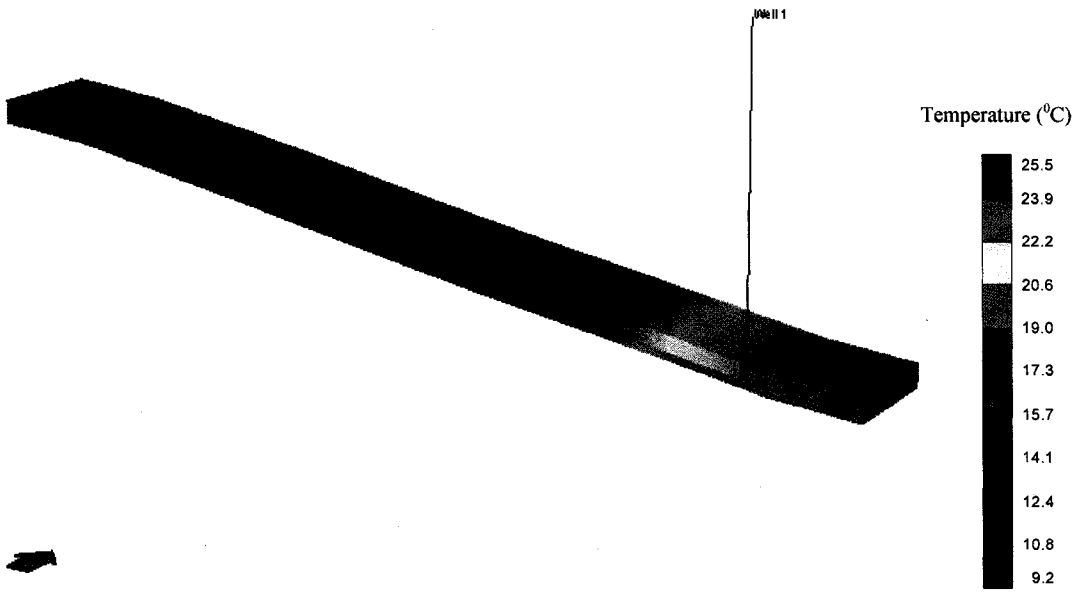

Figure 5.13: Temperature at the End of Simulation

Because of this drop in temperature, the hydrates can sometimes form in the dissociated hydrate zone, so keeping the well bore heated is suggested. Otherwise, if hydrates are formed near the well bore then the dissociated gas will not have any passage to escape the reservoir and this would lead to an increase in the reservoir pressure and hence lead to more hydrate formation. However, this heated well bore would increase the cost of the project and the feasibility of this needs to be studied further.

Effect on hydrate saturation:

Figure 5.14 shows initial hydrate conditions in the reservoir. As described earlier, the reservoir has a free gas zone and a gas hydrate zone. As seen from the figure, the hydrate saturation in the free gas zone is close to zero and the hydrate saturation in the hydrate zone is nearly 0.74.

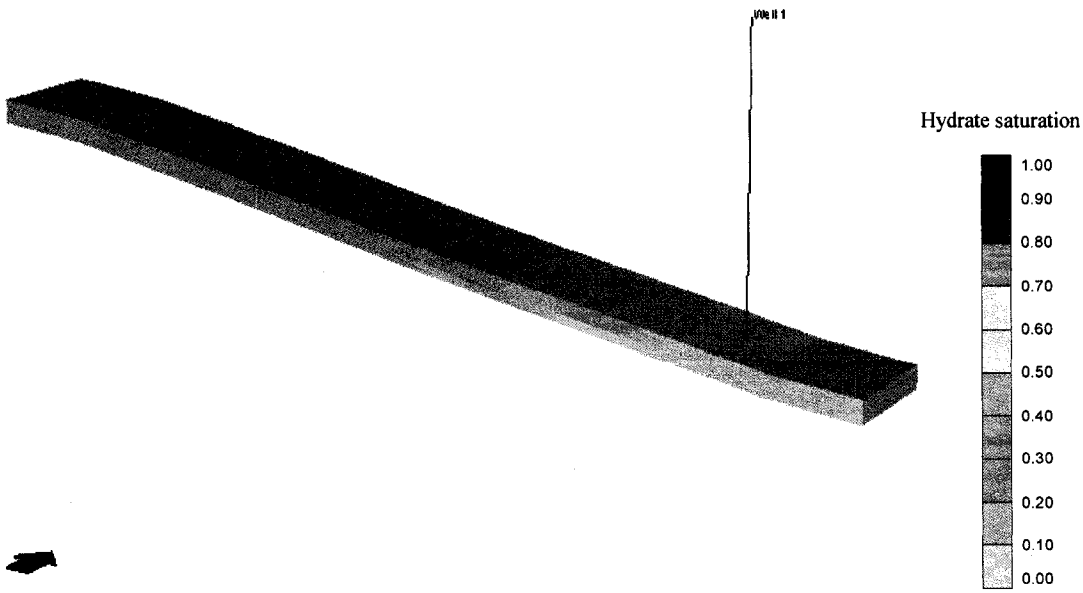

Figure 5.14: Hydrate Saturation at the Start of Simulation

As the gas starts getting produced from the free gas zone, the pressure in the reservoir is reduced and hydrate in the adjacent zone gets dissociated. Hence a drop in hydrate saturation in the adjacent region is observed (Figure 5.15) and dissociated gas is seen as free gas and hence an increase in free gas is observed in the region. As time passes more hydrates get dissociated and a drop in hydrate saturation (Figures 5.16 and 5.17) is observed.

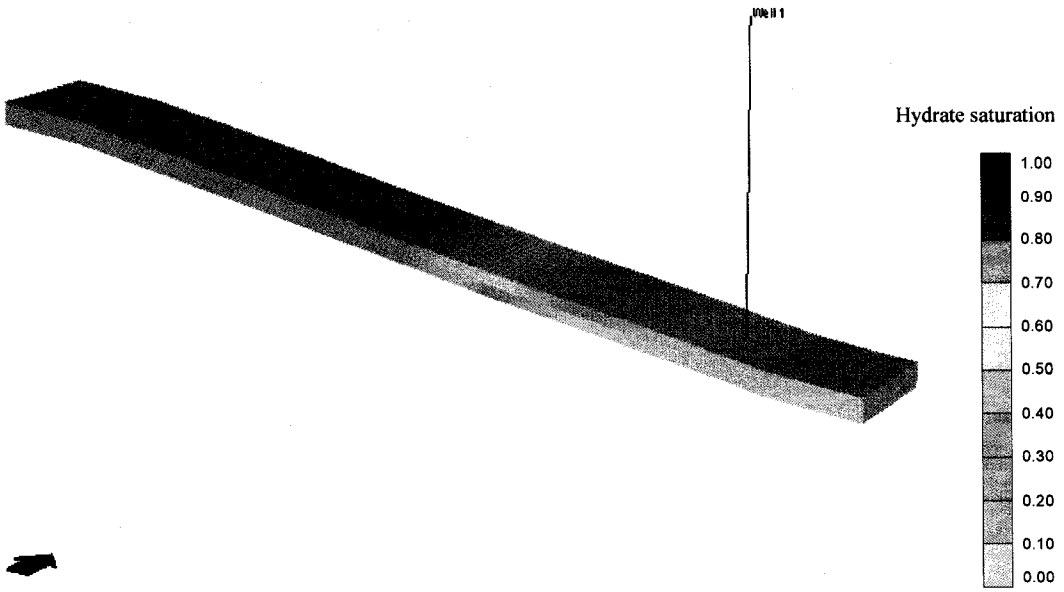

Figure 5.15: Hydrate Saturation after Three Years of Simulation

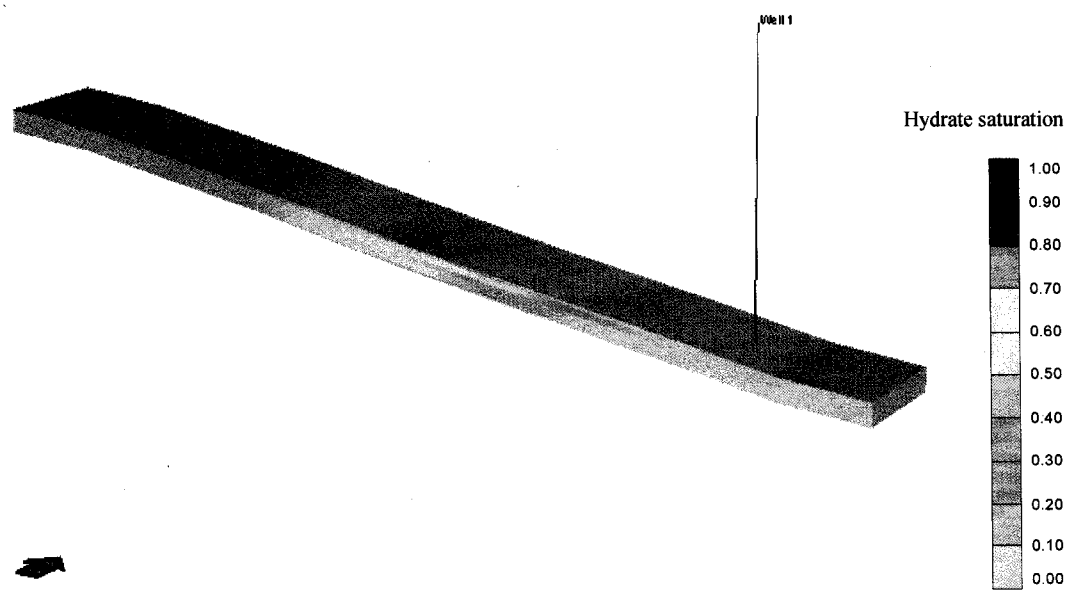

Figure 5.16: Hydrate Saturation after Ten Years of Simulation

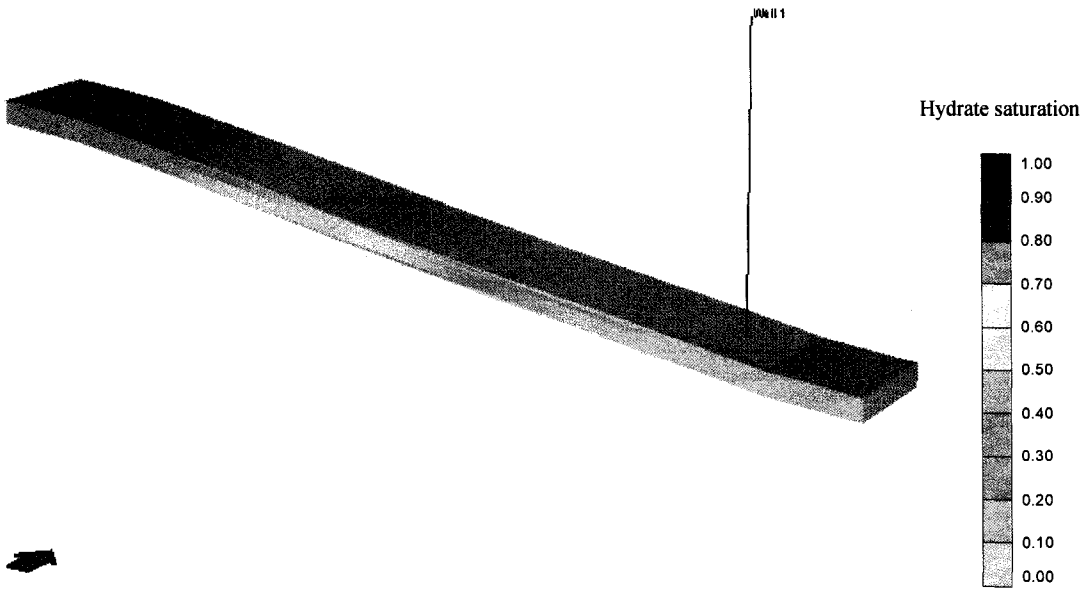

Figure 5.17: Hydrate Saturation at the End of Simulation

Effect on water saturation:

It was assumed that initially there is no water present in the gas hydrate zone as well as the free gas zone. The same is indicated in Figure 5.18.

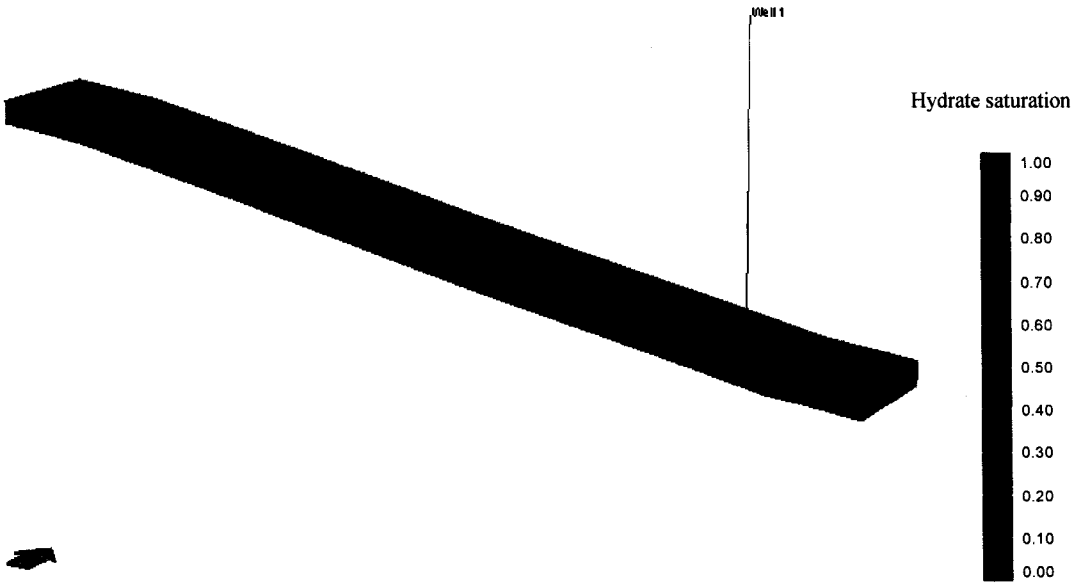

Figure 5.18: Water Saturation at the Start of Simulation

As the hydrates get dissociated, the water from dissociation is released along with free gas because the hydrate contains a gas molecule in a cage formed by water molecule. The water released may get produced or it can drain down to the bottom of the reservoir. But as the well bore bottom hole pressure is maintained low, only small quantities of water are actually produced on the surface. Most of the water produced from hydrate dissociation will stay at the bottom of the reservoir as shown in Figures 5.19- 5.21. The water saturation in the reservoir increases as the time passes.

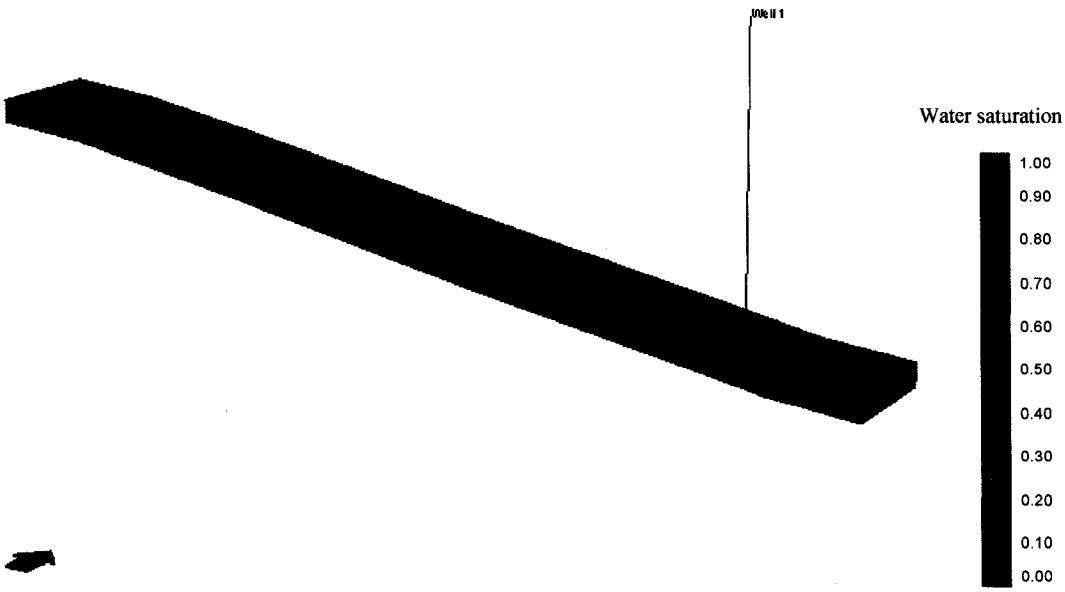

Figure 5.19: Water Saturation after Three Years of Simulation

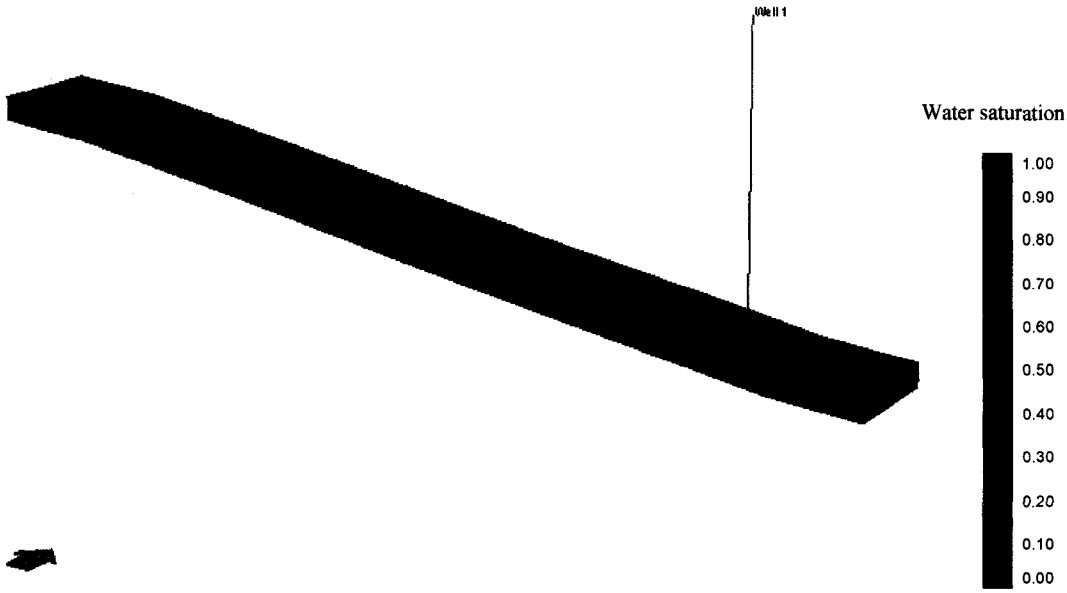

Figure 5.20: Water Saturation after Ten Years of Simulation

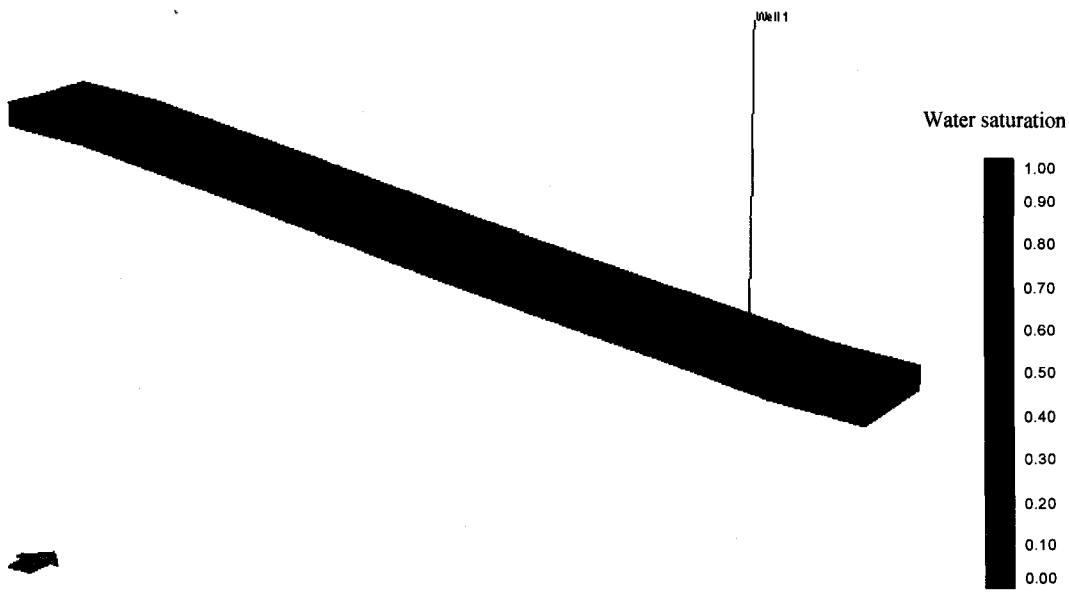

Figure 5.21: Water Saturation at the End of Simulation

Recognizing that at the end of a 15-year production period, only approximately 36% of gas initially in place has been recovered, an extended 30-year production simulation of the base case was performed. At the end of the simulation, the total cumulative production was 54% of the initial gas potential in place. Figure 5.22 shows the gas production rate over the thirty years.

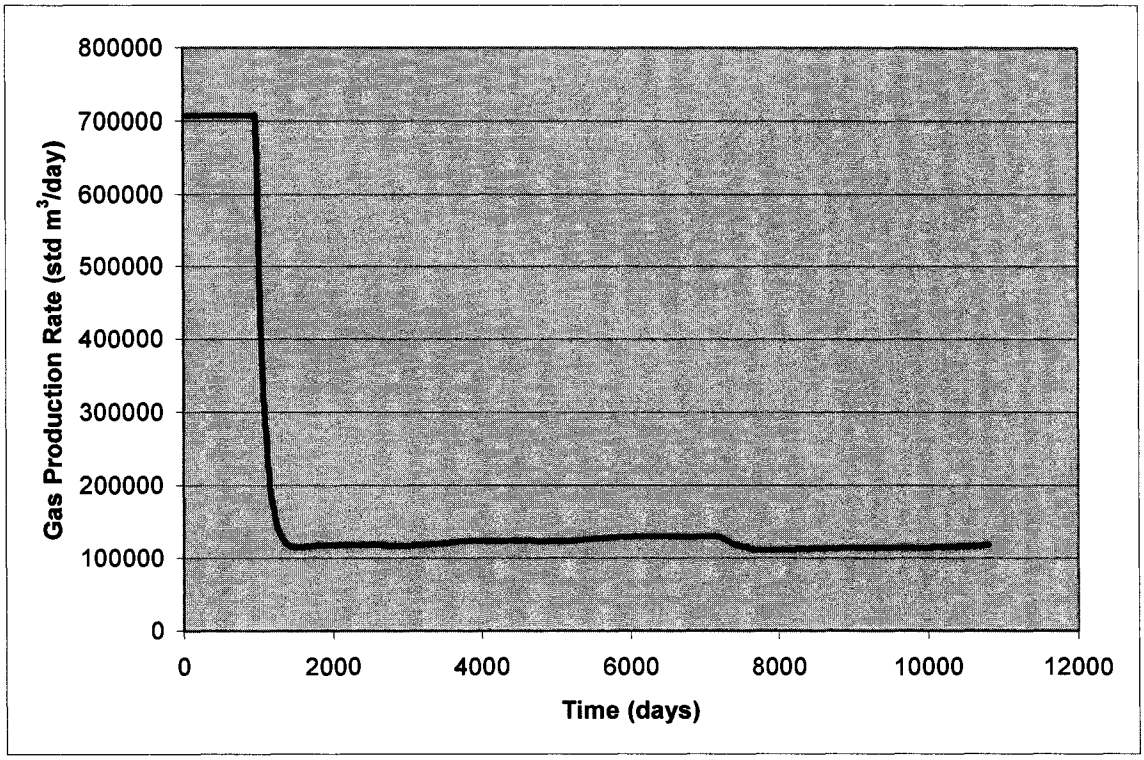

Figure 5.22: Production Rate, 30-Year Simulation

Figure 5.23 shows the hydrate saturation and temperature conditions in the reservoir at the end of the simulation study. At the end of simulation a substantial temperature drop can be observed in the reservoir and this can be attributed to the endothermic nature of hydrate dissociation.

Figure 5.24 shows the comparison of hydrate saturation at the end of 15 years and 30 years of simulation. It can be seen that hydrate saturation is substantially lower in the second case than that in the first case.

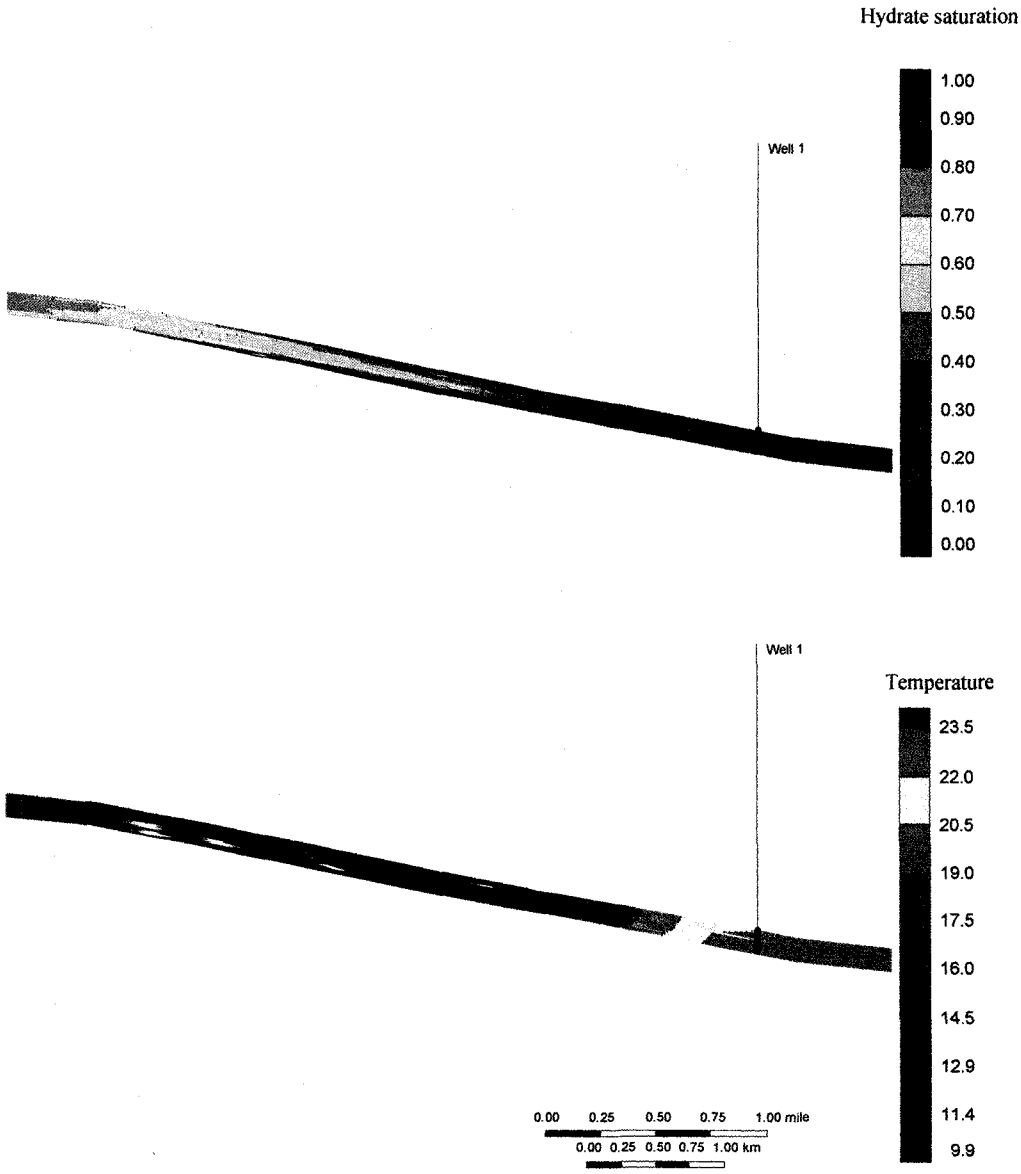

Figure 5.23: Temperature Profile Before and After 30 Years

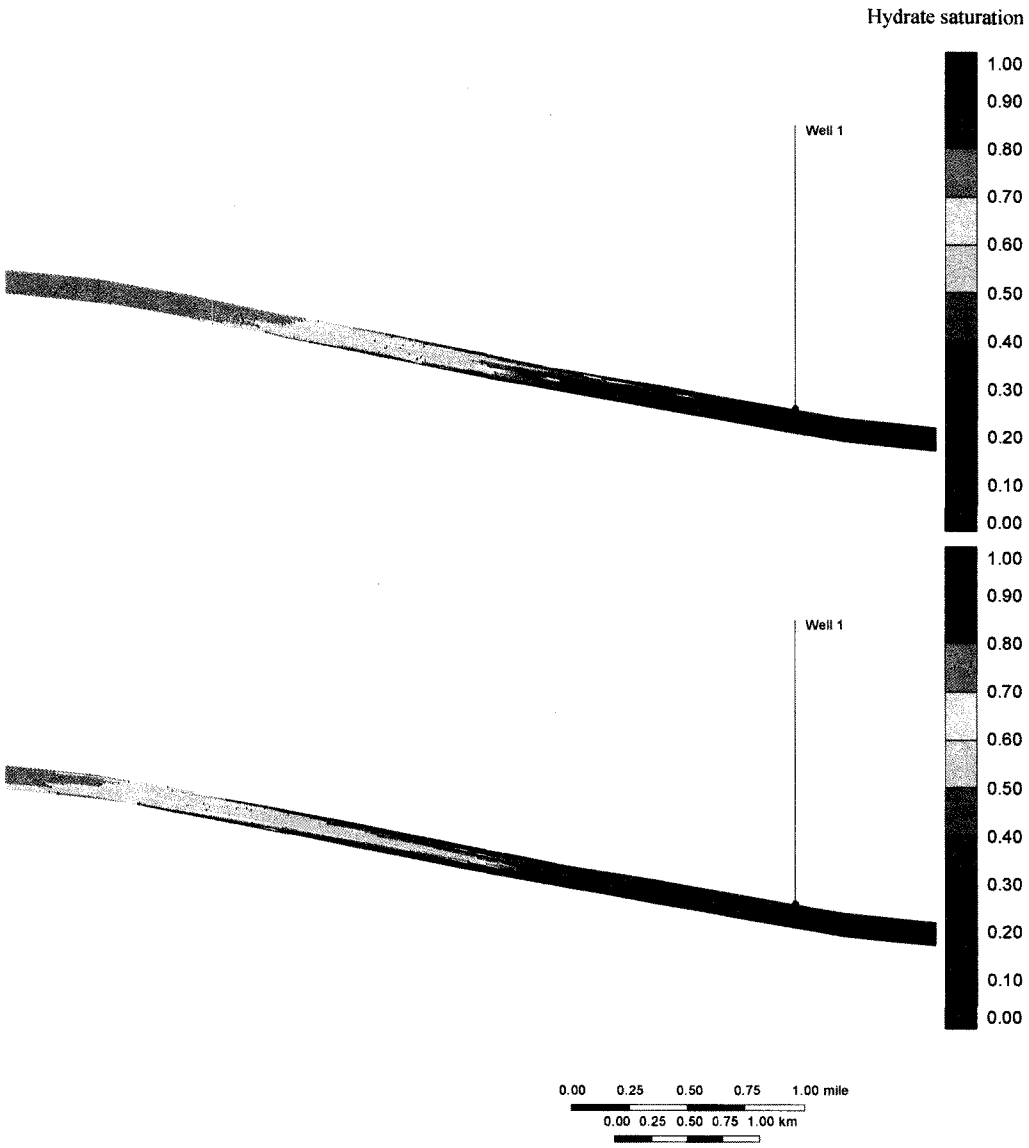

Figure 5.24: Hydrate Saturation Profile at 30 Years

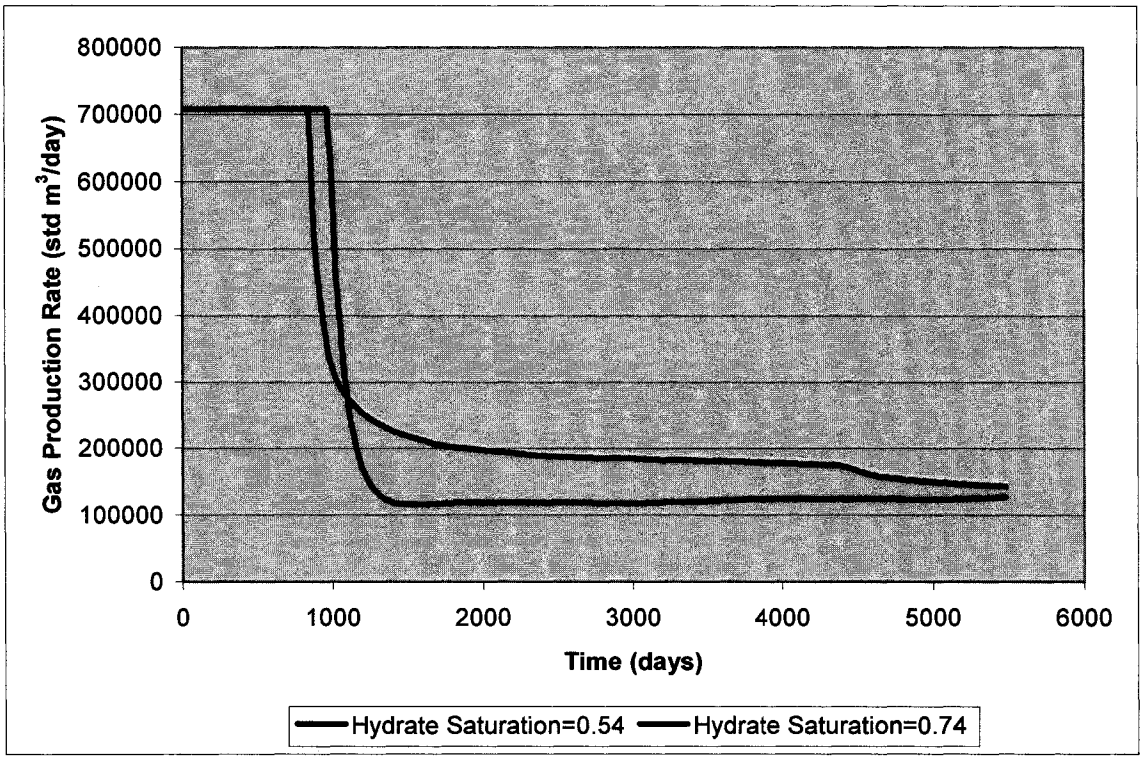

Figure 5.25: Production Rate, Reduced Hydrate Saturation

It is essential to determine which process is more effective in reservoirs containing high hydrate saturation or those having low initial hydrate saturation. So the simulations were run with a reduction of the initial hydrate saturation (0.54 instead of earlier 0.74). The results are shown in Figure 5.25. It can be seen that at higher initial hydrate saturation the peak period will last longer, but after that the production rate falls rapidly and continues that way. In the case of lower initial hydrate saturation, the peak period is shorter, but the production is significantly higher for the rest of the period than that for the earlier case. This could be due to the lower effective permeability of the reservoir when the hydrate saturation is higher. This represents an obstacle for the produced gas and hence the production is lower. Figure 5.26 shows the comparison of water saturation at the end of 15 and 30 years of the simulation run. As expected at the end of 30 years, the water saturation is higher than after 15 years and the water saturation has increased in the region near the production well so water production would have increased significantly.

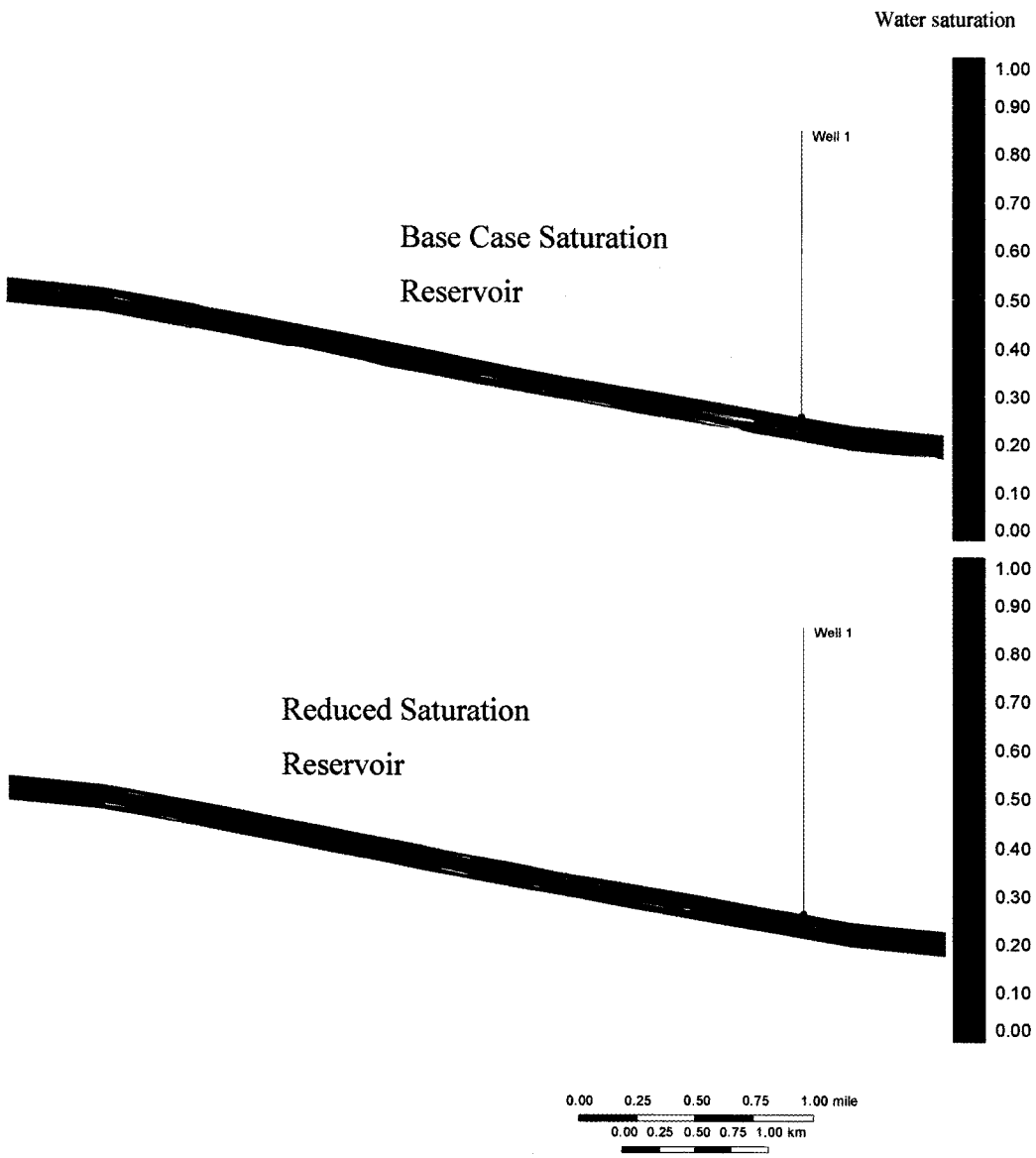

Figure 5.26: Water Saturation at the End of 30 Years

Figure 5.27 shows the effect of reservoir permeability on gas production rate. When the permeability of the reservoir is reduced from 300 md to 30 md the production decreases significantly. This is because with reduced permeability, the ability of rock to transmit the produced gas decreases significantly and hence the production rate becomes lower.

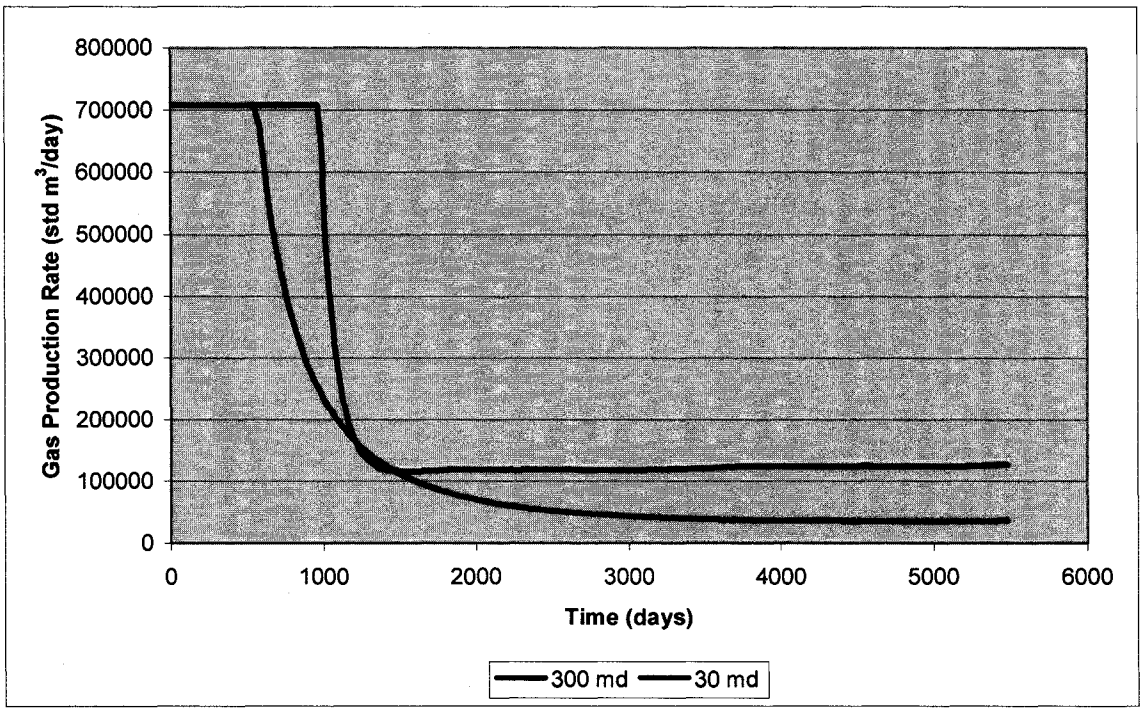

Figure 5.27: Production Rate, Reduced Permeability

Figure 5.28 shows the effect of thermal conductivity on gas production rate. It can be seen from the figure that with higher thermal conductivity the production rate increases. Whenever pressure is lowered, the hydrates dissociate. The hydrate dissociation process is an endothermic process, so the heat required for the dissociation is obtained from the adjacent rock. With higher conductivity, more heat is transferred and more hydrates dissociate and production increases.

Figure 5.29 shows the effect of the kinetic rate constant on cumulative gas production. It can be seen that at a higher rate constant, the cumulative production is higher. At higher rate constant, the hydrates dissociate faster and hence the cumulative production increases over a given span of time.

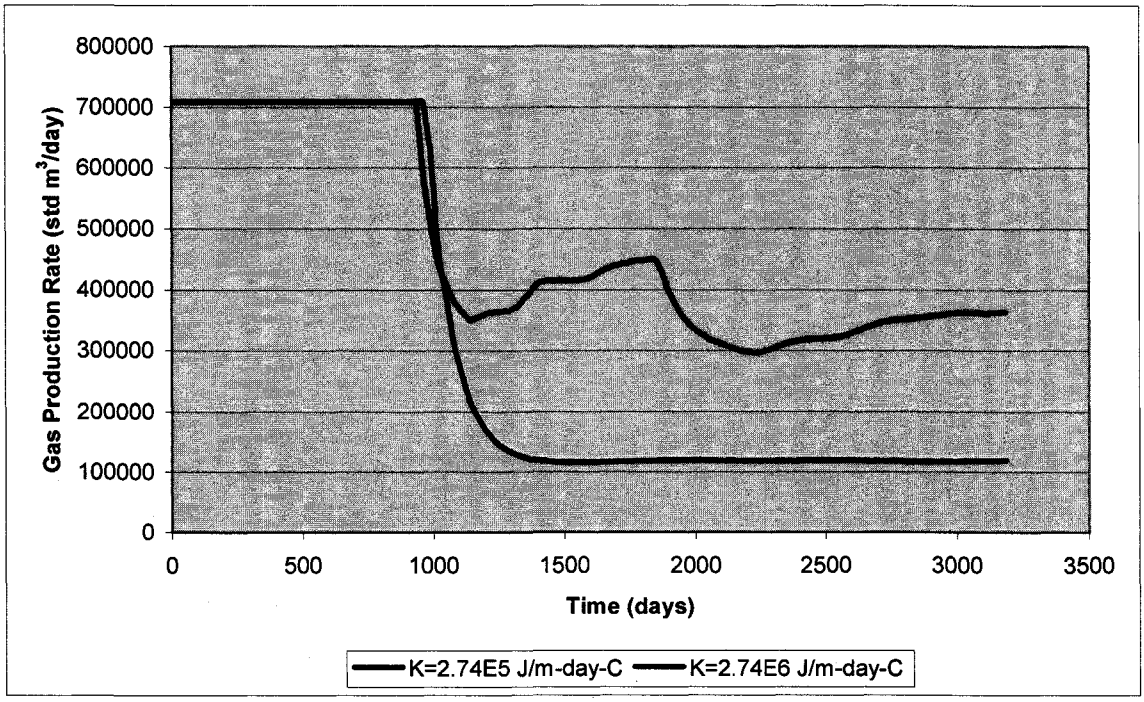

Figure 5.28: Effect of Thermal Conductivity on Production Rate

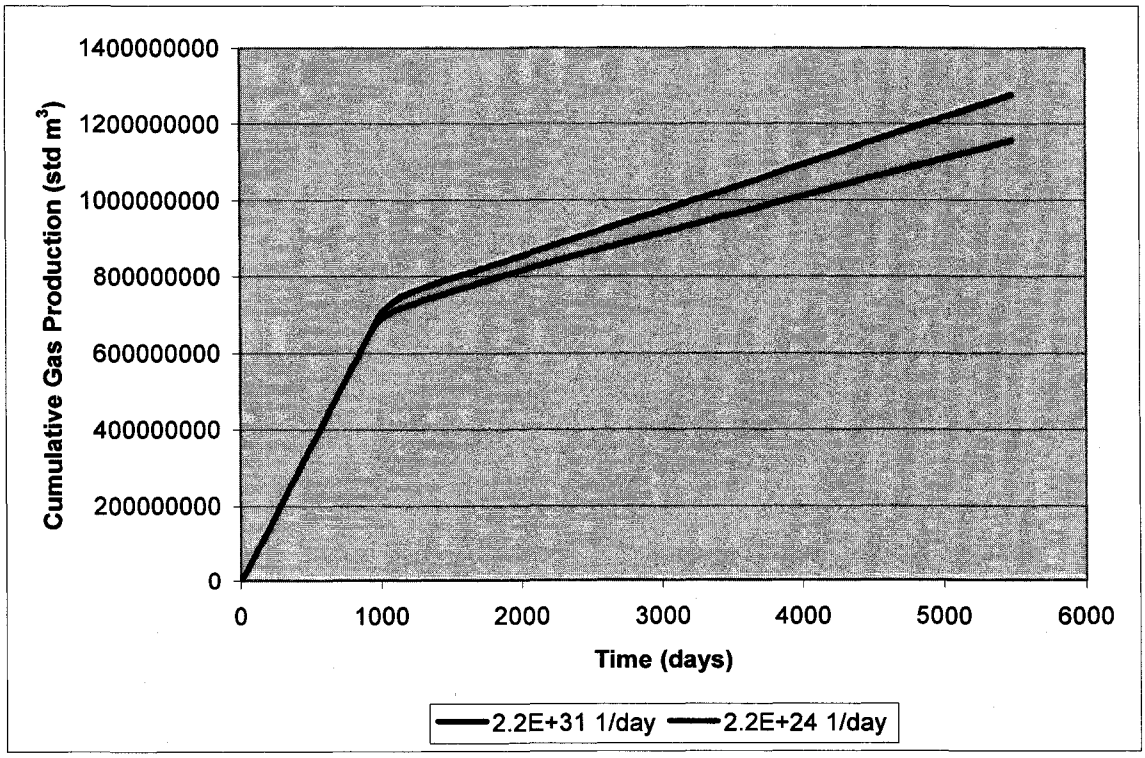

Figure 5.29: Effect of Kinetic Rate Constant on Cumulative Gas Production

Figure 5.30 shows the effect of porosity on cumulative gas production. It can be seen that at a higher value of porosity, the production is higher. It is expected that the production would be higher as the produced gas would be able to move with relative ease.

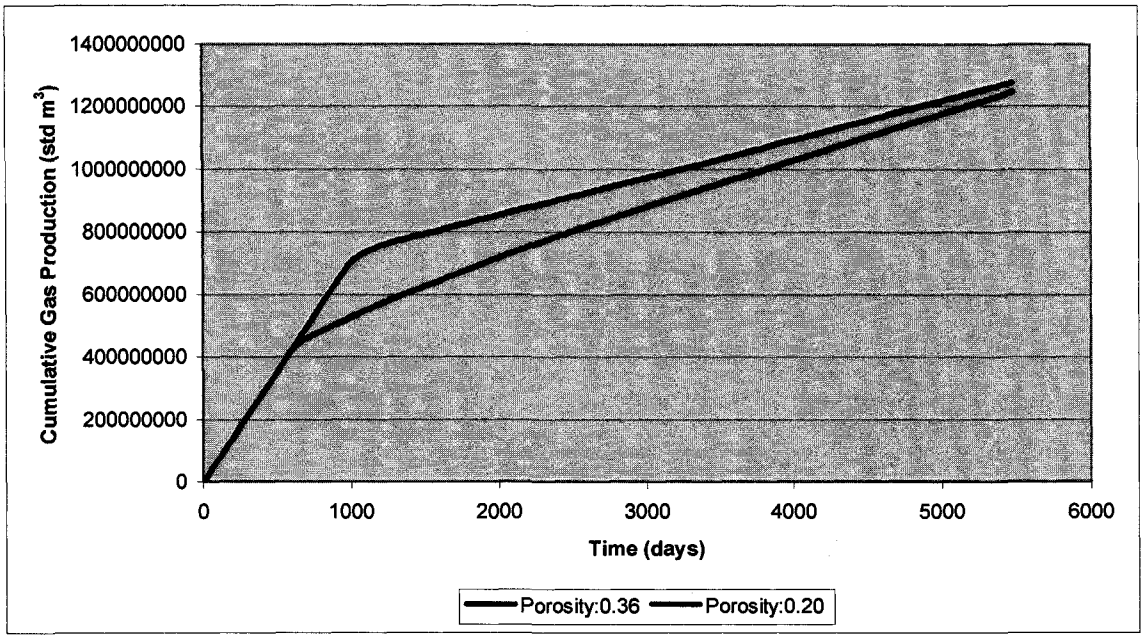

Figure 5.30: Effect of Porosity on Cumulative Gas Production

To account for the effects of rock and fluid properties on gas production, various sands were considered. The production is significantly higher for the rock-fluid data predicted by Stone's model than that for Andarko and Oklahoma sand.

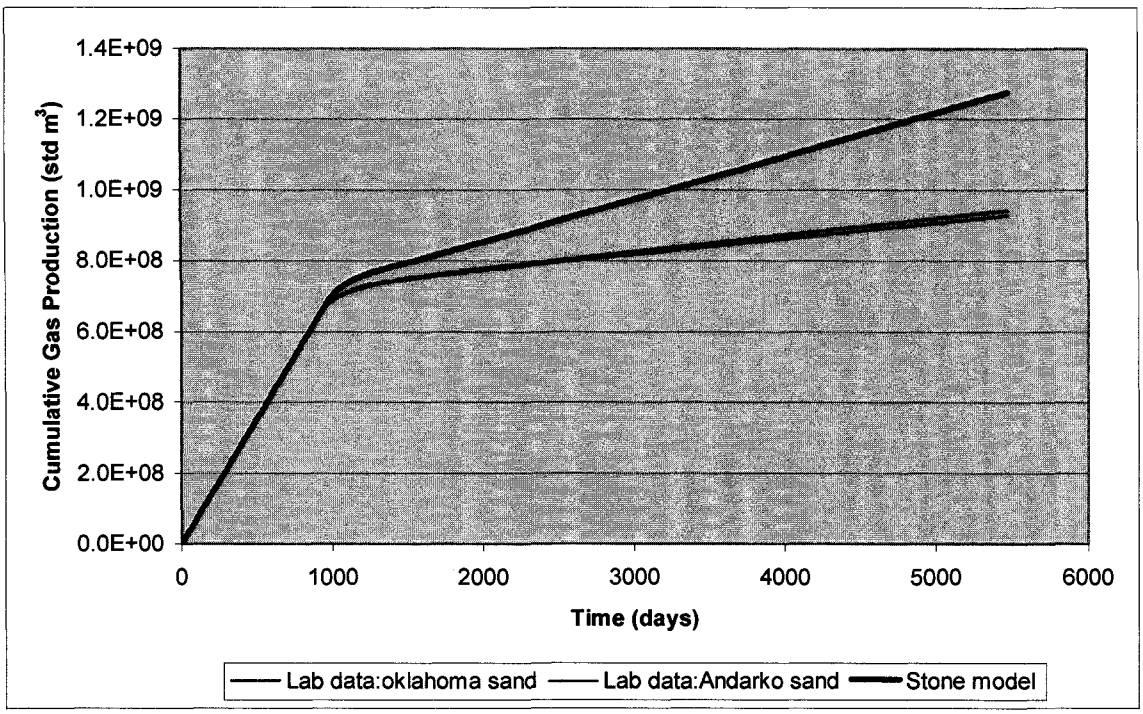

Figure 5.31: Effect of Rock-Fluid Data on Cumulative Gas Production

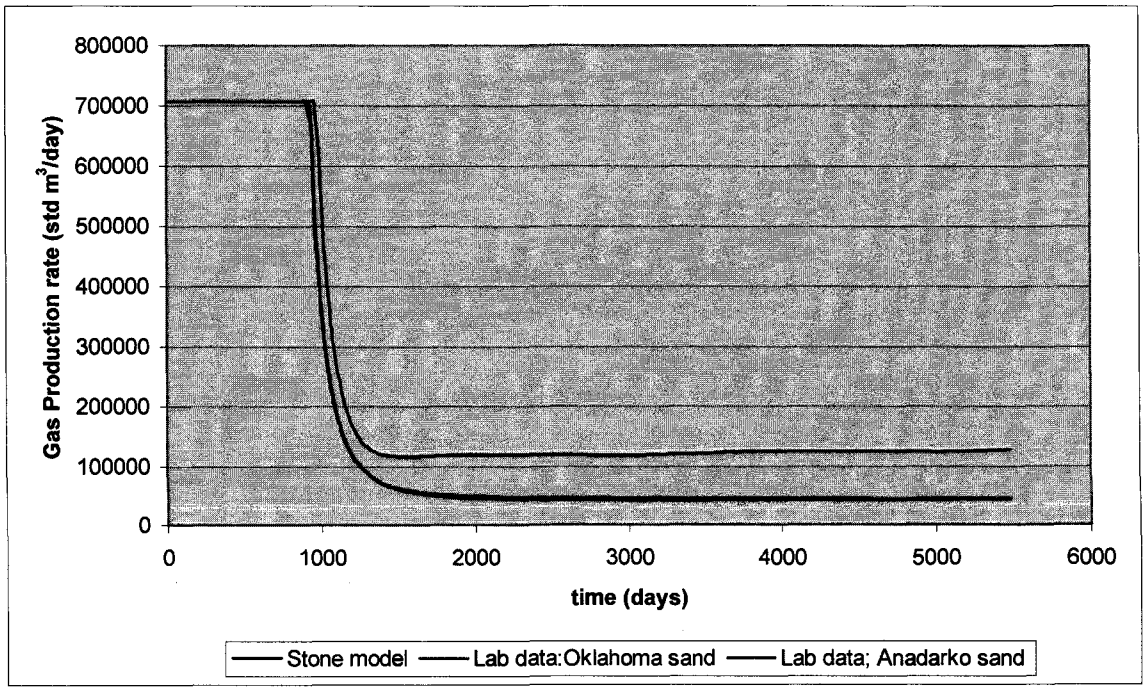

Figure 5.32: Effect of Rock-Fluid Data on Gas Production Rate

5.2 Model 2: Depressurization (with free gas zone and aquifer)

The geometry described in Figure 4.2 is considered for this model. First a gas production scheme using depressurization is considered. Figure 5.33 shows the gas production rate as function of time. Initially the production rate remains constant at 7000 m^3/day and then decreases.

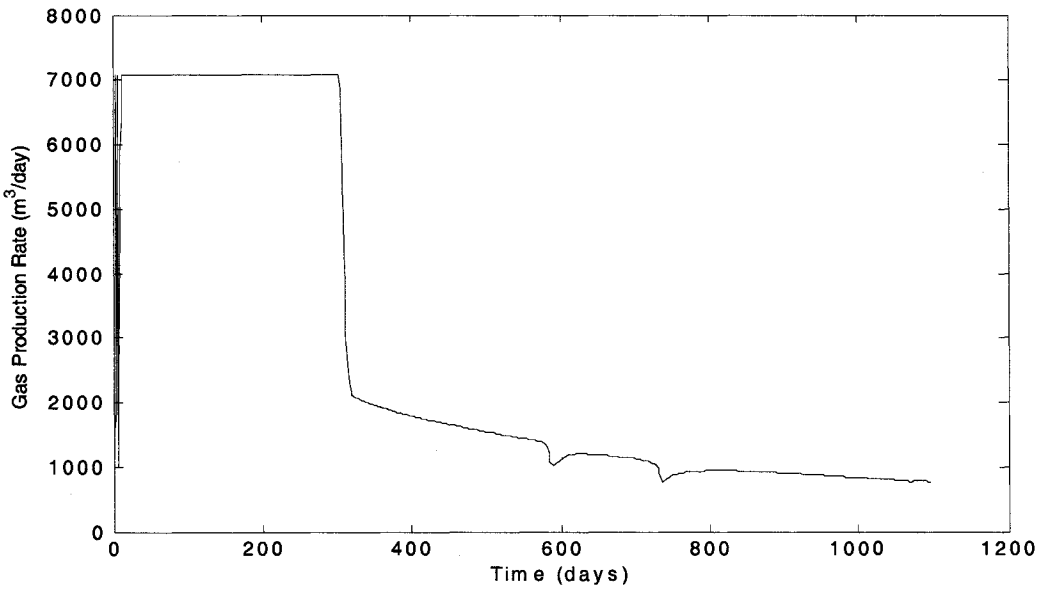

Figure 5.33: Gas Production Rate vs. Time

Figure 5.34 shows the effect of permeability on the cumulative production. The cumulative production decreases significantly when the permeability is reduced. This is because the produced gas has to overcome more resistance to flow out of the reservoir.

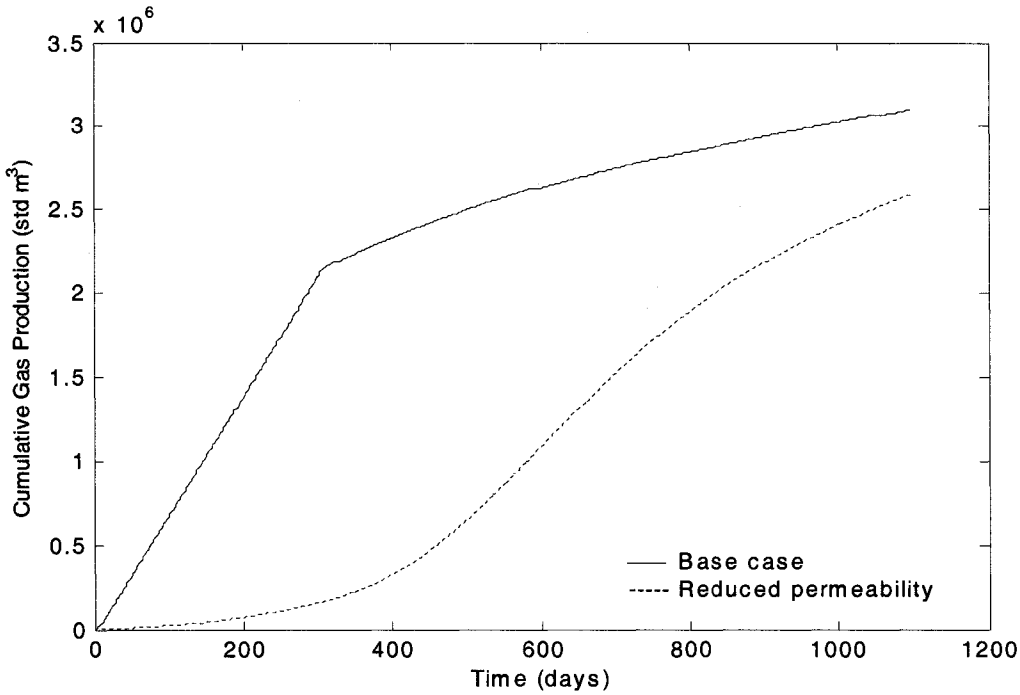

Figure 5.34: Cumulative Gas Production vs. Time

Figures 5.35- 5.37 show the change in hydrate saturation in the reservoir after one, two and three years of production. The figures are top views of the reservoir. It can be seen that initially throughout the reservoir, hydrate saturation is constant (0.6). As the gas production begins, the pressure decreases in the reservoir and hydrates dissociate. Hence, the fall in hydrate saturation near the production well can be seen. As time passes, the hydrate saturation near the well decreases more and more and also the area of low hydrate saturation increases.

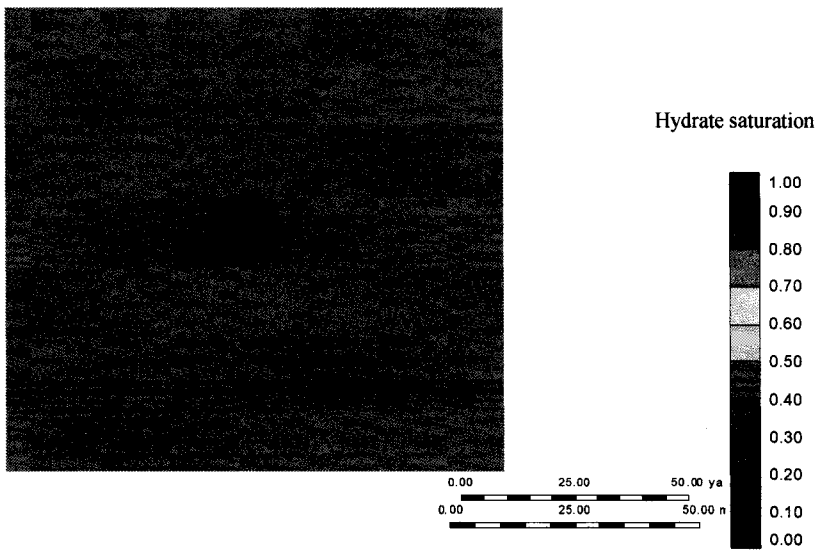

Figure 5.35: Hydrate Saturation Contours after One Year of Production

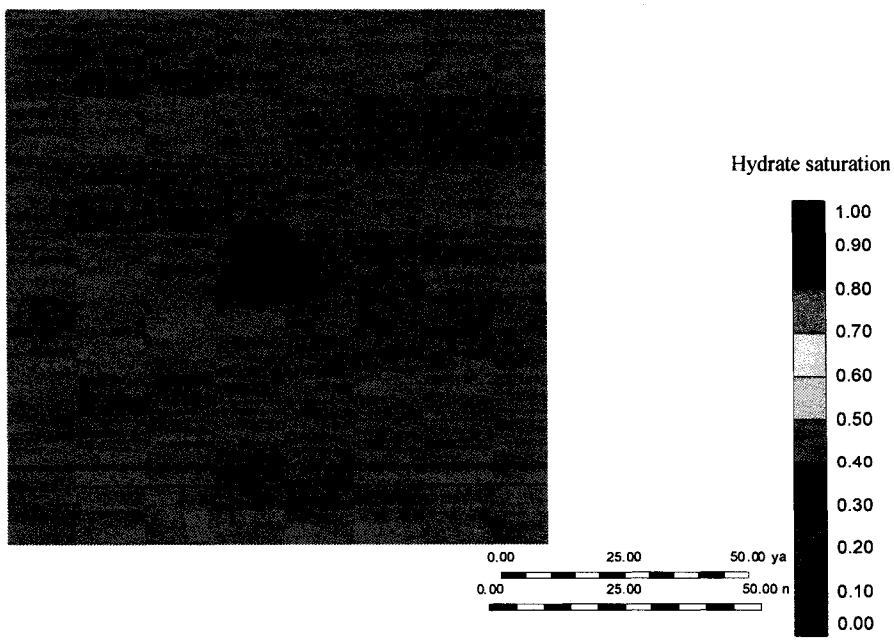

Figure 5.36: Hydrate Saturation Contours after Two Years of Production

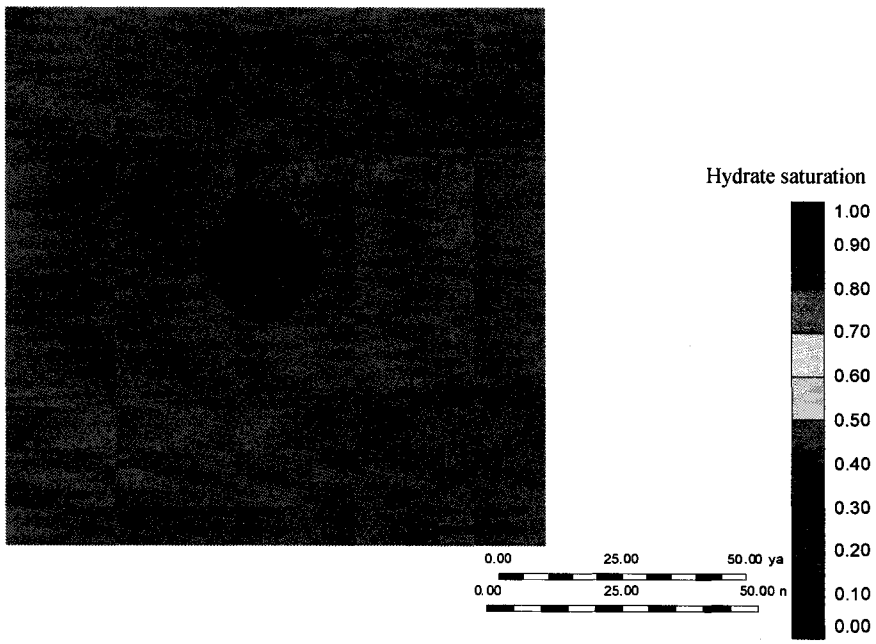

Figure 5.37: Hydrate Saturation Contours after Three Years of Production

Figures 5.38-5.40 show the change in pressure conditions in the reservoir after one, two and three years of production simulation. Initially, pressure in the reservoir is constant and pressure in the well bore is kept at the minimum pressure required for the gas to flow through a 24" pipeline to a separation plant. It can be seen that after one year of simulation, pressure near the production well starts decreasing. As time passes, the area of low pressure starts increasing and after three years of production pressure in the reservoir remains constant but higher than bottom hole pressure.

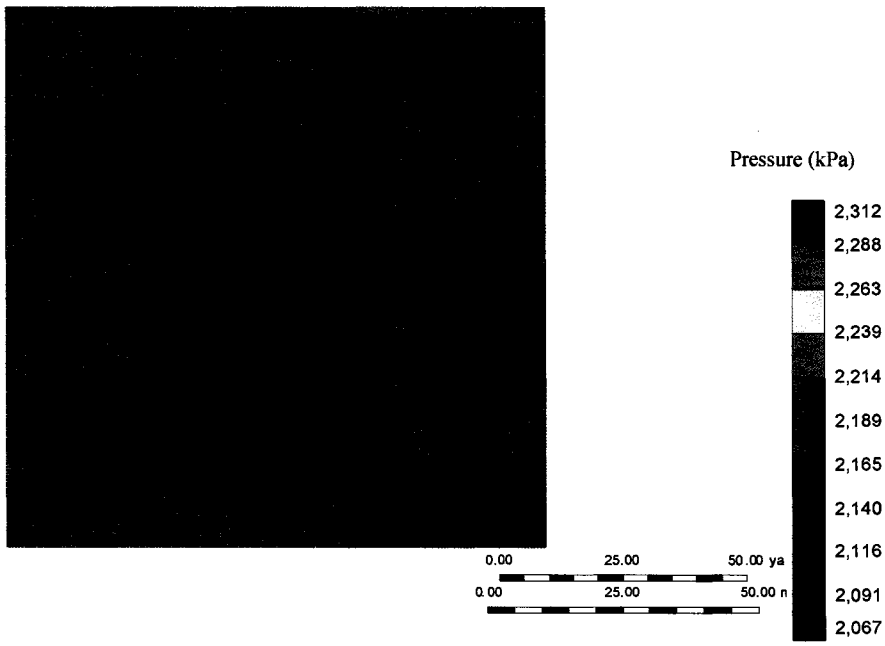

Figure 5.38: Pressure Contours after One Year of Production

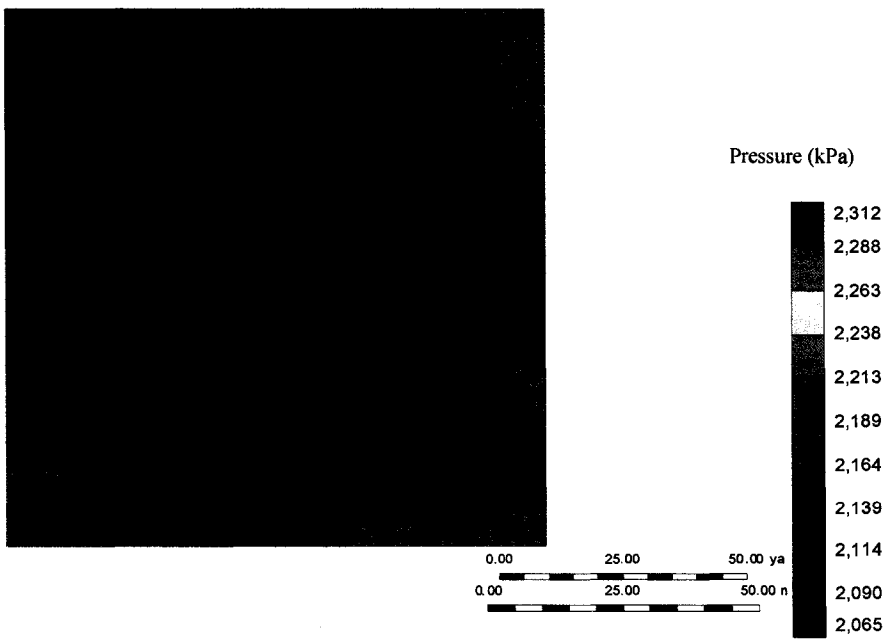

Figure 5.39: Pressure Contours after Two Years of Production

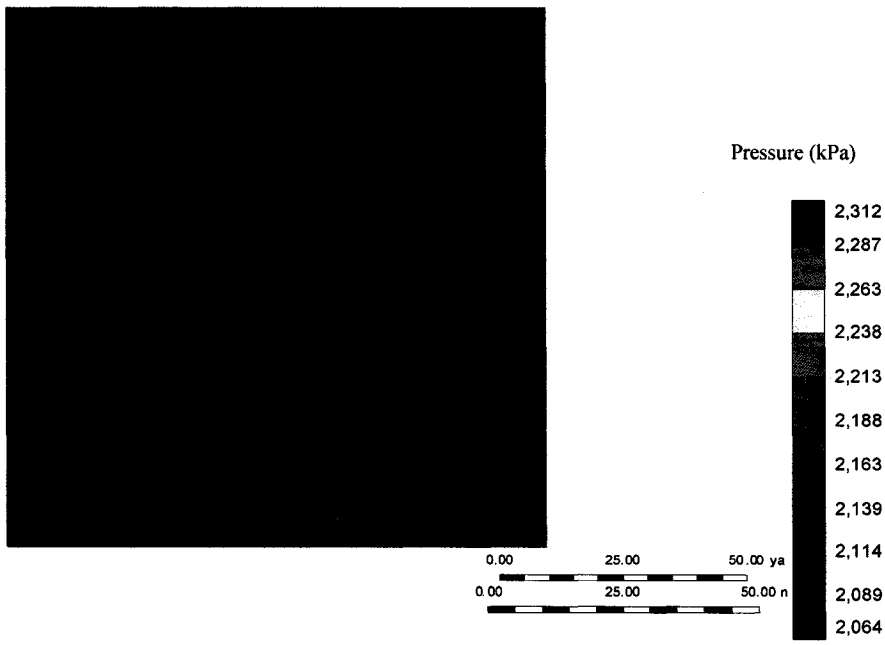

Figure 5.40: Pressure Contours after Three Years of Production

Figures 5.41- 5.43 show the change in water saturation after one, two and three years of production. Initially water saturation in the reservoir is constant. As the depressurization starts, the hydrates near the well bore region begin dissociating. Due to hydrate dissociation, water is released as hydrates are composed of water molecule lattice. Hence, a water saturation increase in the region near the well bore is observed. As more hydrates get dissociated, water saturation increases in the reservoir, but in the region close to the well bore only.

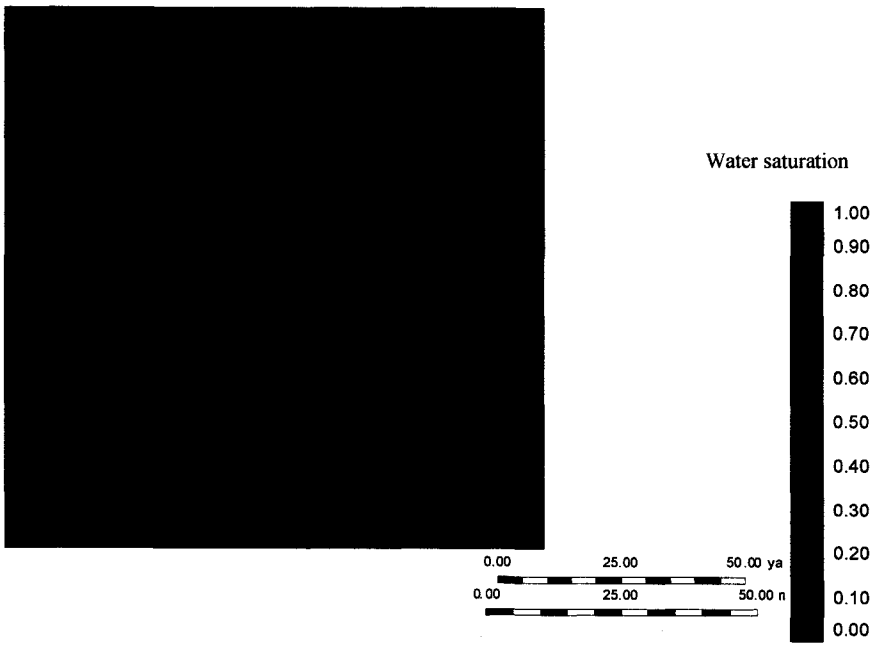

Figure 5.41: Water Saturation Contours after One Year of Production

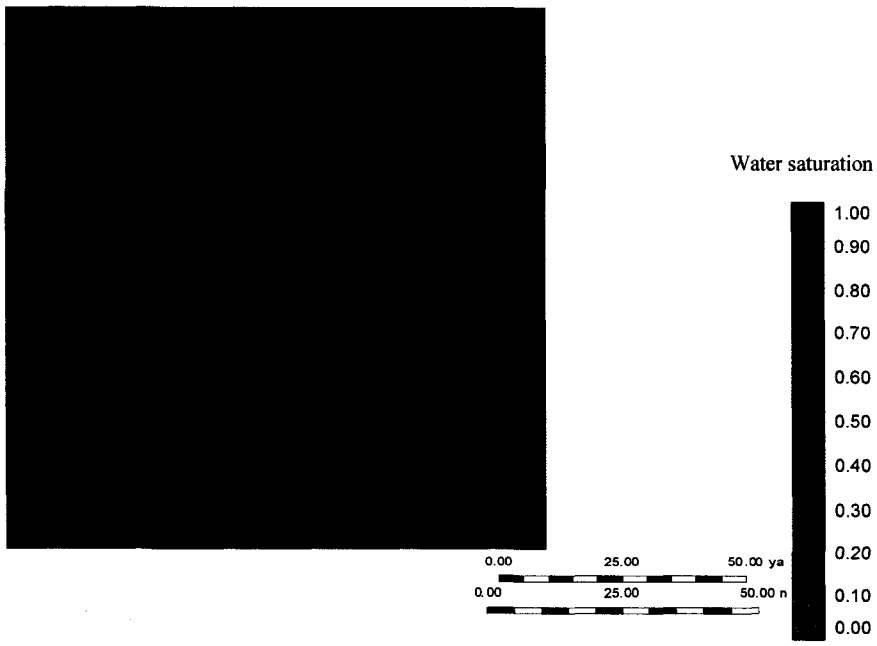

Figure 5.42: Water Saturation Contours after Two Years of Production

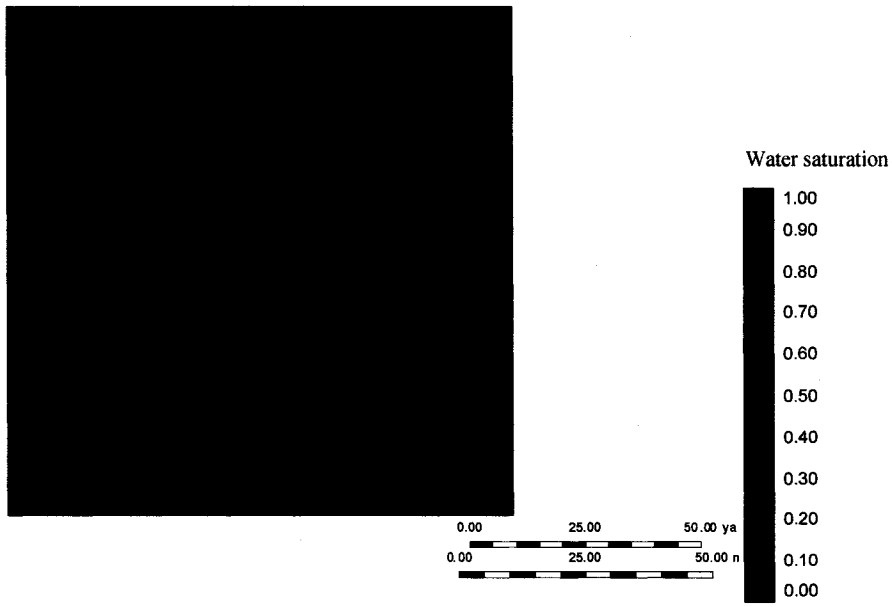

Figure 5.43: Water Saturation Contours after Three Years of Production

Figure 5.44 shows the comparison of cumulative gas production between base case and loose hydrates. As expected the production is higher for loose hydrate reservoir as the produced gas moves easily to the production well.

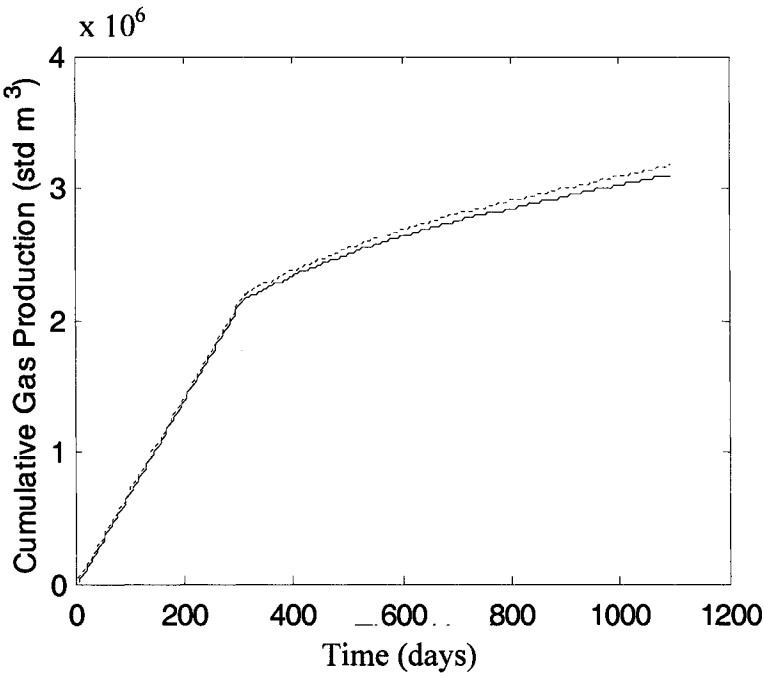

Figure 5.44: Cumulative Gas Production for Loose Hydrate vs. Time

Figure 5.45 shows the comparison of cumulative gas production by depressurization and by hot water injection at various temperatures. The production for hot water injection is higher than that for depressurization as the hot water injection process is actually a combination of depressurization (low pressure in the well bore) and thermal stimulation (injection of hot water).

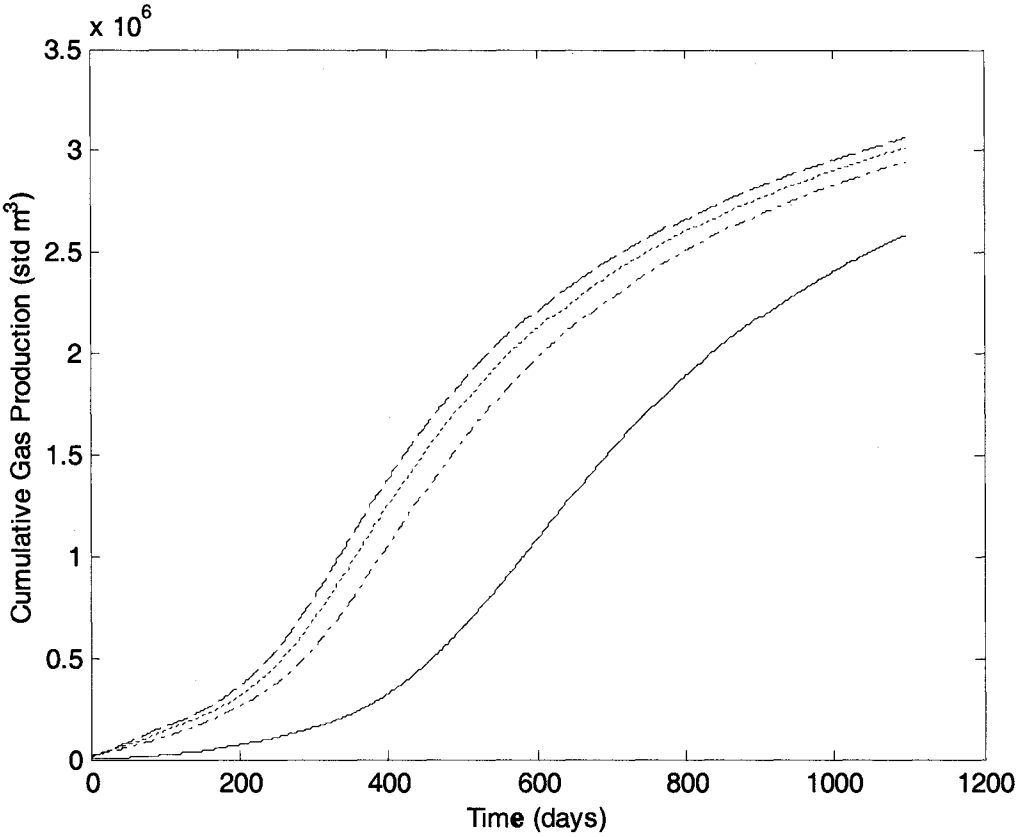

Figure 5.45: Cumulative Gas Production for Tight Hydrate vs. Time (solid line: Depressurization, dashed-dotted line: 40 °C, dotted line: 60 °C, dashed line: 80 °C)

5.3 Model 2: Heated Well

In this section the production scheme of using a heated well method is studied. The geometry is as described in Chapter 4.2. In this method, the well bore is heated. Because of the increase in well bore temperature the hydrates in the adjacent zone dissociate and gas is produced.

Figures 5.46 and 5.47 show the change in temperature profile after two and three years of production. As seen from the figures, temperature in the region near the well bore starts increasing as the time passes. In this production scheme, the heat required for hydrate dissociation is obtained from the heated well.

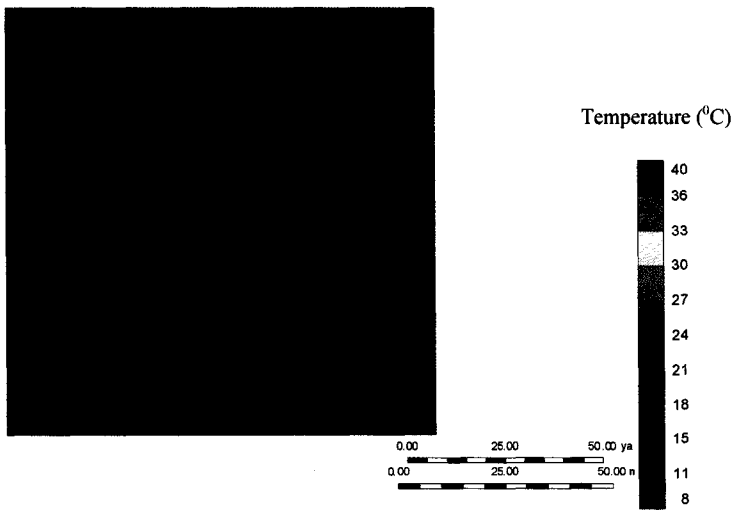

Figure 5.46: Temperature Contours after Two Years of Production, Heated Well Method

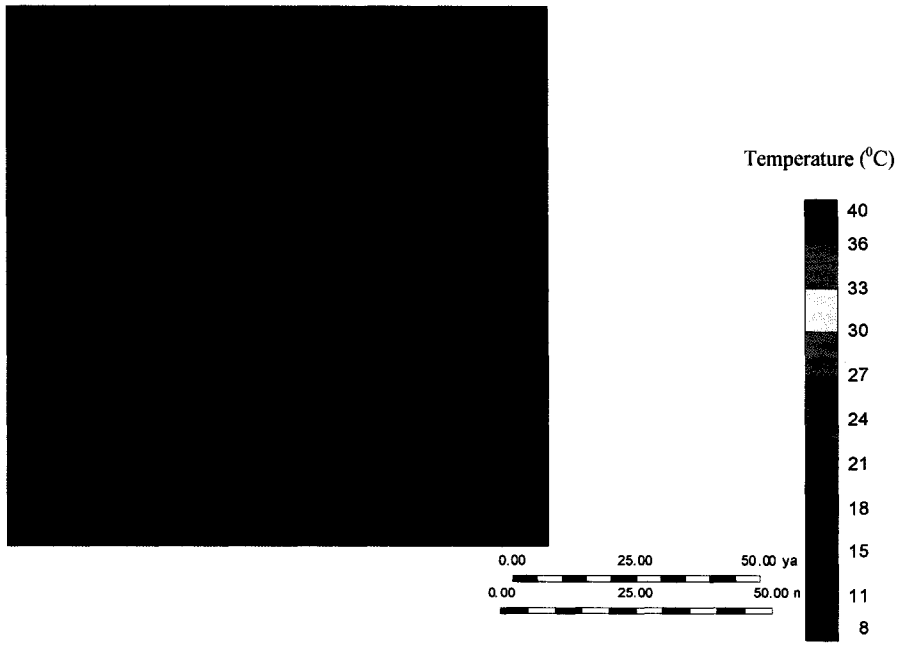

Figure 5.47: Temperature Contours after Three Years of Production, Heated Well Method

Figures 5.48- 5.50 show the change in water saturation contour after one, two and three years of production. Initially, the water saturation is constant throughout the reservoir. As the hydrates get dissociated near the well bore, the water near the well bore is produced. As the production time increases, more and more hydrates dissociate and hence more and more water is produced. Thus, an increase in water saturation is observed in the figures.

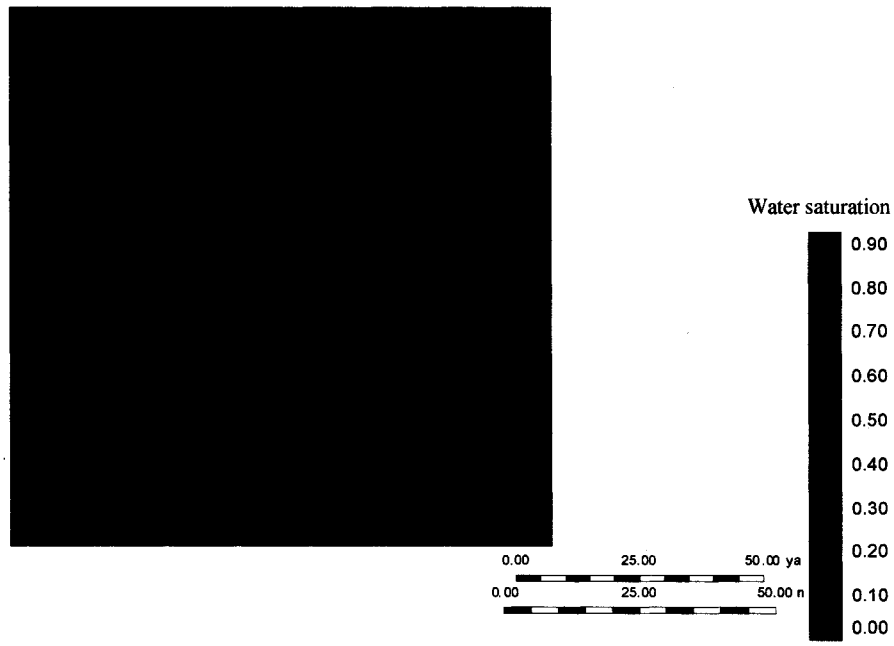

Figure 5.48: Water Saturation Contours after One Year of Production, Heated Well Method

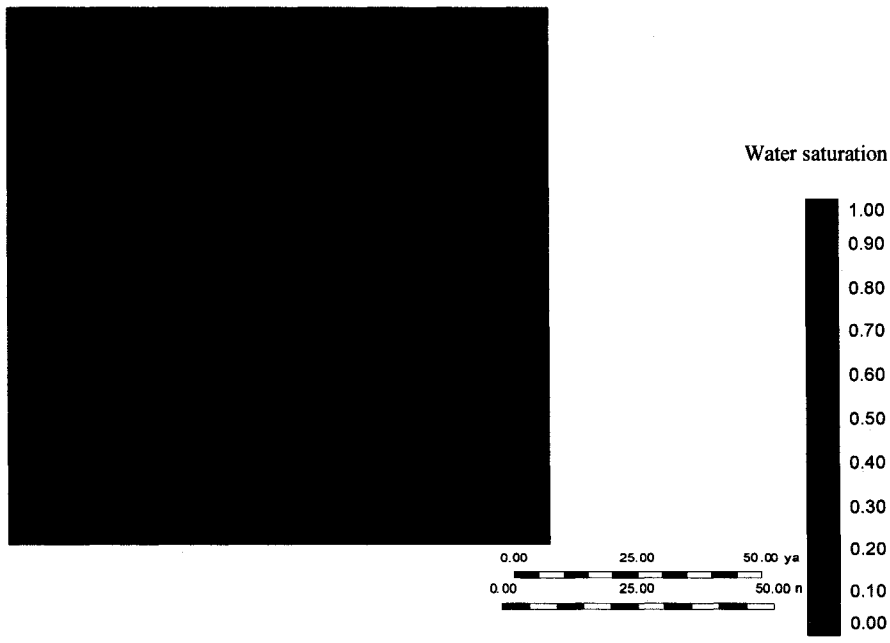

Figure 5.49: Water Saturation Contours after Two Years of Production, Heated Well Method

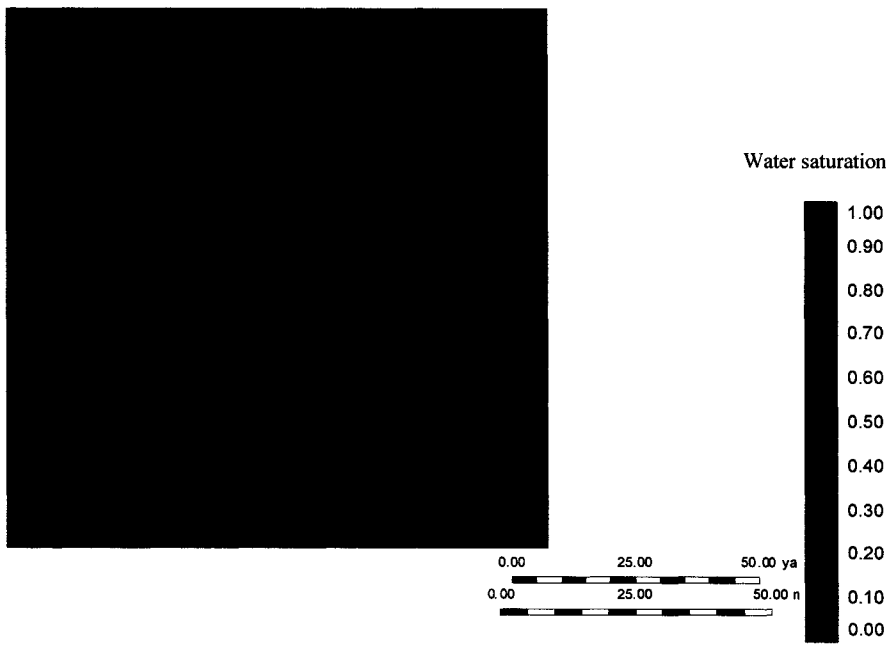

Figure 5.50: Water Saturation Contours after Three Years of Production, Heated Well Method

Figures 5.51- 5.53 show the changes in the pressure contours after one, two and three years of production. Initially the pressure is constant throughout out the reservoir. But as gas production starts, pressure in the region near the well bore decreases and this dissociates the hydrates in the nearby region. Soon the pressure in the reservoir becomes constant at a lower value than the initial pressure and the region near the well bore has an even lower value. As the gas production continues, this region of low pressure increases as more and more hydrates get dissociated.

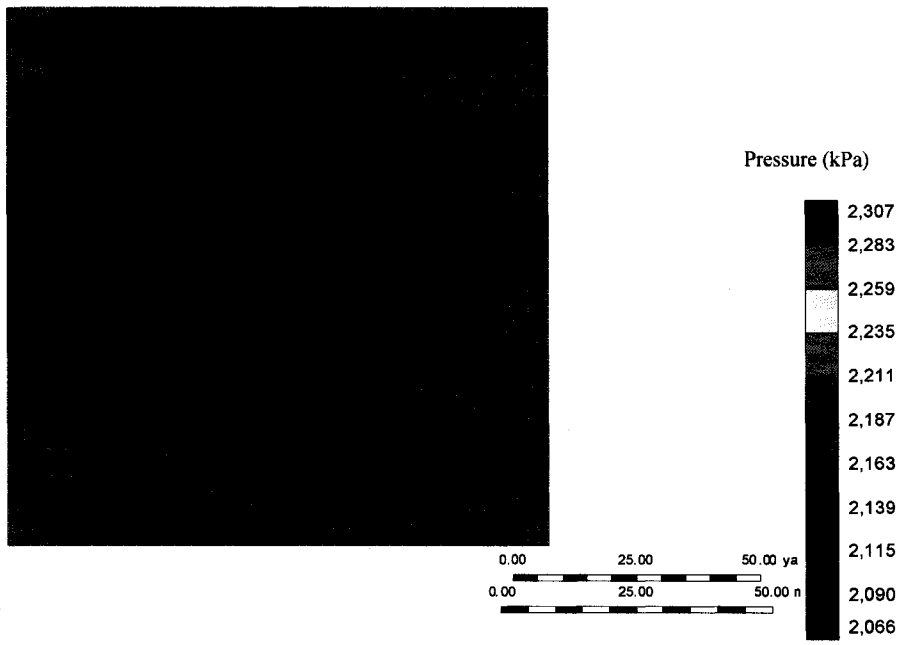

Figure 5.51: Pressure Contours after One Year of Production, Heated Well Method

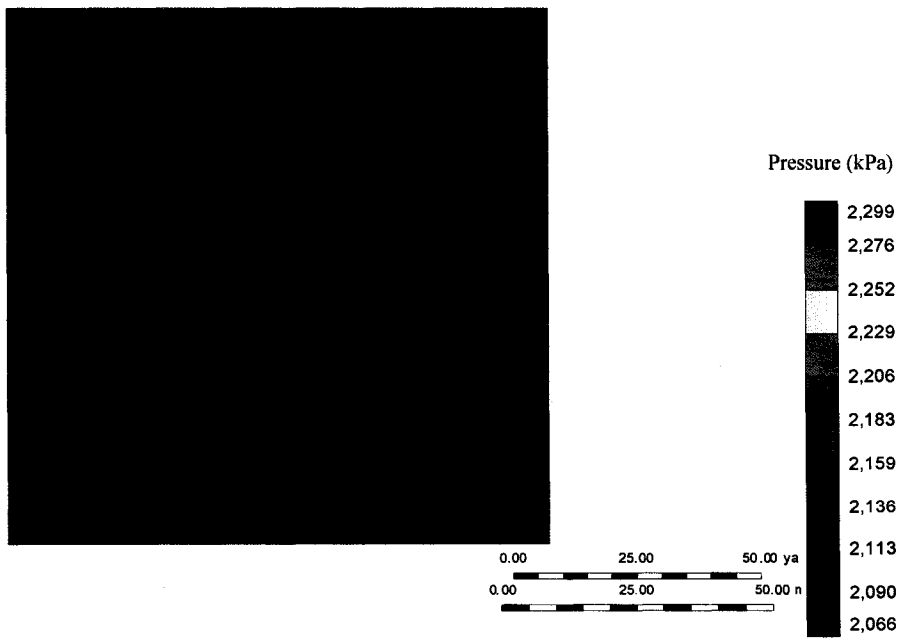

Figure 5.52: Pressure Contours after Two Years of Production, Heated Well Method

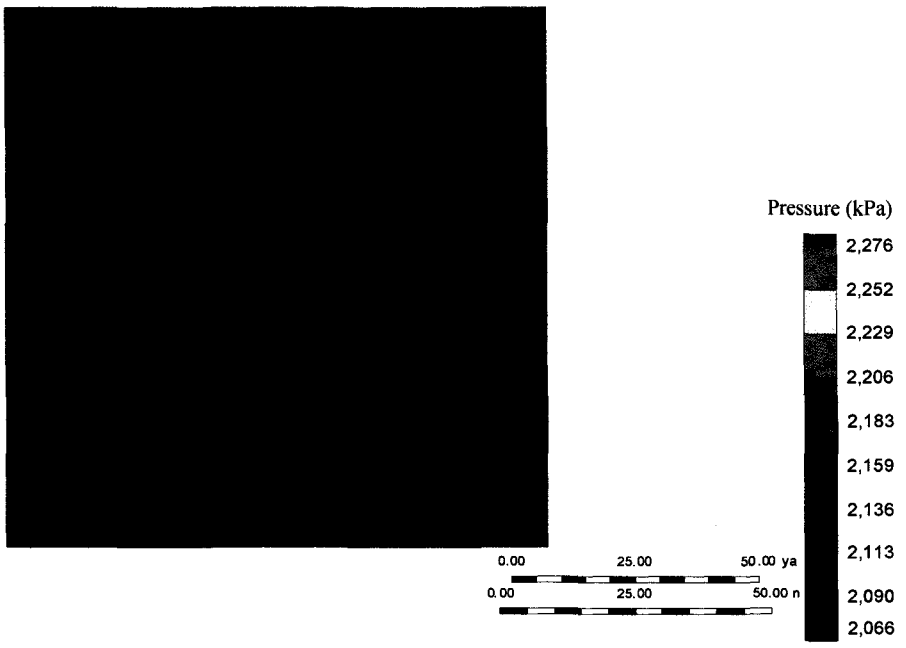

Figure 5.53: Pressure Contours after Three Years of Production, Heated Well Method

5.4 Model 2: Hot Water Injection

In this section, the reservoir geometry described in Chapter 4.2 is considered and the production scheme of hot water injection is studied. A typical five spot pattern is used in which four injector wells are used for injecting hot water and one well is used for production as shown in Figure 5.54.

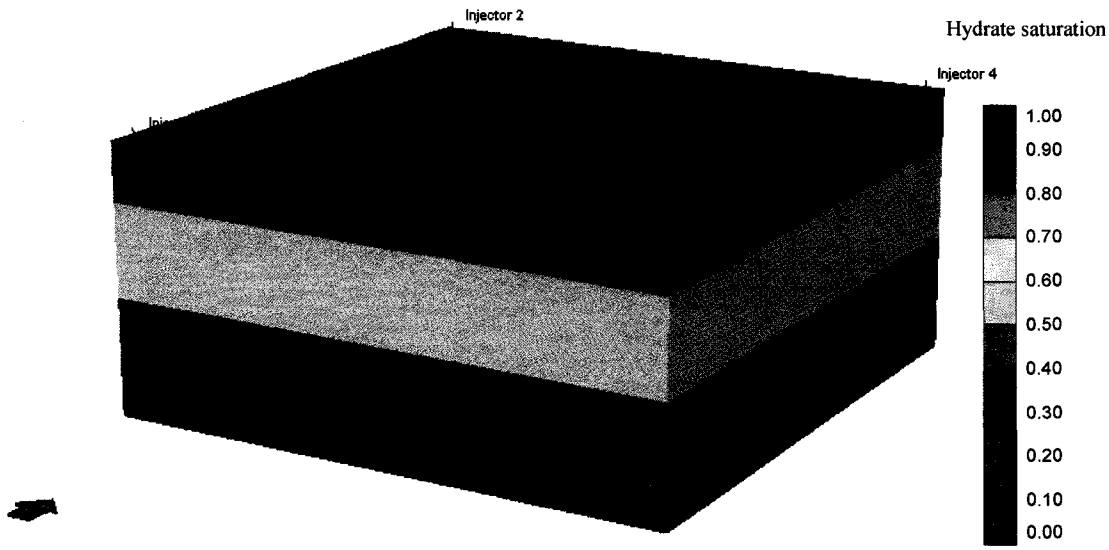

Figure 5.54: Location of Injection and Production Wells Completed in Hypothetical Formation Model

Figure 5.55 shows the cumulative gas production as a function of time for water injection at different temperatures. It can be seen that the production is the highest for the highest water injection temperature (80 °C) and the lowest for no injection (which is depressurization). This is expected because when water is injected at higher temperature, the heat is transferred to the hydrate zone and hydrates get dissociated and gas is produced; naturally the more heat available (i.e. higher the temperature of water injected) the greater the production.

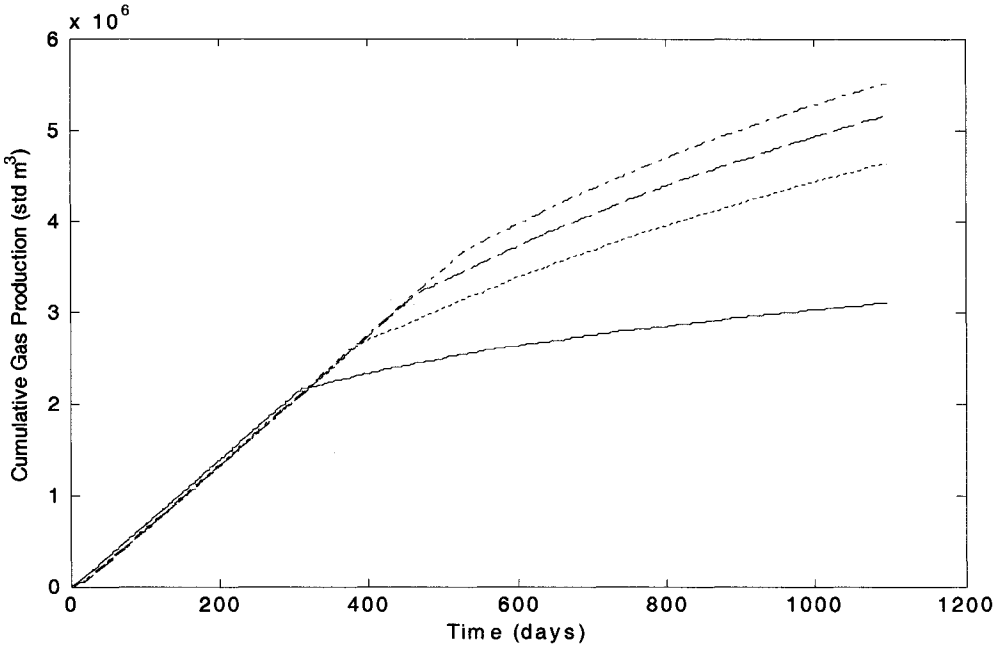

Figure 5.55: Cumulative Gas Production vs. Time (solid line: no injection, dotted line: 40 °C, dashed line: 60 °C, dashed-dotted line: 80 °C)

Figure 5.56 shows the initial temperature conditions in the reservoir. It can be seen that the temperature is the same throughout the reservoir. As the hot water injection starts, the temperature near the injection wells increases and approaches the injection temperature (40 °C). The heat is transferred to the adjacent hydrate zones and the hydrates in that zone get dissociated and the gas is produced from the production well.

Figures 5.57- 5.59 show the change in temperature contour after one, two and three years of hot water injection. It can be seen that as the time passes a larger portion of the reservoir reaches the hot water injection temperature and the overall temperature of the reservoir increases. Also it should be noted that the heat required for hydrate dissociation is taken from the non-dissociated hydrate zone and hence a temperature drop in the non-dissociated hydrate zone can be observed.

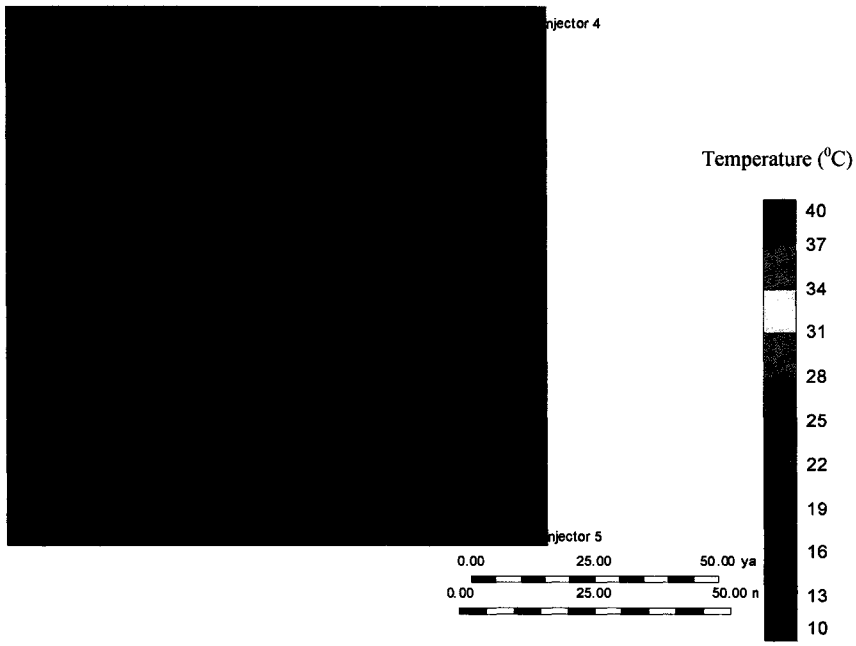

Figure 5.56: Temperature Contours at the Start of Production, Hot Water Injection Method

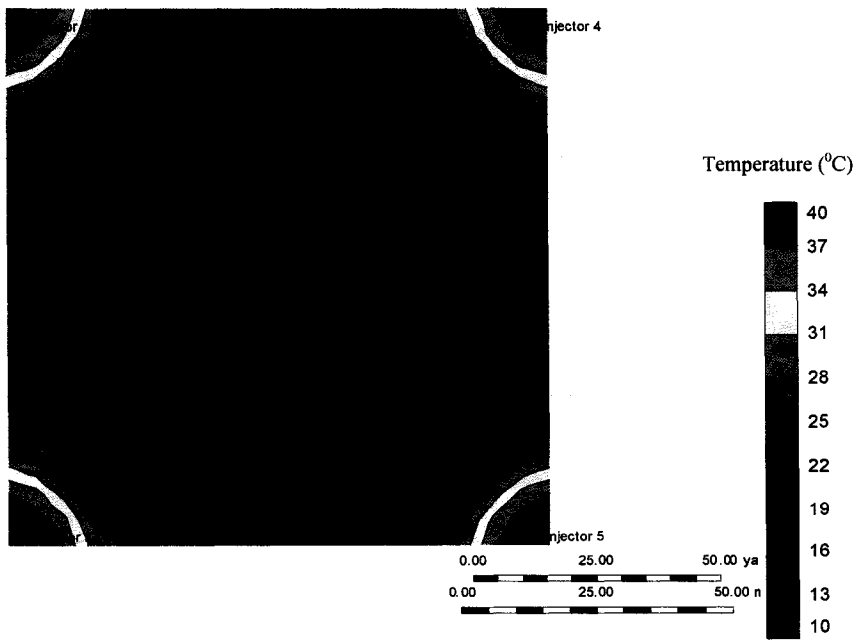

Figure 5.57: Temperature Contours after One Year of Production, Hot Water Injection Method

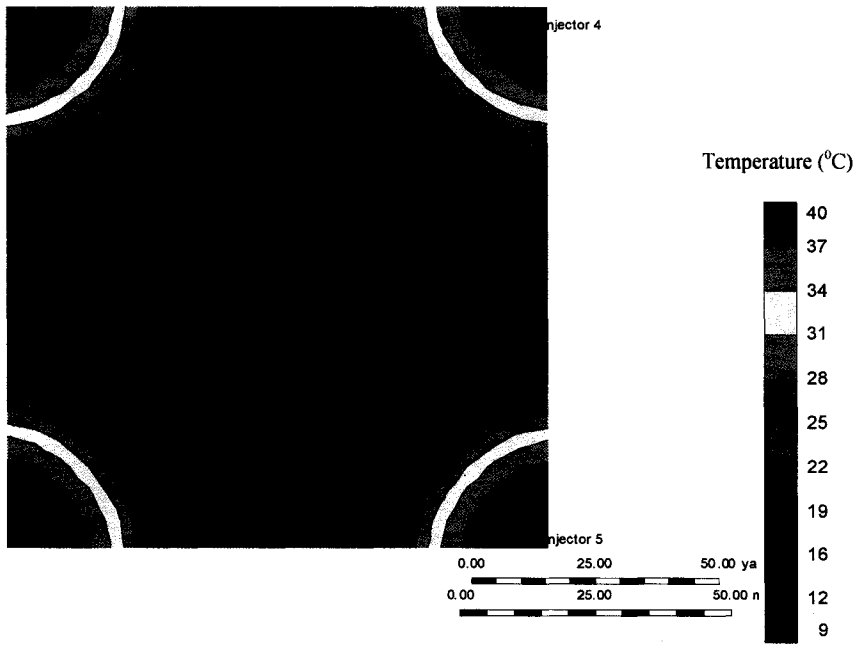

Figure 5.58: Temperature Contours after Two Years of Production, Hot Water Injection Method

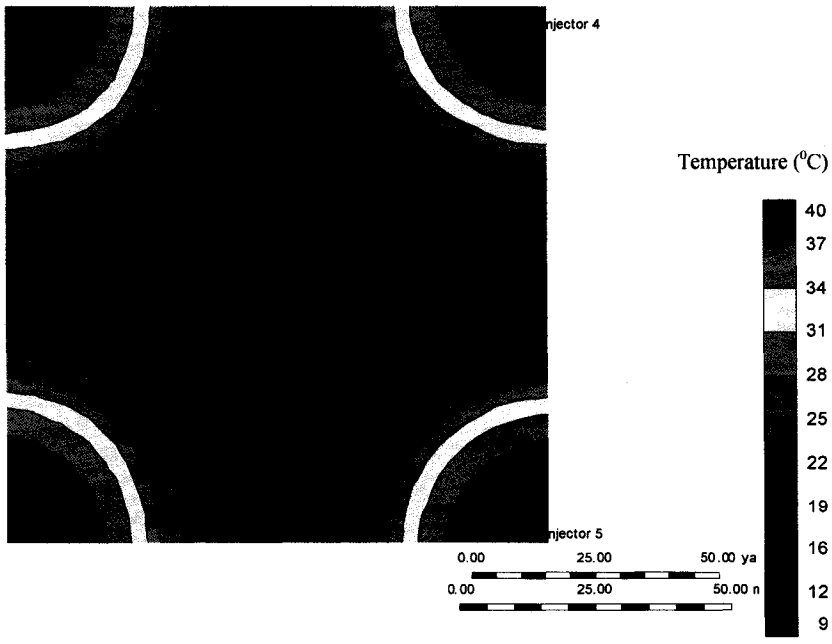

Figure 5.59: Temperature Contours after Three Years of Production, Hot Water Injection Method

Figure 5.60 shows the initial pressure conditions in the reservoir. It can be seen that the pressure throughout the reservoir is the same and it should be noted that this is before any injection or drilling of any well.

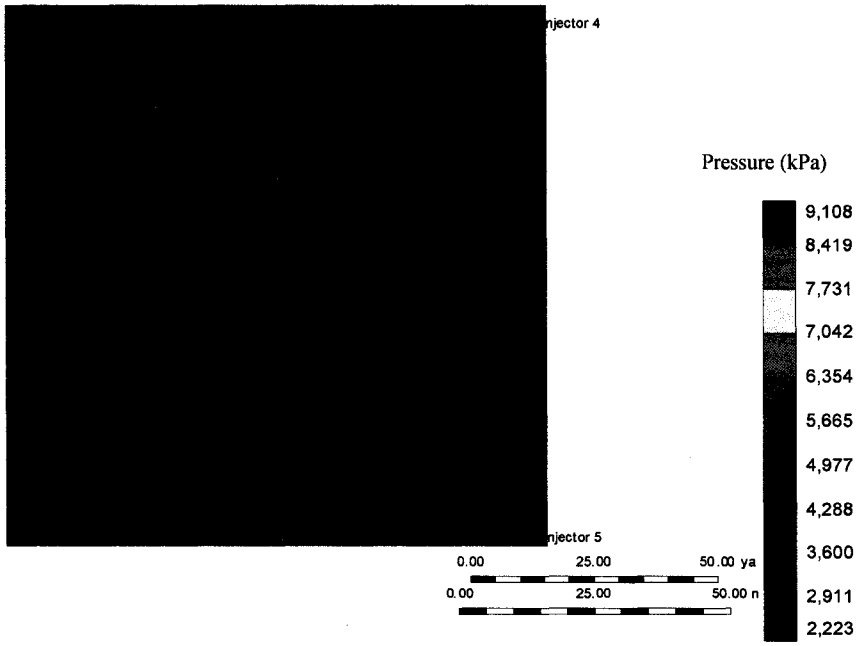

Figure 5.60: Pressure Contours at the Start of Production, Hot Water Injection Method

Figures 5.61- 5.63 show the changes in pressure contours after one, two and three years of production. The pressure near the production well is kept at the minimum pressure required to transport the gas in a 24" pipeline. Because of this, pressure in the adjacent zone decreases and hydrates dissociate. As the gas production starts, the pressure is lowest near the production well and highest near the injection wells because the gas released from hydrate dissociation near the injection wells needs to move towards the production well. The low pressure zone increases in the reservoir with increasing production time.

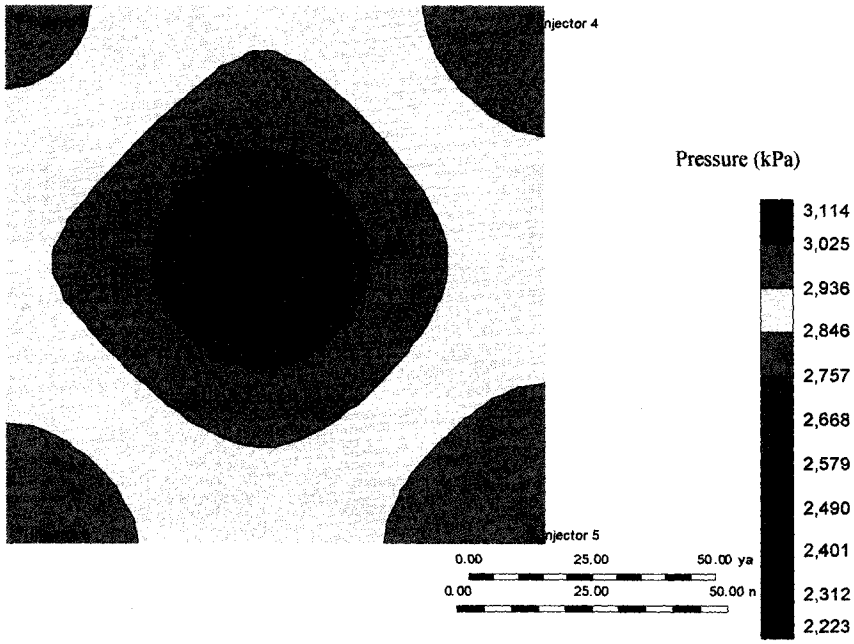

Figure 5.61: Pressure Contours after One Year of Production, Hot Water Injection Method

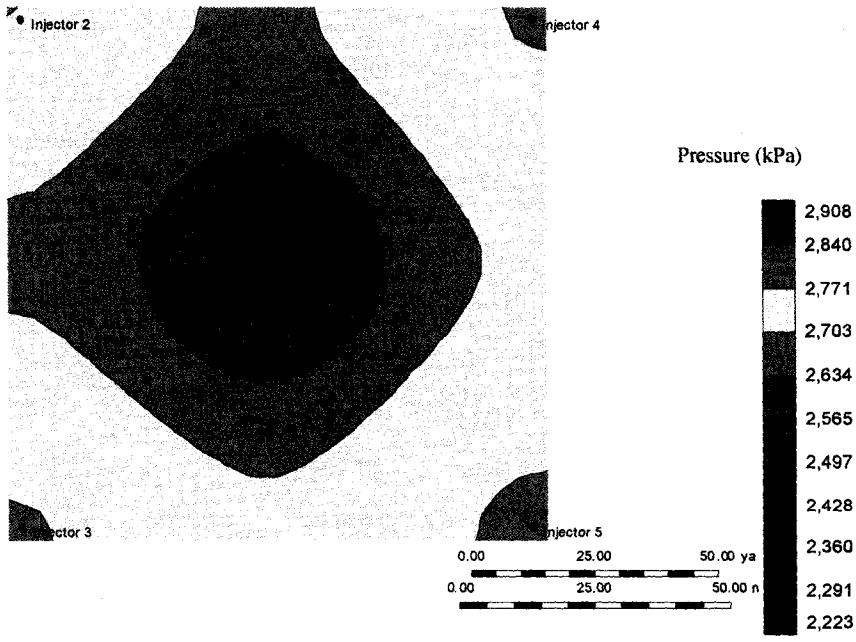

Figure 5.62: Pressure Contours after Two Years of Production, Hot Water Injection Method

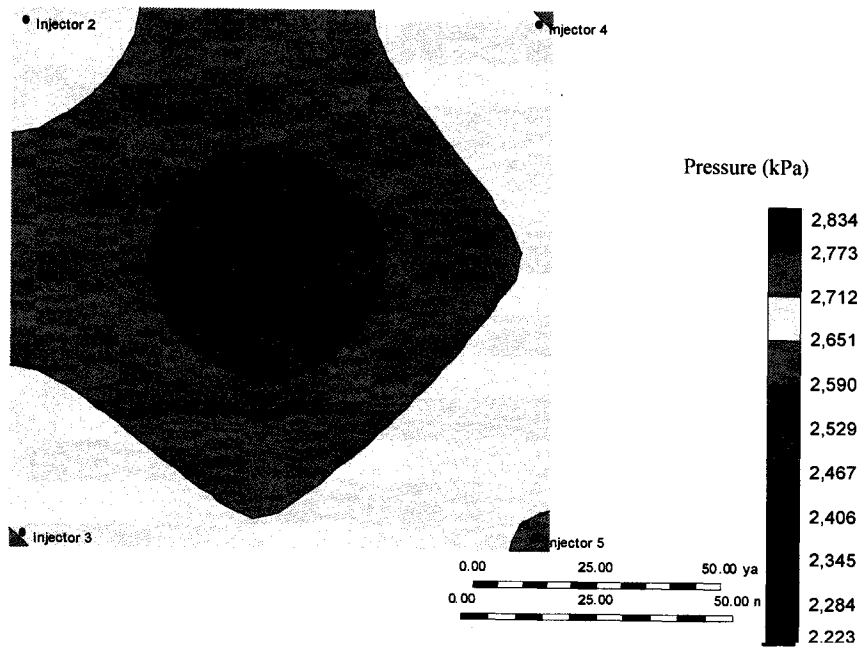

Figure 5.63: Pressure Contours after Three Years of Production, Hot Water Injection Method

Figure 5.64 shows the initial hydrate saturation in the reservoir, which is the same throughout the reservoir. Figures 5.65- 5.67 show the changes in hydrate saturation contours at various stages of production. As hot water is injected into the reservoir, an increase in the temperature near the injection wells dissociates the gas hydrates and hence a drop in hydrate saturation near the injection well is observed. As the pressure in the production well is lowered, the pressure in the adjacent region decreases and the hydrates in that zone dissociate. Thus, the hydrate saturation in that region is lowered. Generally, the rate constant for thermal stimulation (which depends on the temperature, however) is higher than that for depressurization, so the drop in hydrate saturation due to thermal stimulation (near the injection wells) is higher than that due to depressurization (near the production well) at a given time.

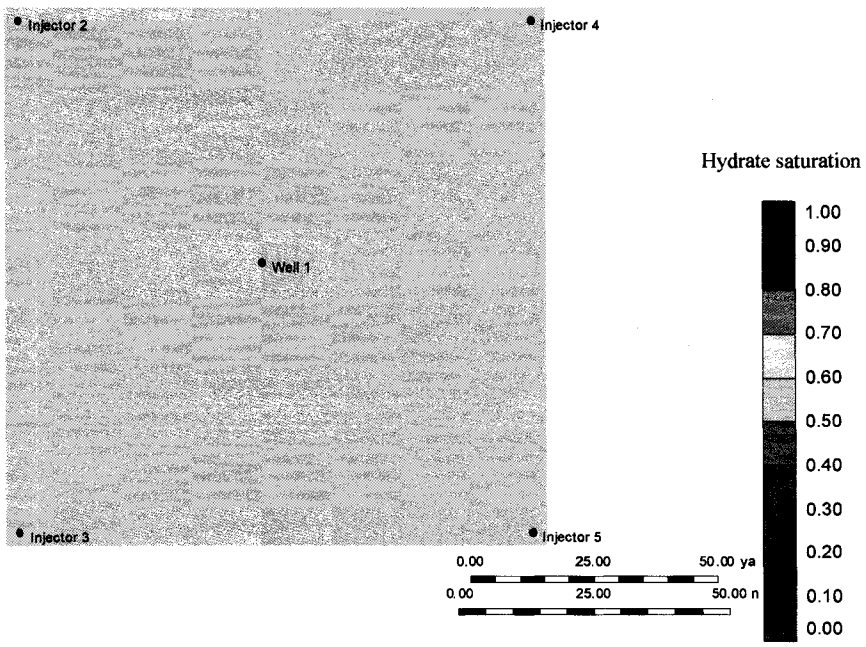

Figure 5.64: Hydrate Saturation Contours at the Start of Production, Hot Water Injection Method

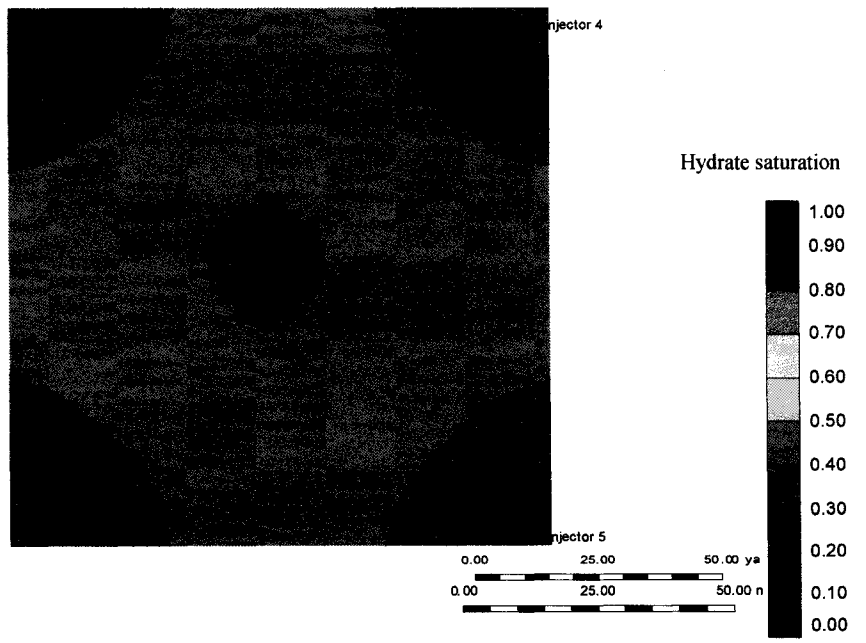

Figure 5.65: Hydrate Saturation Contours after One Year of Production, Hot Water Injection Method

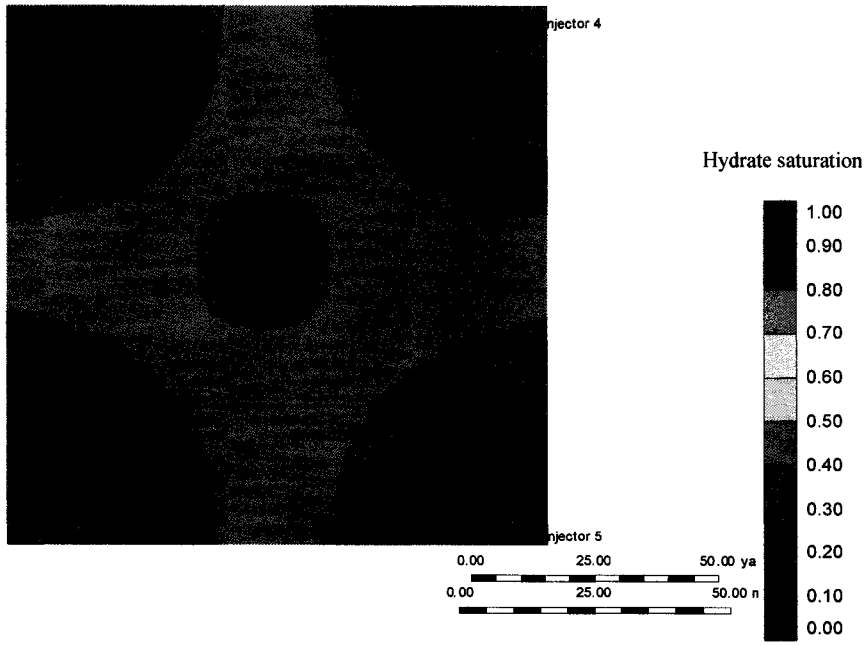

Figure 5.66: Hydrate Saturation Contours after Two Years of Production, Hot Water Injection Method

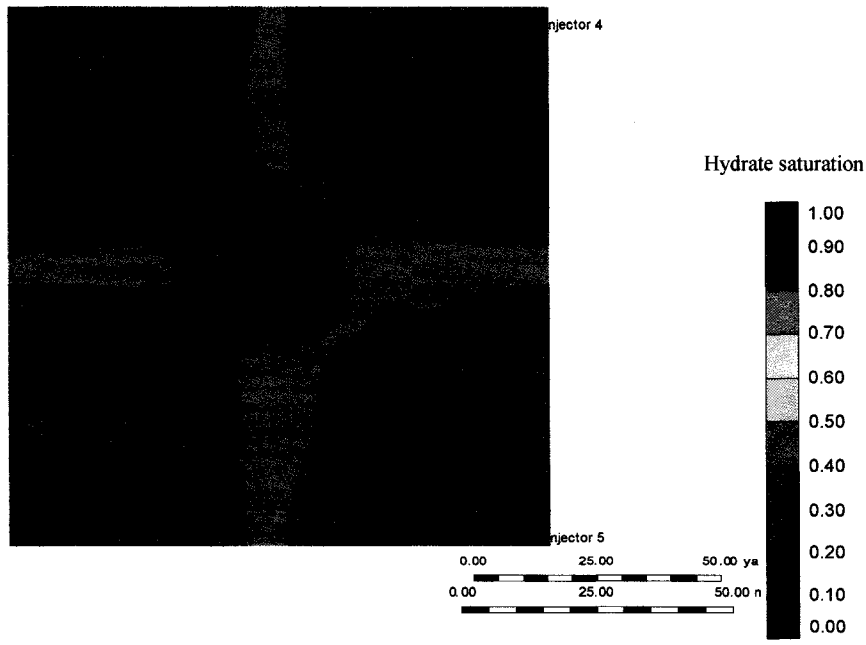

Figure 5.67: Hydrate Saturation Contours after Three Years of Production, Hot Water Injection Method

Figure 5.68 shows the initial water saturation in the reservoir. It is assumed to be constant in the reservoir at 0.4.

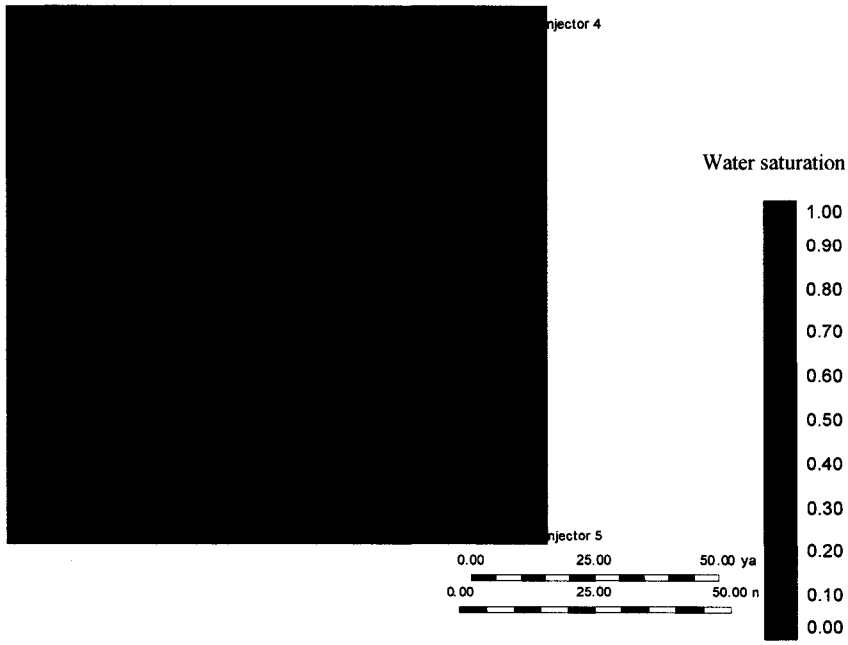

Figure 5.68: Water Saturation Contours at the Start of Production, Hot Water Injection Method

Figures 5.69- 5.71 show the change in the water saturation contours after each year of production. They are quite analogous to the hydrate saturation contours because a water saturation increase is observed when water released due to hydrate dissociation adds to the water present in the region. Low quantities of water are produced on the surface because the produced gas moves much faster than the water. The increase in water saturation near the production well is due to hydrate dissociation caused by depressurization and near the injection wells it is due to hydrate dissociation caused by thermal stimulation.

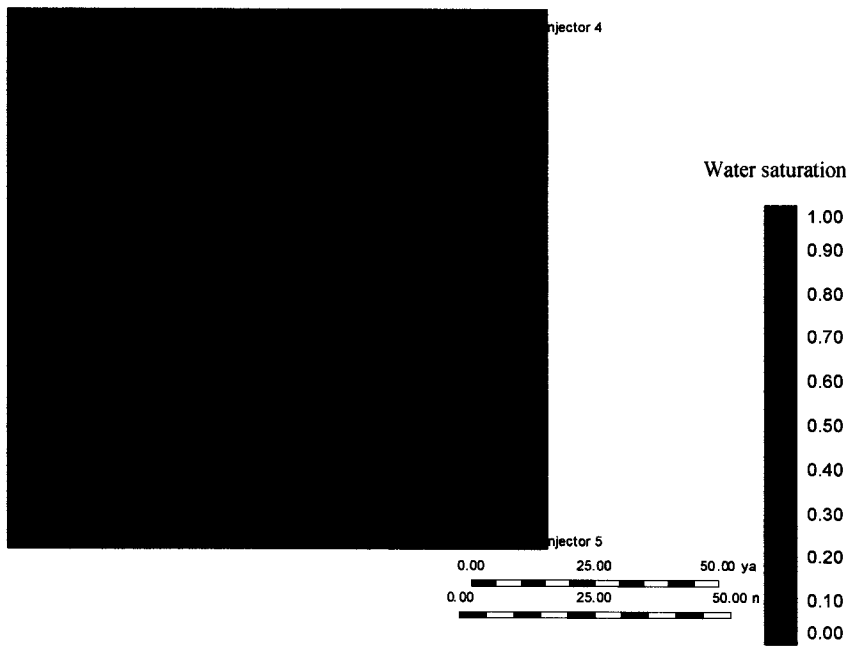

Figure 5.69: Water Saturation Contours after One Year of Production, Hot Water Injection Method

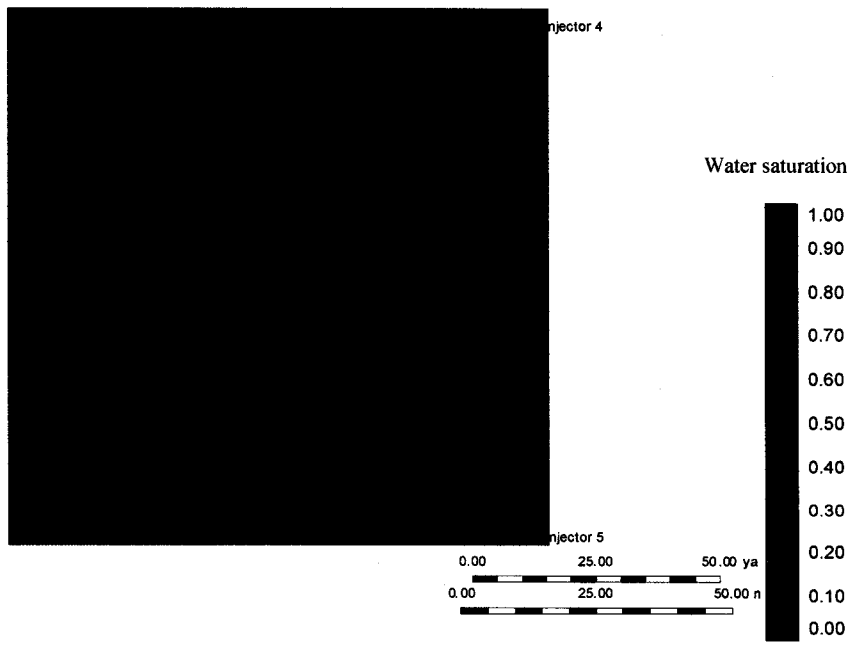

Figure 5.70: Water Saturation Contours after Two Years of Production, Hot Water Injection Method

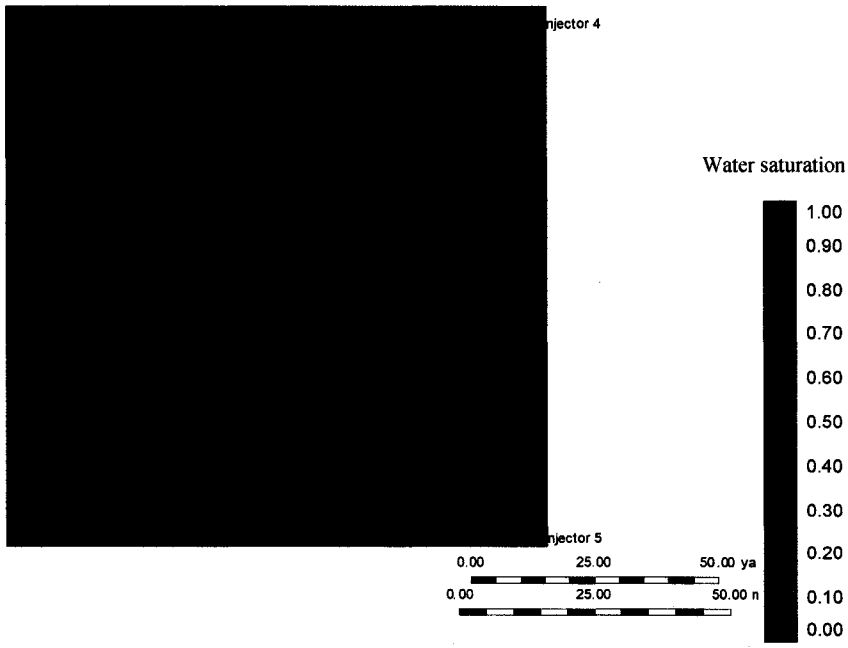

Figure 5.71: Water Saturation Contours after Three Years of Production, Hot Water Injection Method

5.5 Energy Efficiency Calculations

The effectiveness of thermal stimulation is largely dependent on the total energy supplied as well as energy efficiency of the technique. Both these values will affect the economic feasibility of the project.

Energy efficiency is defined as follows:

$$\text{Energy Efficiency} = \frac{\text{Heat Recovered in the form of } CH_4}{\text{Heat Added to the Reservoir}}.$$

Heat added to the reservoir is in the form heat content in the hot water, which is being injected from the injection wells. At any time during production, the total amount of water injected is known. The standard enthalpy per unit mass of water at the water injection temperature is available in the literature. That enthalpy multiplied by the amount of water injected gives the total amount of heat injected in the reservoir at that time.

The cumulative production of CH_4 at any time is given by Figure 5.55. The heating value of CH_4 (kJ/kg) is available in the literature. Heating value multiplied by cumulative production of methane gives the heat recovered in the form of CH_4. By putting these values in the energy efficiency equation, the energy efficiency ratio is obtained.

The energy efficiency ratios for thermal stimulation using different water injection temperatures are given in Figure 5.72. The nature of the graphs is very similar to that of the production curves as expected (Figure 5.55). The production remains constant for the first few days and then declines. Hence the amount of heat recovered from the reservoir in the form of CH_4 also remains constant and then declines. As seen from Figure 5.55, the production remains constant for the first few days irrespective of the water injection temperature, so it is expected that the energy efficiency ratio is low for high water injection temperature and high for low water injection temperature and the same trend is observed in Figure 5.72. However, this should not be taken as the only factor for choosing the water injection temperature as the economic feasibility depends on other factors such as total amount of CH_4 produced in the long run, etc.

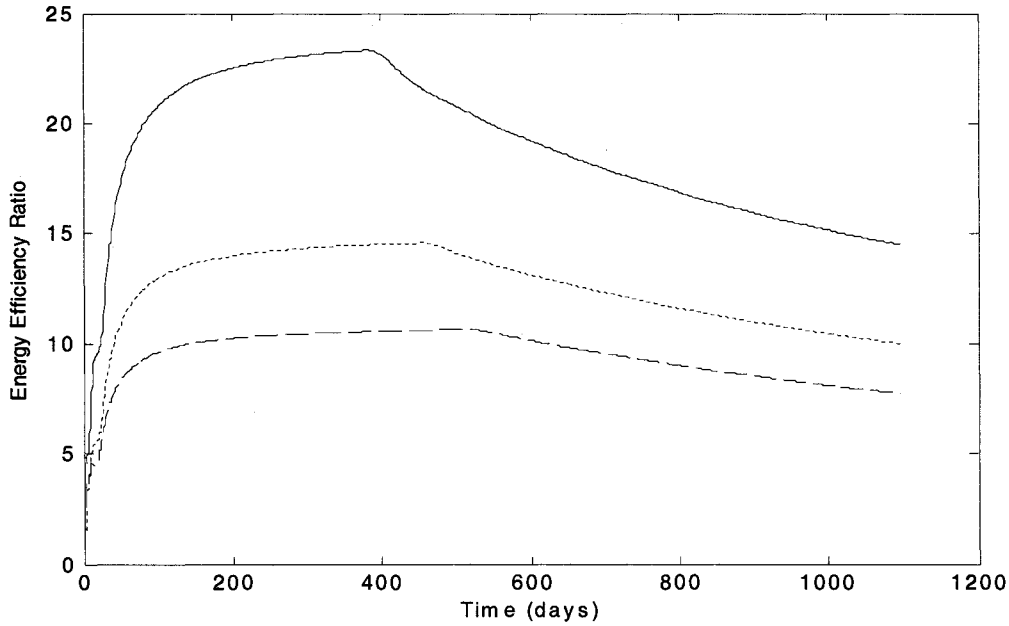

Figure 5.72: Energy Efficiency Ratios vs. Time
(solid line: 40°C, dotted line: 60°C, dashed line: 80 °C)

Figures 5.73 and 5.74 show (in a vertical slice of the reservoir) the comparison of temperature contours when the gas is produced from the reservoir at maximum production rate and at maximum energy efficiency. It can be seen that when the gas is not being produced at maximum energy efficiency, the heat required for the hydrate dissociation is not totally obtained from the hot water, it is also obtained from the non-dissociated hydrate zone. Hence the temperature drop in that zone is observed and it is more than the temperature drop for the case in which the production is achieved at maximum energy efficiency because in the latter case most of the heat required for hydrate dissociation is obtained from the hot water.

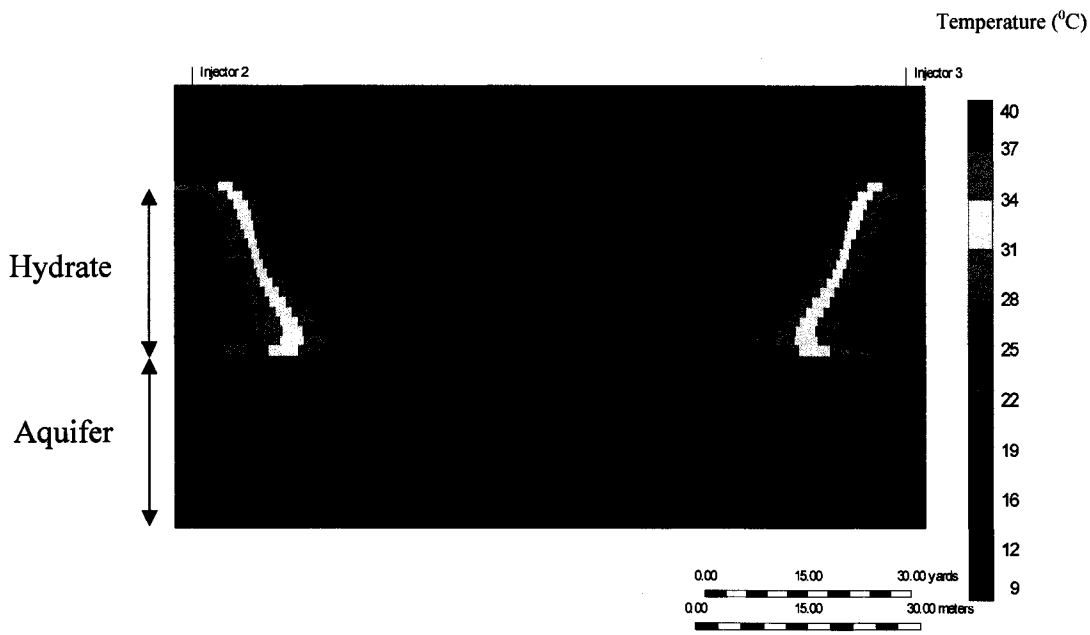

Figure 5.73: Temperature Contours during Hot Water Injection at Maximum Production Rate

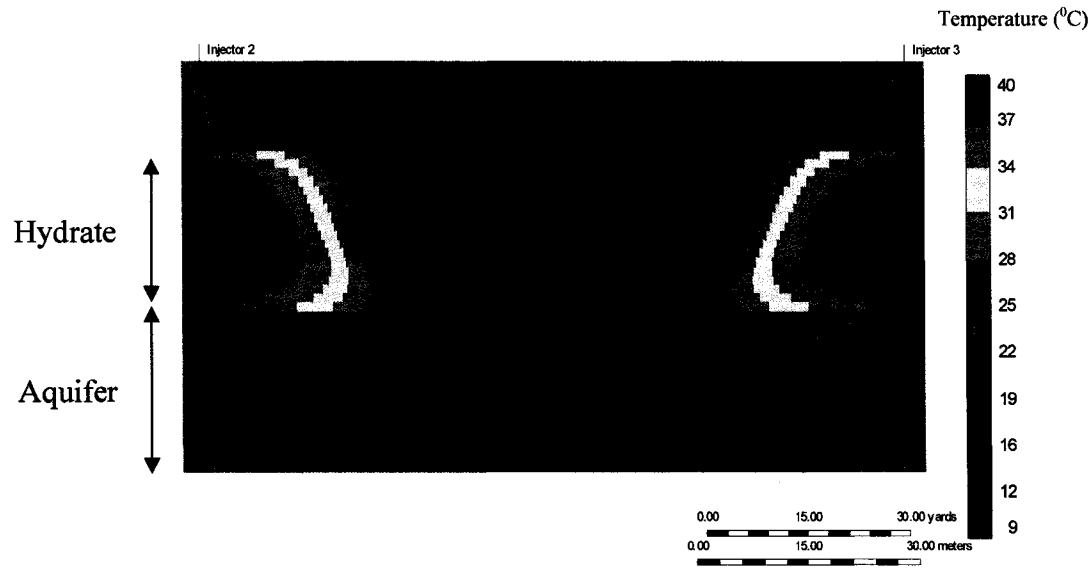

Figure 5.74: Temperature Contours during Hot Water Injection at Maximum Energy Efficiency

Figures 5.75 and 5.76 show the comparison of the hydrate saturation contours when the gas is being produced at the maximum production rate and at the maximum energy efficiency for the same time interval (300 days). These contours are analogous to the temperature contours at maximum production rate. The temperature is lower in the region between the injection and production wells than at maximum energy efficiency. Since at a higher temperature more hydrates dissociate, the hydrate saturation in the region between injection and production well for the maximum energy efficiency is lower than that for the maximum production rate.

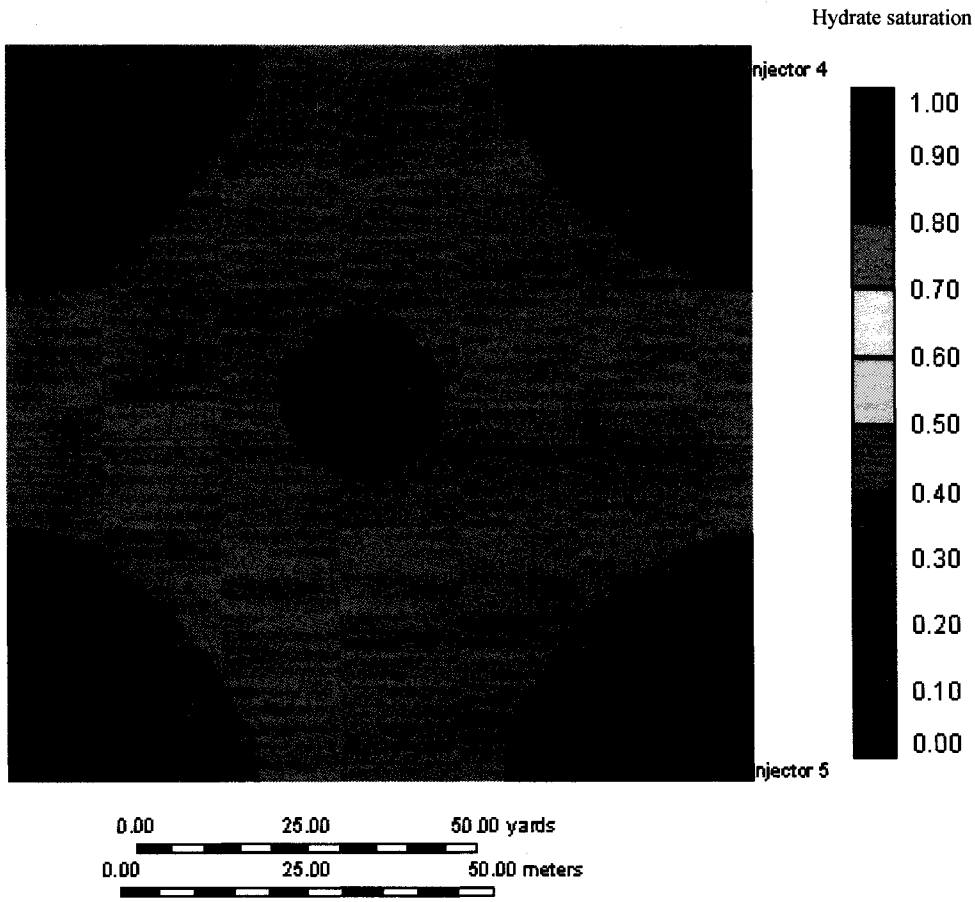

Figure 5.75: Hydrate Saturation Contours during Hot Water Injection at Maximum Production Rate

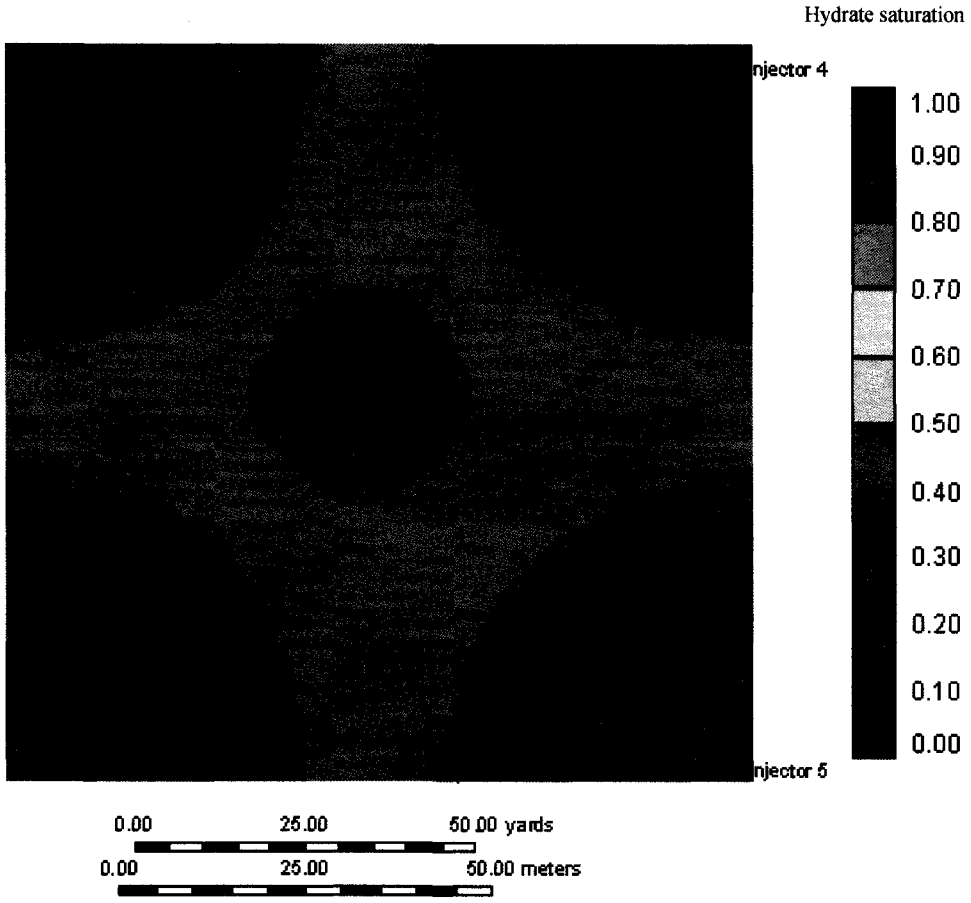

Figure 5.76: Hydrate Saturation Contours during Hot Water Injection at Maximum Energy Efficiency

5.6 Sensitivity Analysis - Axisymmetric Model

Methane gas production from hydrate containing porous media by depressurization is presented in Section 3.3. An analytical model is developed to predict reservoir performance of a hydrate reservoir containing excess methane gas and low hydrate saturation. It is an equilibrium model of hydrate dissociation in axisymmetric infinite homogenous hydrate reservoir and can evaluate pressure, temperature and gas flow rate profiles as functions of time. The effects of variations in well boundary conditions, reservoir temperature and reservoir zone permeabilities are presented in this section.

The axisymmetric model is simulated for an unbounded hydrate reservoir. The linearization method is used to obtain a rapid estimation of gas pressure, temperature distribution, dissociation front position, and production rates. Time variations of pressure and temperature profiles in a hydrate reservoir are presented in this section under various conditions. In addition to this, time evolutions of methane gas production, mass flux and location of the dissociation front are also evaluated. A parametric study and the sensitivity of natural gas production to various parameters are discussed. In this section, numerical results of two base cases are shown, one with constant well pressure and the other with fixed gas output. Finally, the results are compared to study the effect of boundary conditions on gas production. The pressure boundary condition of constant well pressure will be referred to as *BC1* and of fixed natural gas production rate as *BC2*, for simplicity. Simulations are done based on the parameters specified in the nomenclature section.

5.6.1 Pressure, Temperature and Total Mass Flow Profile Distributions for Well Pressure of 2 MPa

For different well pressures and reservoir temperatures the solutions to the non-linear system are listed in Table 5.1. Based upon the present linearized axisymmetric model, the

resulting values of dissociation pressure and temperature and the position of the moving front are fixed. Table 5.1 shows that when the well pressure increases, the dissociation pressure and temperature change only slightly. The value γ, which controls the movement of the front and gas production rate, decreases sharply with increase of well pressure. Keeping the well pressure at 2 MPa, a decrease of 2 K in the reservoir temperature lowers the value of dissociation pressure by about 16%. In addition, dissociation temperature and the parameter γ decrease with the drop in reservoir temperature.

Time variations of temperature and pressure profiles in the reservoir for a well pressure of 2MPa and a reservoir temperature of 287K are plotted in Figure 5.77. Here, the permeability in the gas zone is 5.2md and the hydrate zone permeability is 0.4md. As can be seen from the Figure 3.1, the whole reservoir can be divided into two distinct regions: the gas zone and the hydrate zone. The gas zone is immediately adjacent to the production well, and the temperature is dropped to its minimum value at the well. The pressure at the well is reduced to a constant value below the dissociation pressure and maintained at that value. Near the well, the pressure gradient becomes quite high. No appreciable change in the slopes of temperature profiles is noticed at the decomposition front. However, a small jump in the values is observed at the front. The hydrate zone lies far away from the decomposition front. In this region, the temperature and pressure decreases gradually from the equilibrium reservoir values to the dissociation temperature and pressure at the front. In these regions, variations in distribution of temperature and pressure are quite different. Temperature and pressure profiles for different times are also self-similar and expand outward as the decomposition front moves away from the well.

Table 5.1: Values of Dissociating Temperature and Pressure and Parameter γ for Given Reservoir and Well Conditions.

p_{in} (MPa)	T_{in} (K)	p_W (MPa)	T_D (K)	p_D (MPa)	γ (m^2/s)
15	287	2	279.89	5.418	$1.629*10^{-6}$
15	287	3	280.002	5.473	$6.917*10^{-7}$
15	287	4	280.29	5.628	$1.778*10^{-7}$
15	287	5.5	280.96	6.006	$3*10^{-8}$
15	285	2	277.963	4.535	$1.266*10^{-7}$
15	283	2	276.02	3.826	$9.862*10^{-9}$

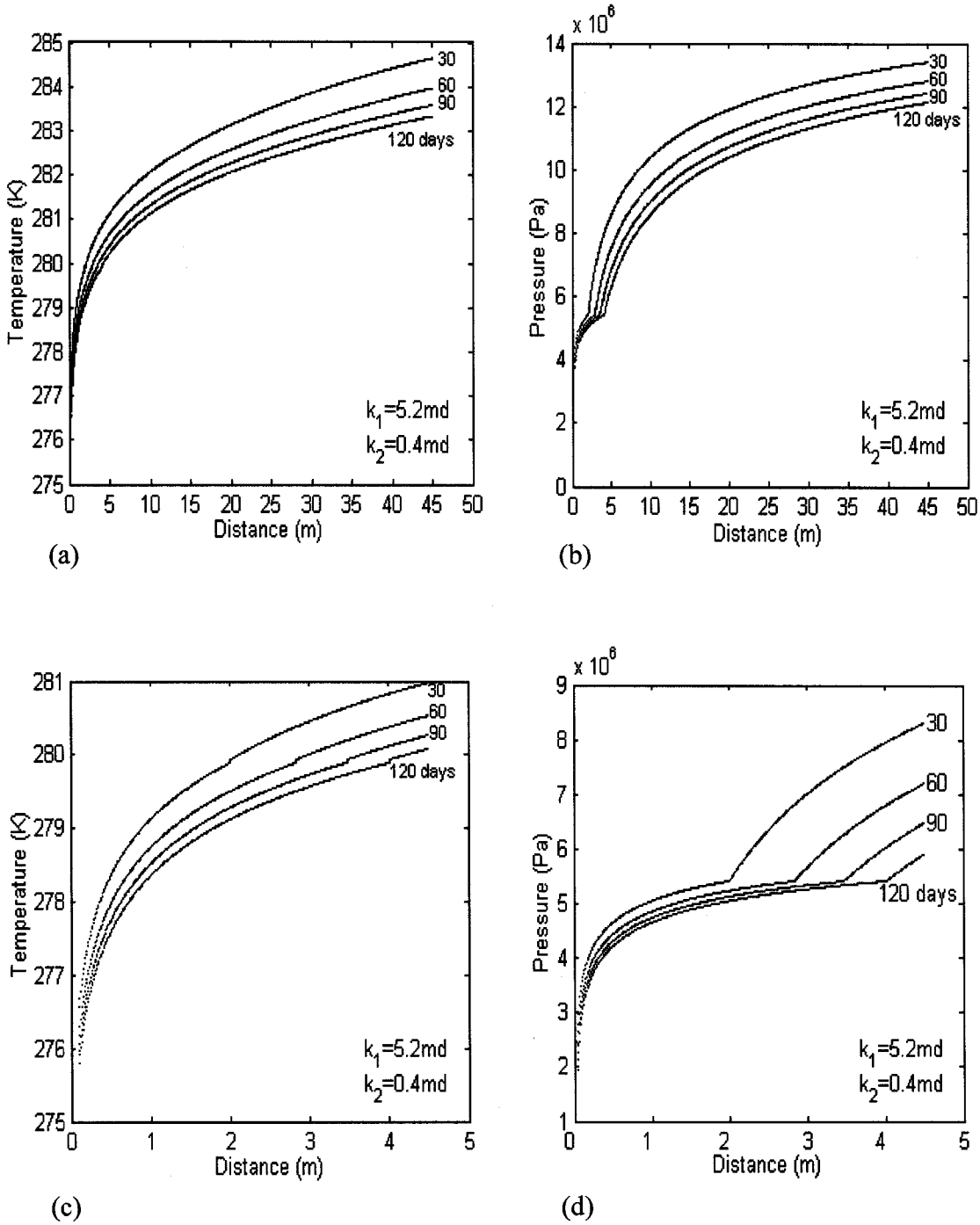

Figure 5.77: Temperature and Pressure Profiles in an Extended Field (a), (b) and in Near-Well Zone (c), (d).

Figure 5.78 shows the time evolutions of gas mass flux (ρv) and the total mass flow ($2\pi r\rho v$) across the reservoir for a well pressure of 2 MPa. Mass flux increases towards the well and decreases with time. This figure clearly displays that the variation of the mass flux and the amount of natural gas produced is independent of time in each zone. It is also seen that there is a jump in the gas mass flux and the total mass flow at the decomposition front and the jump propagates with time as the decomposition front penetrates deeper into the hydrate zone. Obviously, the sudden jump in these profiles indicates the production of gas from hydrate decomposition.

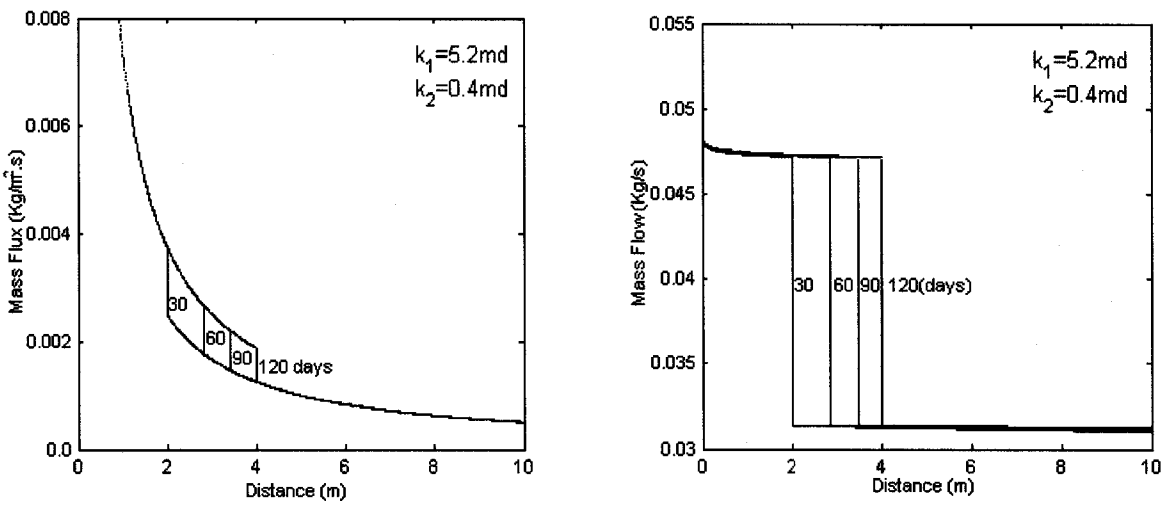

Figure 5.78: Mass Flux and Total Mass Flow Profiles

In this section, the effect of reservoir temperatures and well pressure on variations of pressure, temperature and gas flow is studied. Figure 5.79 compares the profiles of pressure, temperature and natural gas flow for a well pressure of 2 MPa and 285 K (2 K lower than the previous case) with the basic reservoir condition case. These profiles are quite similar to those shown for 2 MPa well pressure and 287 K reservoir temperature. Comparatively, the dissociation pressure and temperature in this case are noticeably smaller. The movement of the dissociation front slows down because of lower reservoir temperature. If the reservoir temperature is lowered, then the natural gas production is

decreased. Thus, the reservoir temperature becomes an important controlling parameter in estimating the gas production. This observation shows the importance of heat transfer to hydrate dissociation and production processes. The energy balance is modeled by considering the system to be adiabatic. Because of this fact, heat transferred from the surroundings, which is not taken into account, could significantly affect the production process. When the reservoir temperature increases, the dissociation pressure and temperature change noticeably as shown in Table 5.1. The value γ, which controls the gas production rate, increases sharply with increase in initial temperature. Comparison of the pressure, temperature and natural gas flow distribution for a well pressure of 4 MPa and 287 K with the base case of 2 MPa and 287 K is also shown in Figure 5.79. No significant change in the variation of these profiles is noted except for large gradients at the front in the hydrate zone. As the pressure increases, the dissociation pressure and the temperature at the front become close to the well conditions and the moving boundary slows down. Thereby, the pressure gradient in the gas zone decreases causing the lower gas production. But at a high well pressure, the well can be operated a long time as the outward motion of the dissociation front is slow. For high well pressure, the pressure and temperature profiles approach their reservoir values near the well bore, for lower radial distance from the well, and the gas zone is comparatively small.

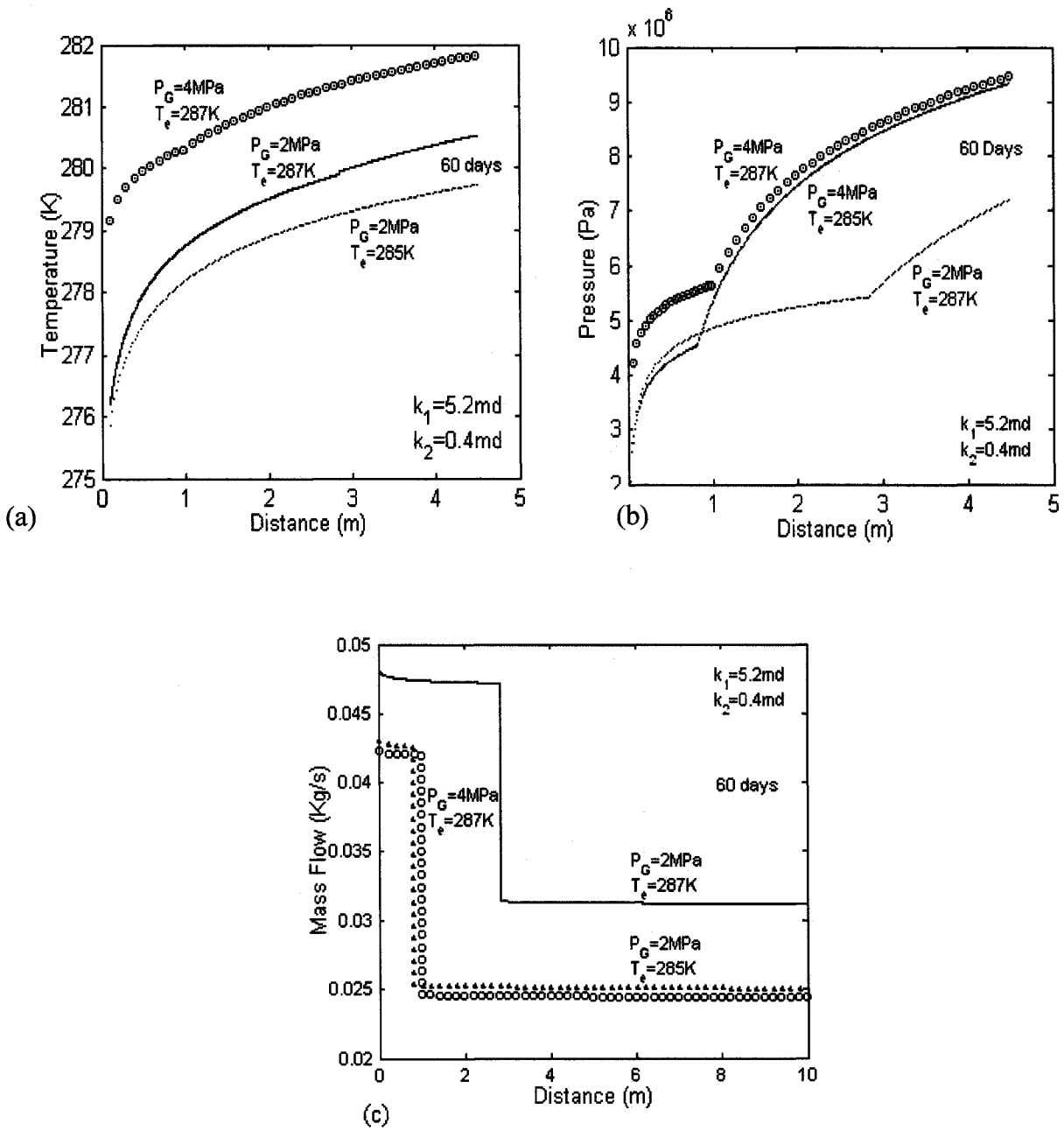

Figure 5.79: Comparison of Temperature, Pressure and Natural Gas Flow for Different Well Pressures and Reservoir Temperatures.

The effect of well pressures on movement of the dissociation front is studied in this section. Here the reservoir conditions are kept constant. The distance of the front from the well is proportional to the square root of time as expected and schematically shown in

Figure 5.80a. As the well pressure increases, the motion of the front decreases, especially as the well pressure approaches the decomposition pressure. The position of the decomposition front for a well pressure of 2 MPa and for different initial reservoir temperatures is shown in Figure 5.80b. It is shown that the reservoir temperature significantly affects the motion of the front as well as natural gas output. This study gives a quick estimation of natural gas output for different reservoir temperatures.

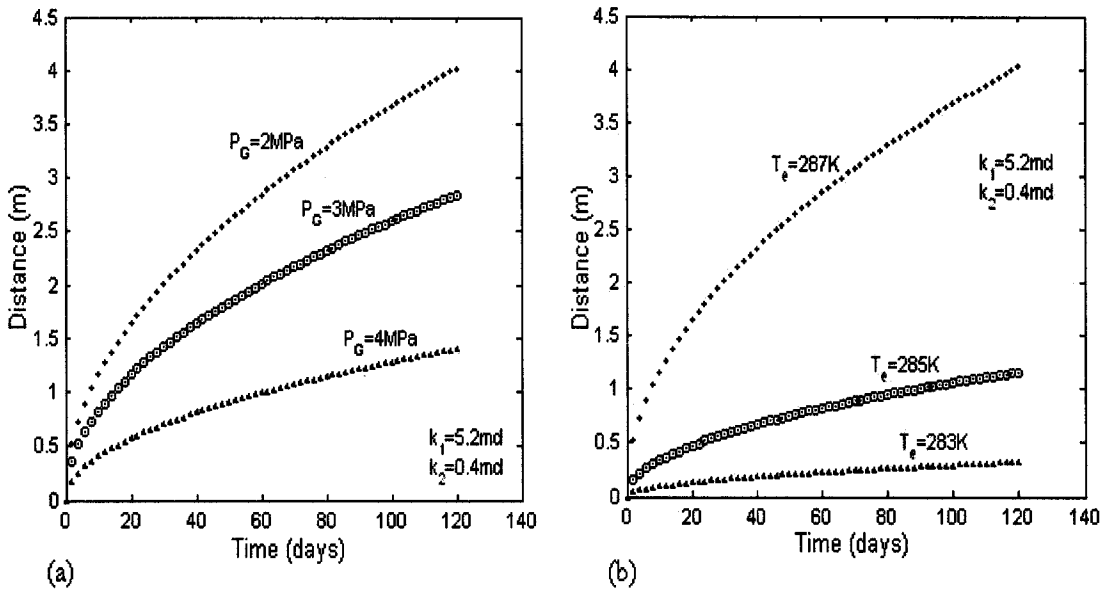

Figure 5.80: Comparison of Location of Dissociation Front for Different Well Pressures and Reservoir Temperatures.

In this section, variations of natural gas production rate, as well as the reservoir pressure and temperature profiles for different permeabilities are studied. Here, the porosity and hydrate saturation are kept constant at $\phi = 0.2$ and $S_H = 0.19$. It should be understood that the permeability and porosity are related by the Kozeny-Carman equation and constant porosity in this simulation is an idealization. Sensitivity analysis to the reservoir parameter porosity when permeability is a function of porosity is discussed in the next section. Computed values of dissociation pressure and temperature and parameter γ for

different values of the zone permeabilities are listed in Table 5.2. Dissociation pressure and temperature decrease and parameter γ increases with increase in gas zone permeability. Variations of the temperature, pressure and gas flux profiles and the displacement of the front when the permeability of the gas and hydrate zone vary as a function of time are presented in Figure 5.81. In this case, there is an obvious pressure gradient change at the dissociation front, controlling the movement of the dissociation front and natural gas output. It is observed that the variation in the hydrate zone permeability has a significant effect on the gas production and a negligible effect on the gas output. Relative permeability for the gas in the gas zone is expected to be somewhat greater than that in the hydrate zone. It is shown that the flow rate decreases with time and with increase in hydrate permeability. When the hydrate zone permeability decreases, the amount of gas flow towards the front also decreases allowing low dissociation values at the front. As noticed in Table 5.2 the change in dissociation values is not very significant. In order to maintain the same pressure gradient in the gas zone, more hydrate has to dissociate, and therefore, the dissociation front penetrates deeper into the hydrate zone as the hydrate zone permeability decreases. Decrease in hydrate zone permeability reflects the change in the nature of the pressure distribution. Large pressure gradients are observed at the front in the hydrate zone and the pressure gradient in the gas zone increases with an increase in hydrate zone permeability. Pressures in the gas zone decrease from the dissociation pressure at the front to the well pressure, with a slope that is a sensitive function of permeability in the hydrate zone. Temperature decreases gradually in the hydrate zone and decreases with a sharper slope in the gas zone as hydrate zone permeability increases. The effect of gas zone permeability on the temperature distribution and values of dissociation temperature is not very significant.

Table 5.2: Values of Dissociating Temperature and Pressure and Parameter γ for Different Zone Permeabilities

p_{in} (MPa)	T_{in} (K)	p_W (MPa)	k_1 md	k_2 md	T_D (K)	p_D (MPa)	γ (m^2/s)
15	287	2	5.2	0.4	279.89	5.418	$1.629*10^{-6}$
15	287	2	5.2	1	280.53	5.75	$3.94*10^{-8}$
15	287	2	5.2	3	280.97	6.003	$3.94*10^{-10}$
15	287	2	1	1	281.3	5.945	$8.335*10^{-9}$

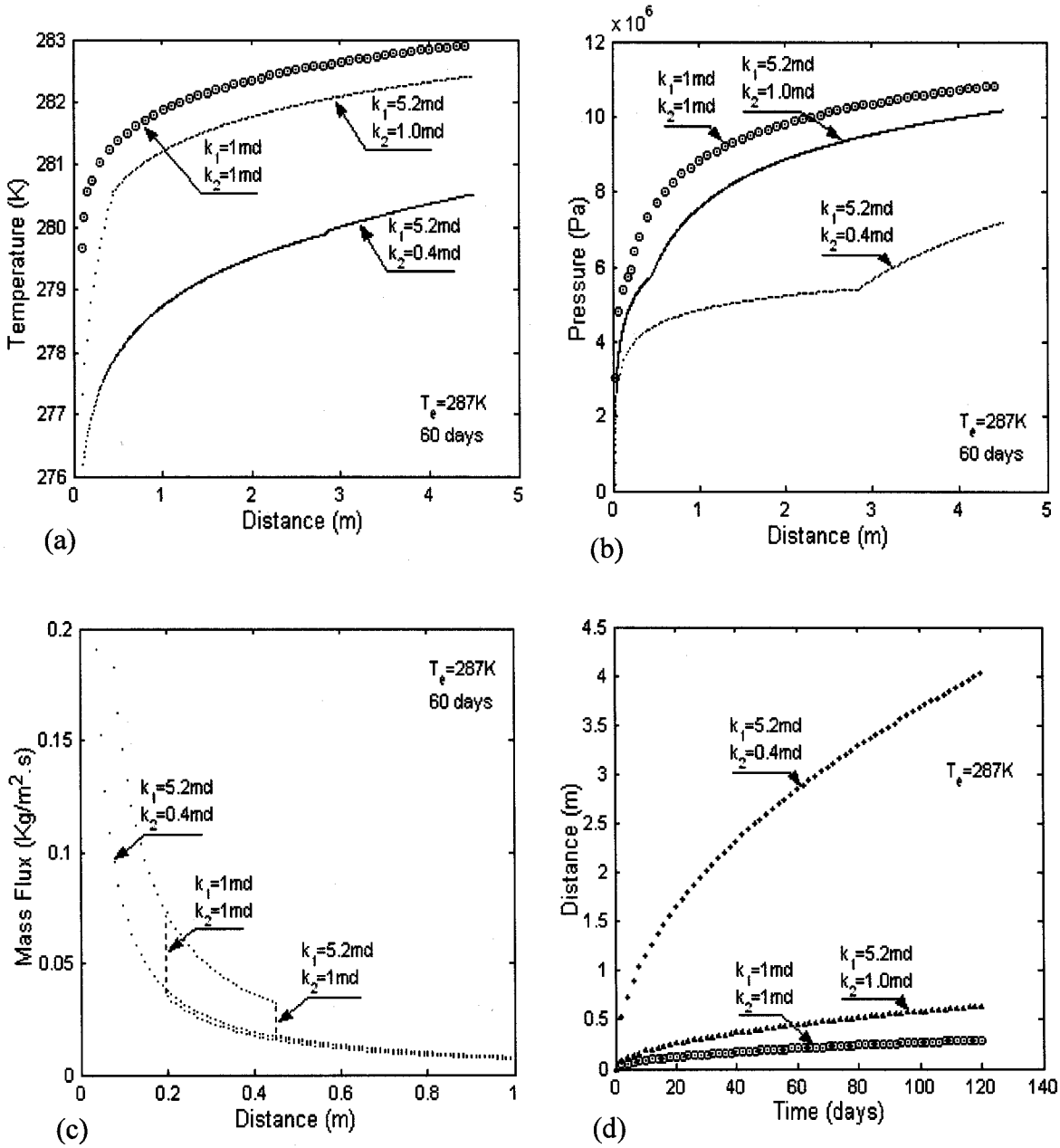

Figure 5.81: Comparison of Temperature, Pressure, Gas Flux Profiles and Location of Dissociation Front for Different Permeabilities

Reservoir porosity is one of the important parameters, which can control the production rate. In this case, the zone permeabilities are allowed to change as a function (Kozeny-Carman equation) of porosity and hydrate saturation and other reservoir conditions are kept constant. Variations of the temperature, pressure, and gas flux profiles and the displacement of the front with change in reservoir porosity are displayed in Figure 5.82. Table 5.3 lists the dissociation pressure and temperature and parameter γ for different reservoir porosities. It is observed that the dissociation pressure and temperature and the parameter γ decrease with increases in reservoir porosity and permeability. With an increase in reservoir porosity, the decomposition front moves more slowly and both the hydrate and gas zone temperatures decrease. Gas output increases, as there is a large amount of hydrate available to dissociate with an increase in zone permeabilities and porosities. The pressure profiles are self-similar but with an increase in porosity, the magnitude of the pressure increases in the hydrate zone as the driving force is large, and decreases in the dissociated zone as the driving force is small.

Table 5.3: Values of Dissociating Temperature and Pressure and Parameter γ for Different Reservoir Porosities

p_{in}(MPa)	T_{in}(K)	p_W(MPa)	k_1 md	k_2 md	ϕ	T_D(K)	p_D(MPa)	γ (m^2/s)
15	287	2	5.2	0.4	0.2	279.89	5.418	$1.629*10^{-6}$
15	287	2	17.55	1.35	0.3	278.21	4.639	$3.968*10^{-7}$
15	287	2	41.6	3.2	0.4	276.95	4.151	$1.417*10^{-7}$

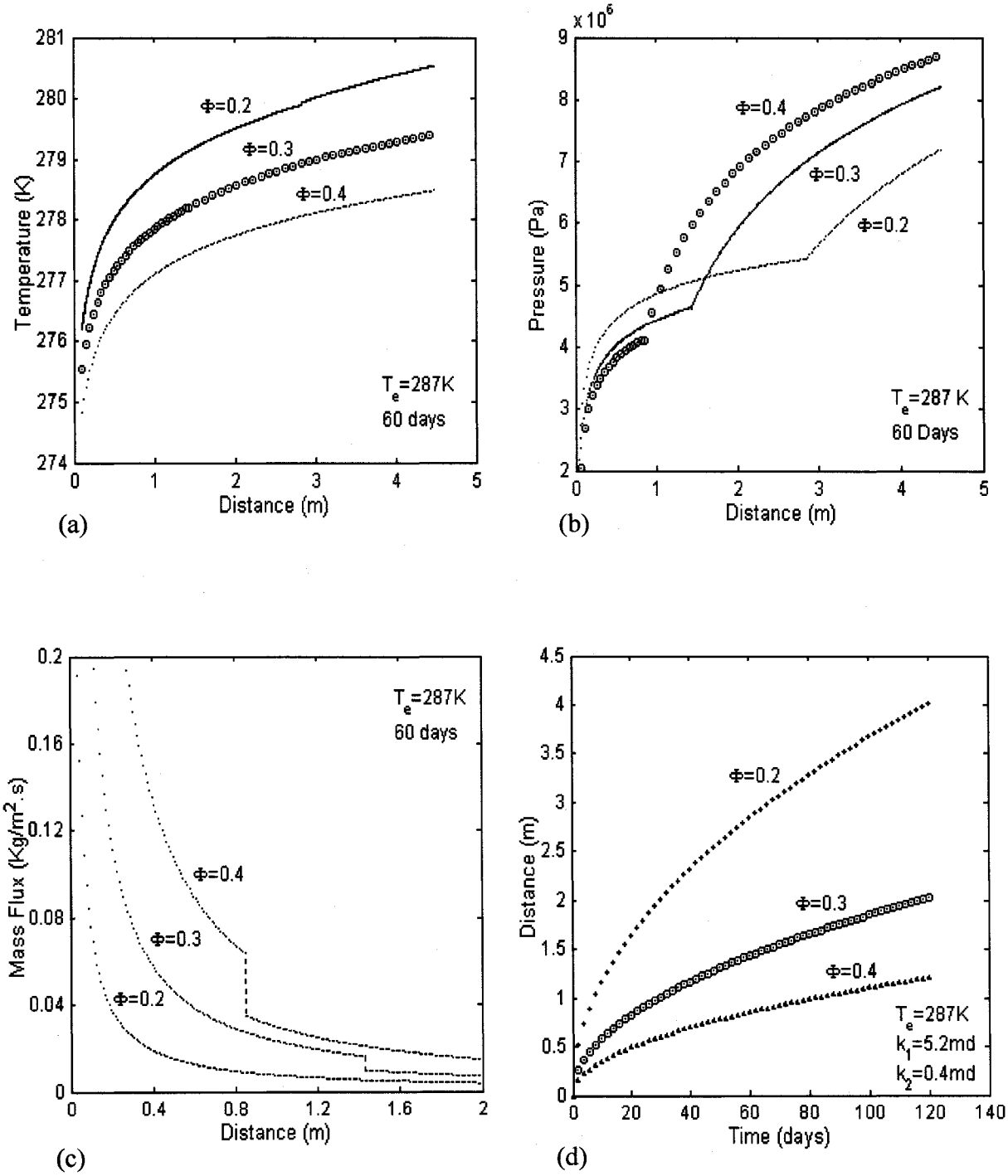

Figure 5.82: Comparisons of Temperature, Pressure, Gas Flux Profiles and Displacement of Dissociation Front for Different Porosities

Time variations of pressure, temperature and mass flow profiles in a reservoir for fixed gas production rates are discussed and compared with those for constant well pressure. Effects of different well boundary conditions are emphasized in this section. Values of dissociation pressure, temperature and parameter γ for different gas output rates are tabulated in Table 5.4. Except for a different well boundary condition, the other initial and the boundary conditions and the physical properties discussed earlier are used in these results. The values presented in the Table 5.4 are somewhat different from those obtained by Ji et al. (2003). The dissociation values of temperature, pressure and parameter γ listed in the table and figures displayed in the work of Ji et al. (2003) appear to be inconsistent. For a reservoir temperature of 287K and a pressure of 15 MPa and the natural gas production rate of 0.04 Kg/s, the dissociation temperature and pressure calculated by Ji et al. (2003) are 281.96 K and 6.65 MPa respectively. From Figure 2 of Ji et al. (2003) the dissociation temperature and pressure seem to be around 279.5 K and 5.0 MPa, respectively. The position of the dissociation front calculated from the parameter γ listed in his Table 5.1 is around 12 meters. In comparison with their Figure 2, the dissociation front is at about 9 meters after 60 days. Inconsistencies in these values have been noticed for all different natural gas production rates. The dissociation values for fixed gas output were thus simulated again and compared with the values for constant well pressure. Table 5.4 shows the acceptable values of dissociation temperature and pressure and parameter γ for different gas flow rates.

Table 5.4: Values of Dissociating Temperature and Pressure and Parameter γ for Given Reservoir and Well Conditions (*Constant Gas Output*)

p_{in} (MPa)	T_{in} (K)	Q (Kg/S)	T_D (K)	p_D (MPa)	γ (m^2/s)
15	287	0.04	279.334	5.1409	$1.538*10^{-5}$
15	287	0.03	279.8016	5.3704	$2.4215*10^{-6}$
15	287	0.02	280.471	5.7227	$6.4269*10^{-8}$
15	287	0.01	281.274	6.1811	$4.457*10^{-8}$
15	285	0.03	277.505	4.3535	$1.642*10^{-6}$
15	283	0.03	275.347	3.6137	$1.302*10^{-6}$

Comparison of the temperature and pressure profiles as obtained by the *BC1* and *BC2* boundary conditions is shown in Figure 5.83. It is seen that for both conditions, the trends of temperature and pressure profiles throughout the reservoir are similar. It is observed that the mass flow profile is almost constant across the reservoir when constant flow rate is employed at the well. There is a small decrease in the gas production in the hydrate zone, which is compensated by an equally small increase in gas production at the well. When this case is discussed with the one maintaining constant well pressure it is observed that the *BC1* boundary condition produces more gas output than *BC2*. Also, the movement of the dissociation front is slower in case of *BC1* to *BC2*, allowing the well to be operated for longer periods. As a result, the total gas production is increased.

Table 5.5: Values of Dissociating Temperature and Pressure and Parameter γ for Different Zone Permeabilities (*Constant Gas Output*)

p_{in} (MPa)	T_{in} (K)	k_1 md	k_2 md	T_D (K)	p_D (MPa)	γ (m^2/s)
15	287	5.2	3	281.673	6.4185	$1.245*10^{-8}$
15	287	5.2	1	280.698	5.8484	$1.043*10^{-8}$
15	287	5.2	0.4	279.334	5.1409	$1.538*10^{-5}$
15	287	1	1	280.698	5.8484	$1.043*10^{-8}$

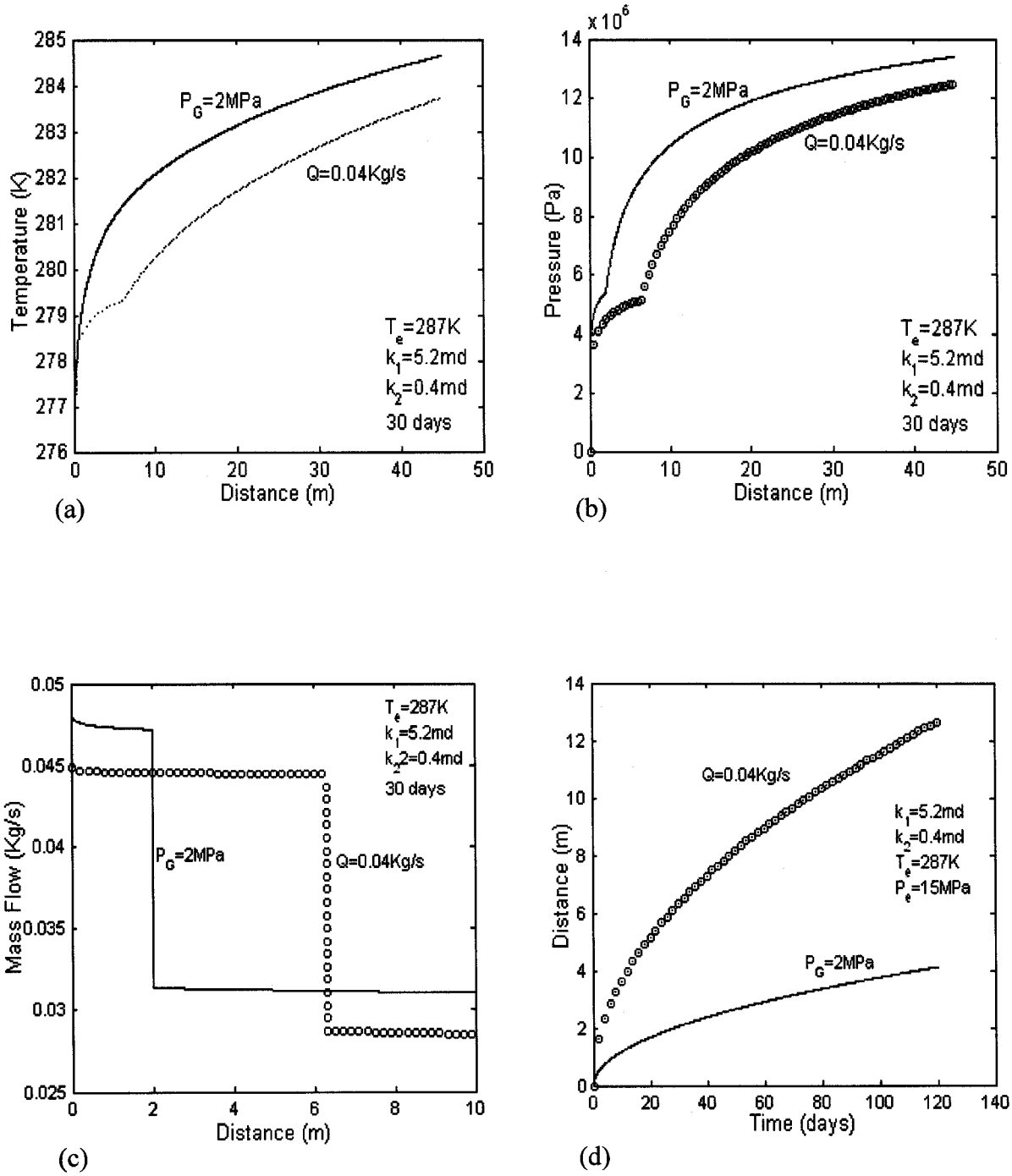

Figure 5.83: Comparisons of Temperature, Pressure, and Gas Flow Profiles and Displacement of Dissociation Front for Different Boundary Conditions

5.7 Simulation Results - Steam Injection

While recognizing that this study has limitations due to the small amount of definitive input data and the approximations used, coupled with the imprecision of the gas hydrate dissociation simulator, useful conclusions can still be drawn from the study. Production profiles generated from the simulations indicate that an accumulation of methane hydrate in a reservoir will begin to dissociate into free gas when the reservoir pressure is lowered.

The base case run used the values given in Table 4.3. An absolute permeability of 300 md was assigned to the reservoir rock and the well had a maximum flow rate of 283168.5 m^3/day (10 mmscfd) resulting in an overall peak production rate of 10 mmscfd. The gas production rate over 15 years of simulation time is shown in Figure 5.84. The production remains on a plateau at a rate of 10 mmscfd for over six years. The main contributor during the plateau is likely to be the free gas present initially and when this is depleted, the rate is dominated by the hydrate dissociation. After the rapid decline from the plateau rate, the production rate declines more gradually, as the dissociation of the hydrate slows down. In depressurization, low productivity is unavoidable because the heat for dissociation of hydrate is controlled by the formation sensible heat. Hydrate dissociation reaches a peak due to pressure reduction from the free gas zone to the hydrate zone through the movable gas phase over six years. After the peak, hydrate decomposition decreases as the reservoir temperature decreases gradually due to expansion cooling. At this stage hydrate dissociation is controlled by the heat supply from the surrounding formations. Because of the steep nature of the reservoir, the large quantities of water produced during hydrate dissociation will drain to the bottom of the reservoir and as such, quantities of produced water will be low. Figure 5.84, showing the produced water profile, appears to indicate that this is the case. Cumulative production after 15 years was 646 million metric standard cubic meters (mmscm) as shown in Figure 5.85. The contribution of gas generated from hydrate dissociation and produced from the free gas zone towards cumulative production is displayed in Figure 5.85. The gas content (at STP conditions) practically storable in natural gas hydrates has a gas to hydrate volume ratio

of 165:1. Complete dissociation of the hydrate would produce 903.4 mmscm of gas at surface conditions. Total gas potential of the reservoir model, including free gas and gas from dissociation is approximately 1.18 billion cubic meters. At the end of a 15-year production period approximately 55% of the gas initially in place has been recovered.

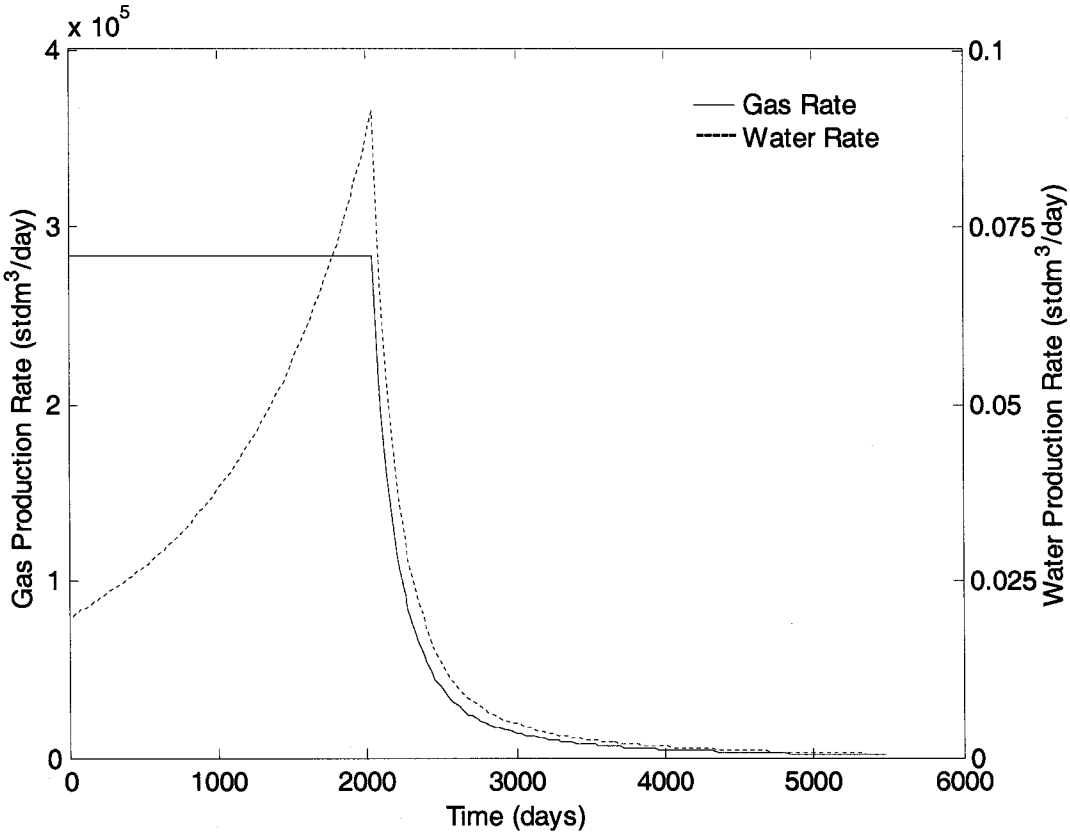

Figure 5.84: Gas and Water Production Rate vs. Time of Base Case

The temperature decrease with time due to the endothermic nature of the dissociation process is shown in Figure 5.86. The reservoir temperature is gradually decreased from the initial formation temperature to zero degrees within six years. Another limitation of the model is noted when the temperature in the main area of hydrate dissociation has reduced to, or near to, zero degrees Celsius. STARS cannot operate at temperatures lower than zero degrees Celsius.

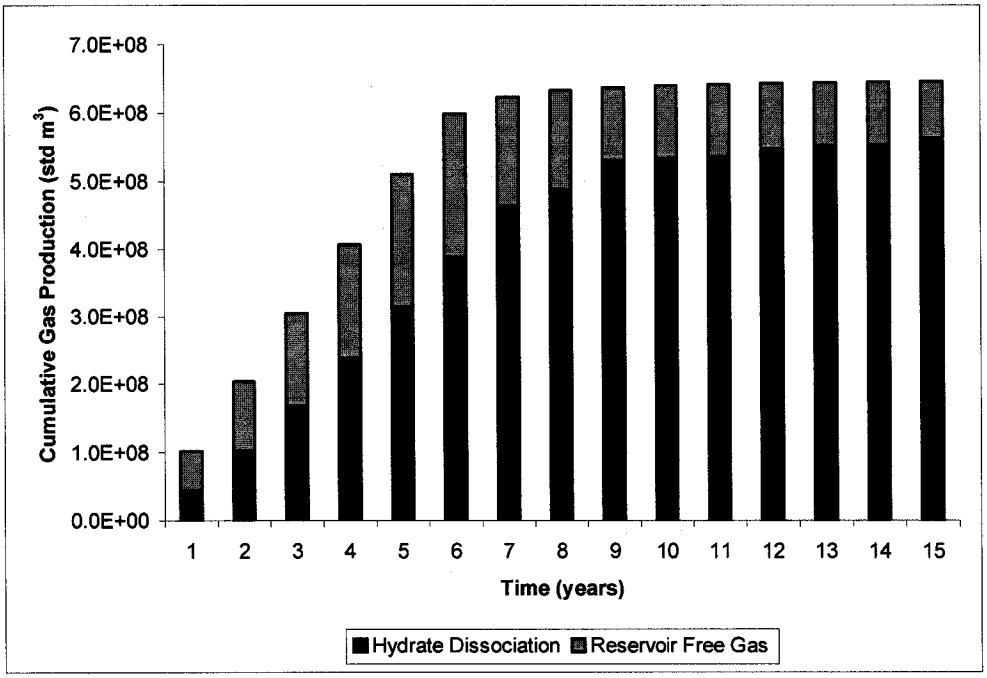

Figure 5.85: Components of Reservoir Voidage

During the simulation, numerous warning messages are received that an attempt was made in various grid blocks to lower the temperature below zero °C. In this circumstance, STARS attempts to recalculate the last time step so that temperature is equal or greater than zero. These multiple iterations are one reason for the long simulation execution time. In reality, the reservoir temperature may reduce below zero °C, and inhibit the hydrate dissociation. However, STARS will reiterate the time steps so that the temperature does not fall below zero degrees by reducing the rates of hydrate dissociation, thereby accounting for some of the reduction in dissociation due to low temperatures that would be experienced in the field. The zero degree temperature limit in STARS can be avoided by shifting the entire system temperature by 10 °C with a complementary shift in the hydrate reaction parameters from 273.15 to 263.15 K. This results in a temperature decrease to –1.6 °C and the reaction slows down thereby. This demonstrates the importance of heat transfer from surroundings for dissociation to occur.

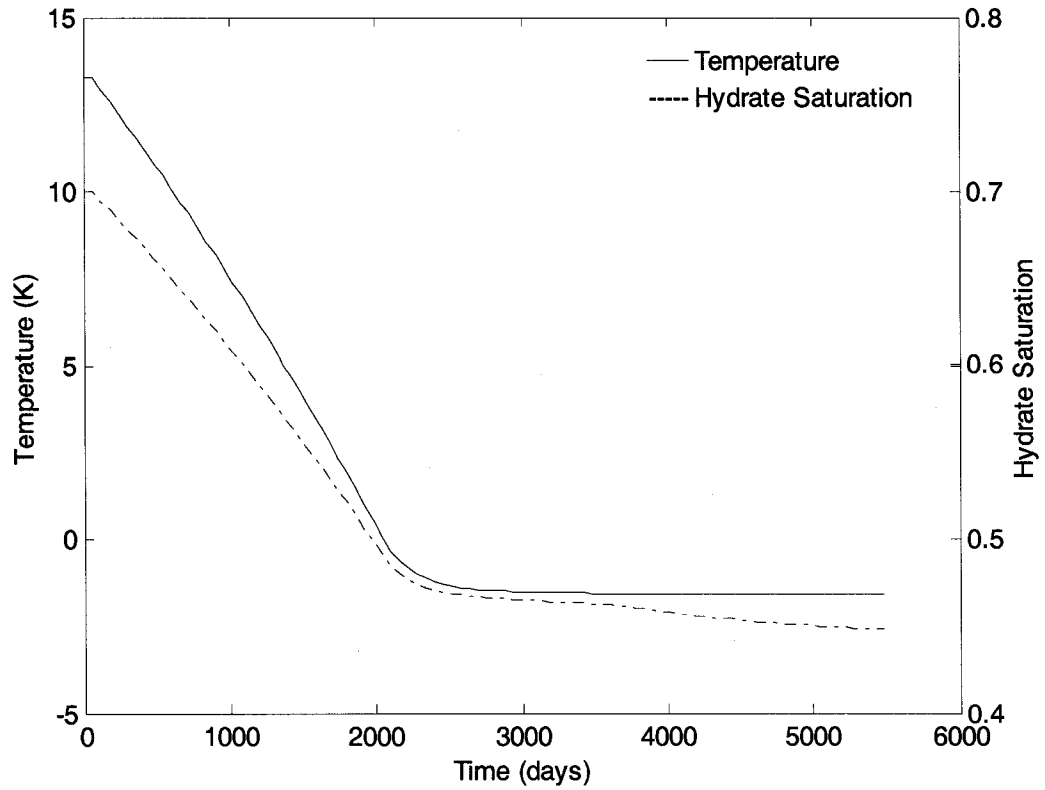

Figure 5.86: Temperature and Hydrate Saturation Distributions vs. Time

The area near the well bore begins to increase in temperature with simulation time, as heat flows from the surrounding rock. And at the same time, the cold zone propagates down the reservoir as the dissociation front moves down the reservoir. Figure 5.86 also shows how the hydrate saturation decreases with time. A sharp reduction in hydrate saturation is noticed at the initial stage which then stabilizes at low hydrate saturation of 0.44 at the end of simulation.

In Case 2, an aquifer is connected to the sides of the reservoir with the water-saturated zone. An aquifer porosity of 20% and a permeability of 250 md are used. The water influx calculation option is based on work by Fetkovitch (1971). The method for heat influx calculations is a semi-analytical formulation which is an extension of the work done by Vinsome and Westerveld (1980). The aquifer models are intended mainly for

drawdown pressure maintenance. Figure 5.87 compares the present cumulative gas and water production profiles with those obtained for Case 2. It is emphasized that less gas is produced and water starts exiting the well after 3100 days when the reservoir is connected to the aquifer. A useful conclusion is that the well can be shut-in after 3100 days for the production to be economical.

Recognizing that at the end of a 15-year production period, only 55% of the initial gas in place has been recovered by the depressurization scheme, hot water and steam injection schemes were employed for improving gas recovery. Hot water was injected into the hydrate zone at a maximum rate of 10,000 m^3/day and at a temperature of 40 °C. The production and the injection intervals were set to be 600 m and an injection well is completed in the hydrate zone as shown in Figure 4.3. The injection well is opened after six years when gas production rate is decreased. The high temperature fronts did not propagate much deeper into hydrate layer since the permeability of hydrate interval is low at the initial hydrate saturation. Comparison of cumulative gas produced by depressurization with the hot water injection scheme is shown in Figure 5.88. The gas recovery factor reaches about 57%. A slight increase in gas productivity is noticed in the case with hot water injection. Gas production rate depends upon several factors like location of injection well, time of injection, number of injection wells and geometry of the reservoir.

In steam stimulation, the conditions were different from the water injection case. The injected fluid was superheated steam with a specific enthalpy corresponding to a pressure of 10 MPa and a temperature of 400 °C. The maximum injection rate was assumed to be the same as that of the water injection case. The cumulative gas release in Figure 5.88 shows a comparison of the steam injection scheme with that of the hot water injection and depressurization production principles. Steam injection is started after six years and the production decline is halted. In this case, the released volumes are large and the gas recovery factor reaches about 65%. The temperature contours of the steam injection

scheme are displayed in Figure 5.89 after three and eight years of simulation, where, P stands for a production well and I for an injection well.

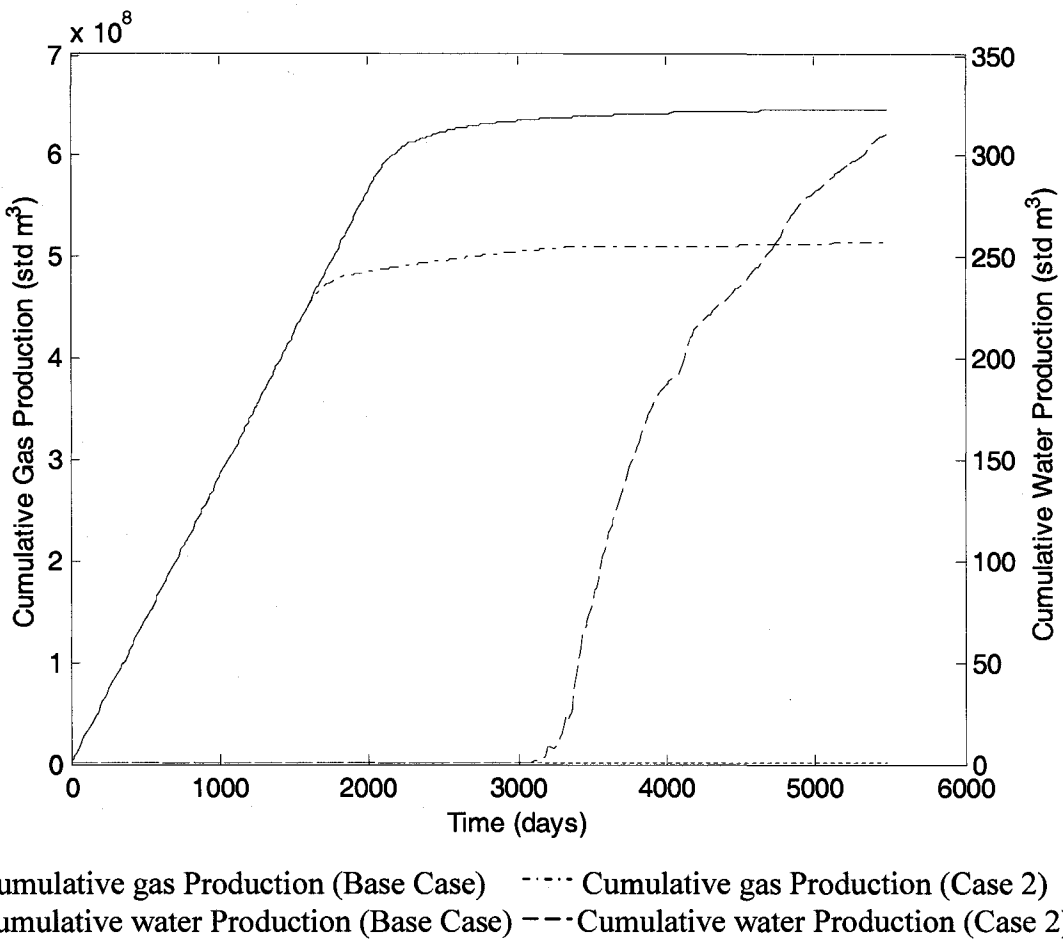

Figure 5.87: Cumulative Gas and Water Production vs. Time

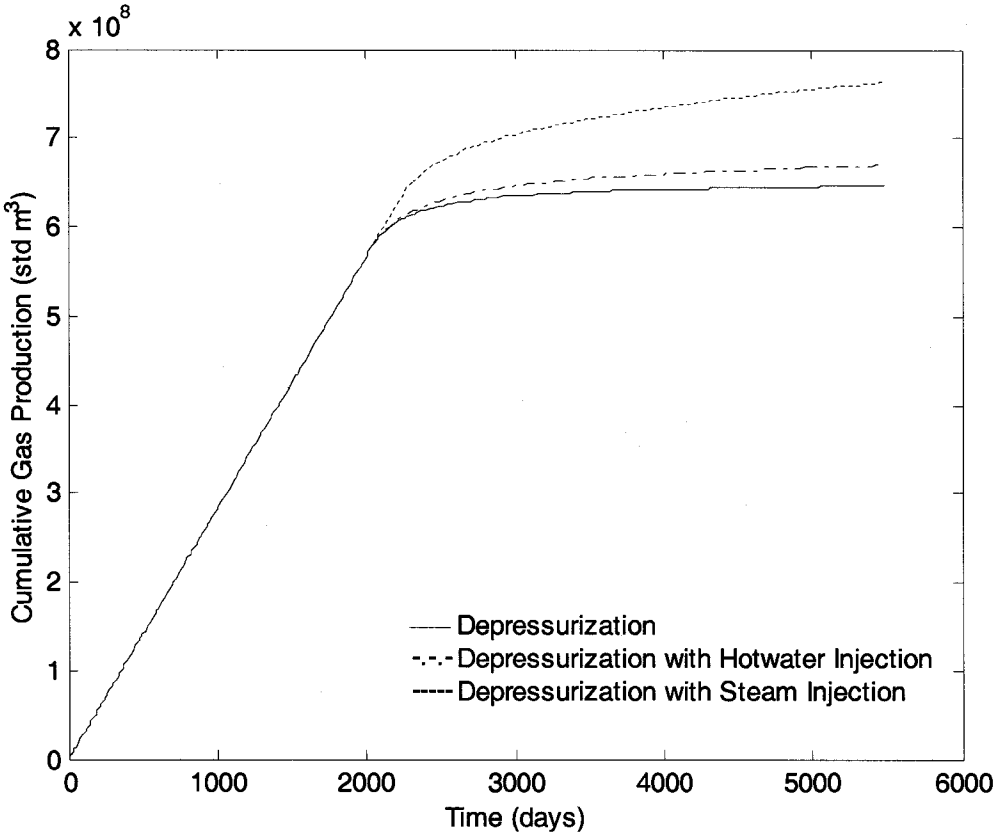

Figure 5.88: Cumulative Gas Production vs. Time for Various Production Schemes

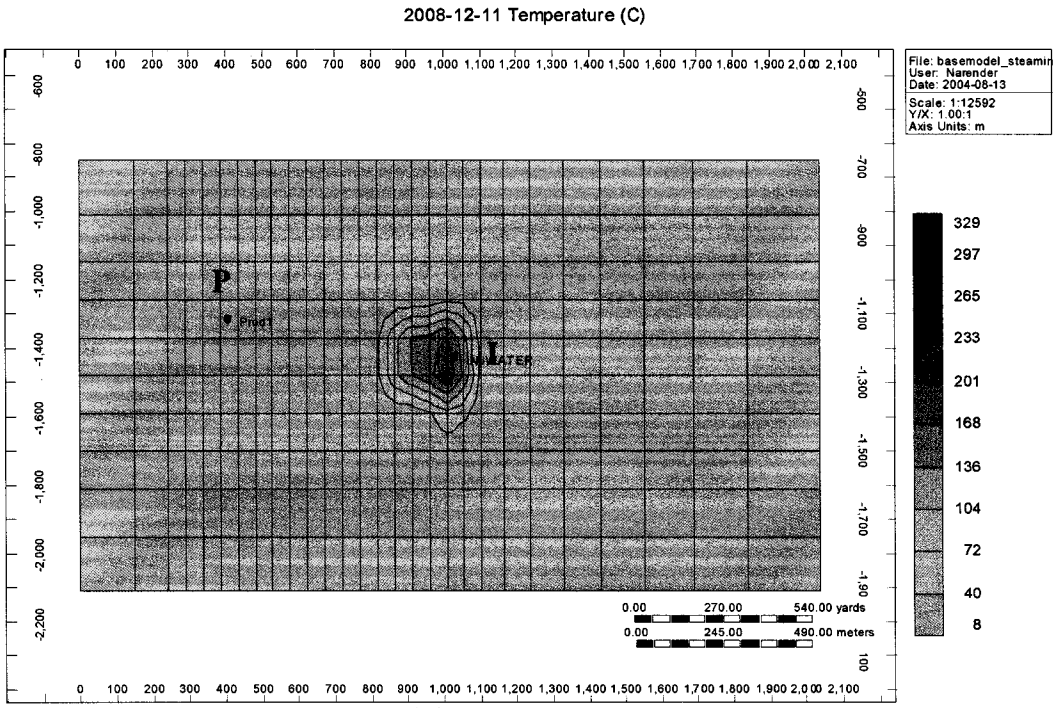

(a)

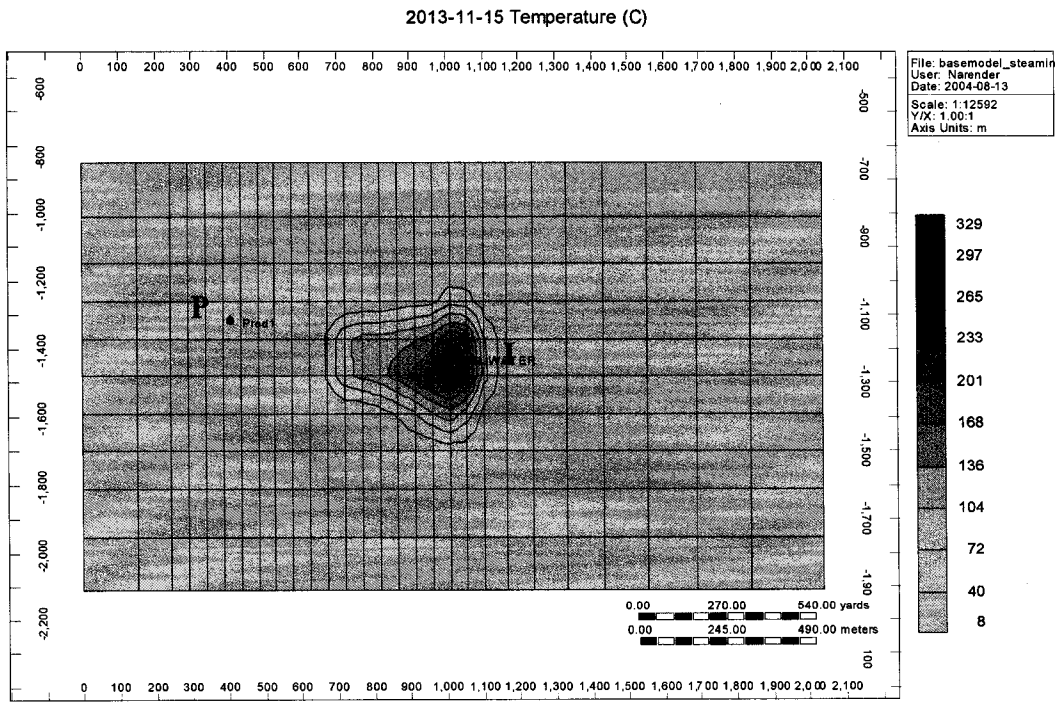

(b)

Figure 5.89: Temperature Profiles During Steam Injection after Three and Eight Years Respectively

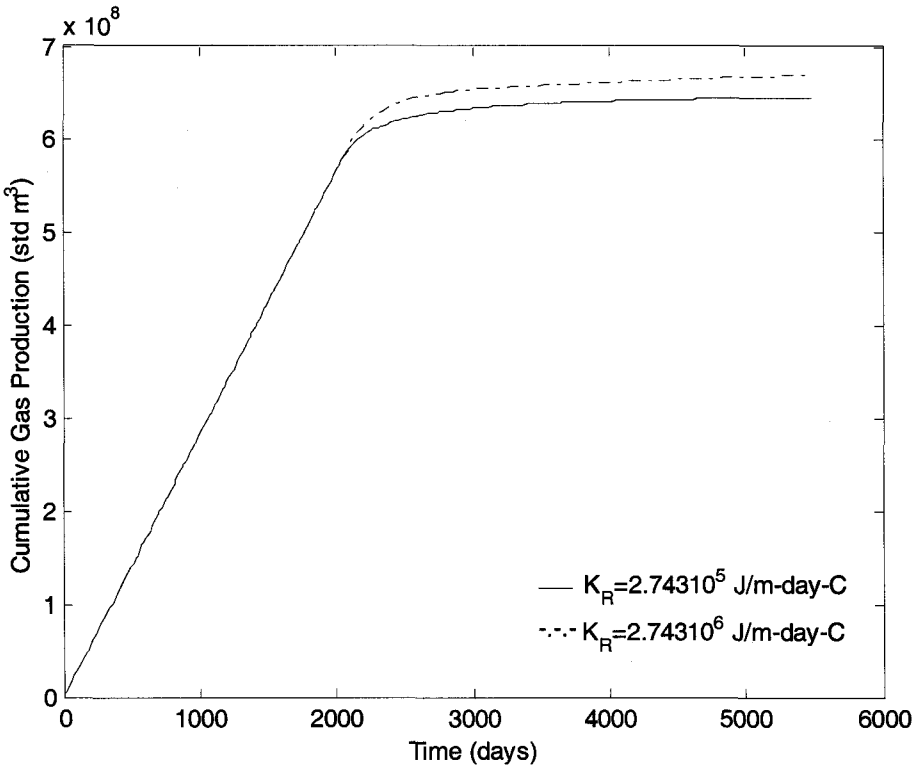

Figure 5.90: Effect of Cumulative Gas Production to the Rock Thermal Conductivity

In order to investigate the effect of reservoir parameters and rate kinetics on gas production, sensitivity studies were conducted. The role of conductive heat transfer behavior is studied by increasing the thermal conductivity of rock 10 fold. An increase in rock thermal conductivity results in an increase of heat transfer of the medium. This results in an increase of cumulative gas production as shown in Figure 5.90. Recognizing that the absolute permeability of the reservoir may be less than anticipated, a simulation with reduced reservoir permeability was also run. Rock permeability was decreased by a factor of 10 to study the importance of fluid flow on cumulative gas release. Figure 5.91 compares the cumulative gas produced by decrease of formation permeability with that of the base case. As expected, the constant production rate is shorter and it is emphasized that the higher the rock permeability the higher the gas production rates. To investigate the importance of reaction frequency factor (*rrf*) in reaction rate kinetics of hydrate

decomposition, *rrf* is varied as presented in Figure 5.92. The kinetics of hydrate dissociation can be a controlling factor in the gas production when the *rrf* is varied by several orders of magnitude. The reaction rate expression had a negligible effect until the *rrf* was reduced by 7 orders of magnitude below the base case. No significant difference was observed on number of well perforations. However, when the vertical well is replaced by a horizontal well relatively large volumes were produced.

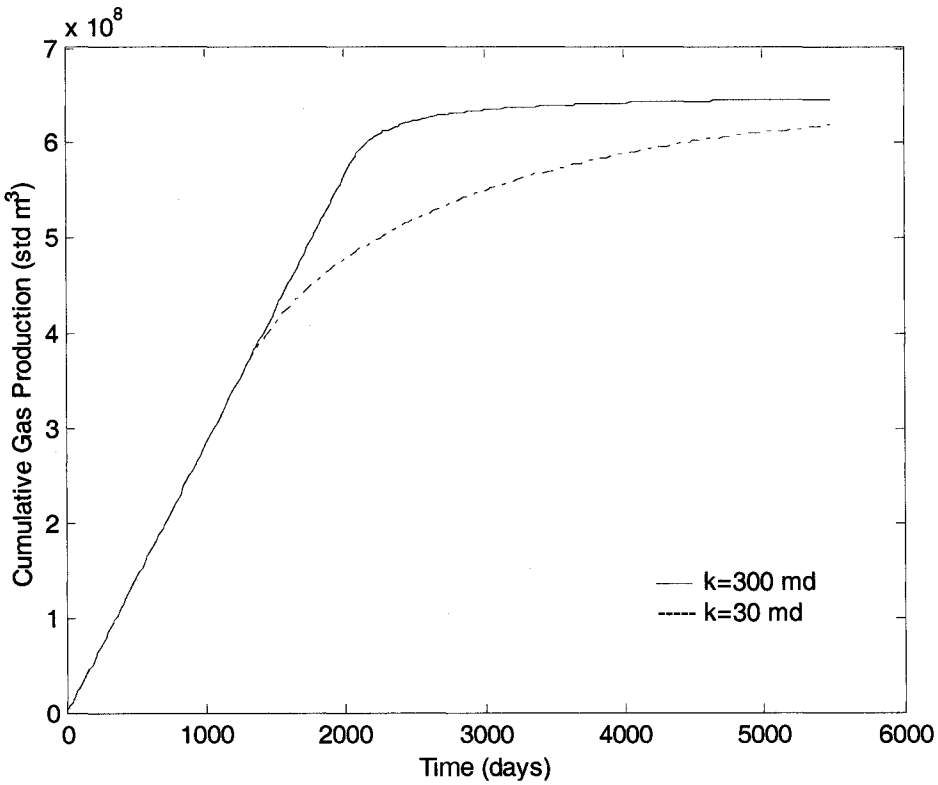

Figure 5.91: Effect of Rock Permeability on Cumulative Gas Production

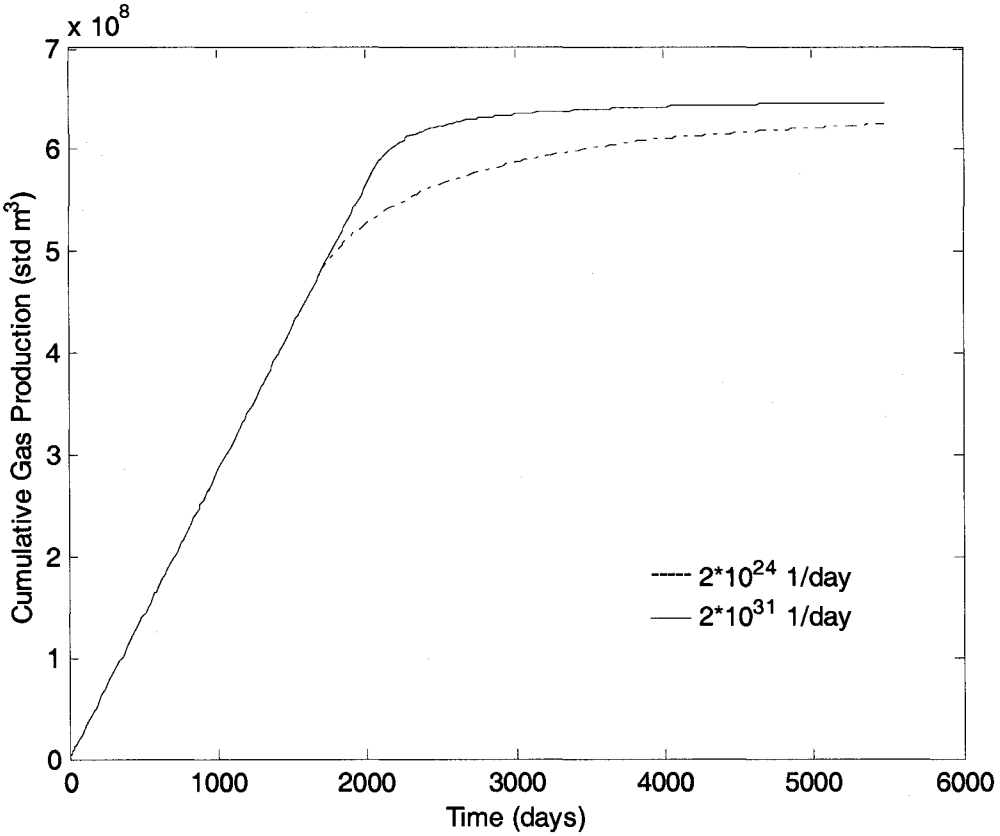

Figure 5.92: Effect of Cumulative Gas Production to the Reaction Frequency Factor

5.8 Comparison of Results from CMG STARS and Analytical Model

Figure 5.33 shows the gas production rate obtained from the geometry described in Figure 4.2 using depressurization as the method of production of methane from the hydrate reservoir. It can be seen that the production is constant approximately for the first 300 days. Therefore, cumulative gas production in the first 120 days will be, 120days * 7079 m^3/day = 849480 m^3. Assuming density of the gas to be 0.677 kg/m^3 (pure methane), the gas produced is 575098 kg. These results have been obtained from CMG STARS.

Figure 5.78b shows the total mass flow profile of the same geometry with different reservoir parameters, but also using depressurization as the production technique. It can

be seen that the mass flow rate is constant near the well bore region. In order to calculate the cumulative production, the value of interest is the mass flow at the well bore i.e. at 0 m distance from the well bore. Therefore, the cumulative gas production in 120 days is calculated as follows: 120 day* 86400 sec/day* 0.048 kg/s = 497664 kg.

It can be seen that the results obtained from the analytical model and CMG STARS are comparable even though the values obtained from CMG STARS are a little bit higher. It should be noted that the permeability of the reservoir was considered to be 300 md for the CMG STARS case whereas in the analytical model it was 5.2 md for the gas zone and 0.4 md for the hydrate zone. In addition, it can be observed from Figure 5.81c that the higher the permeability, the higher is the mass flux and hence the production rate. For higher permeability, the results would have been even closer. This shows that the analytical model is comparable to the CMG STARS model.

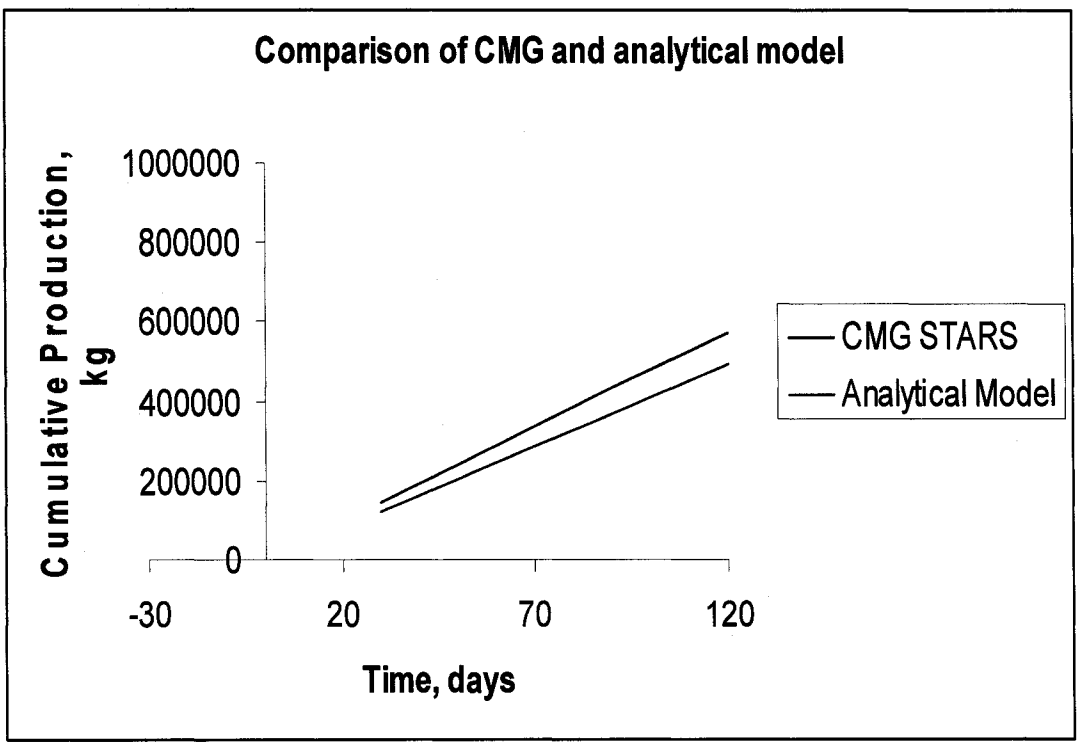

Figure 5.93: Cumulative Gas Production vs. Time Comparison of CMG STARS and Analytical Model

Figure 5.93 shows cumulative production as a function of time obtained from CMG STARS and the analytical model. It can be seen that the production is comparable and the difference can be attributed to the low permeability of the reservoir used in the analytical model. The results are shown up to 120 days only because the analytical model is only run up to 120 days from the start of production.

It should be noted that the comparison between the analytical model and CMG STARS was made only to demonstrate that the analytical model is capable of capturing the physics of gas hydrate dissociation and not to demonstrate that these two models are capable of yielding very similar predictions. CMG STARS is not only able to model the gas hydrate dissociation, but also has the capability to incorporate the gas-water relative permeability data, which is crucial to predict the production of gas from dissociated gas hydrates, in the presence of a hydrate phase.

CHAPTER SIX
CONCLUSIONS AND RECOMMENDATIONS FOR FUTURE WORK

6.1 Conclusions

This study demonstrates a novel approach to adapt a commercial simulator, CMG STARS, for predicting gas production performance from the formations containing hydrates. An off-the-shelf simulator was modified by formulating a kinetic and thermodynamic model to describe the hydrate decomposition. This simulator is used to investigate the feasibility of gas production from a hypothetical hydrate formation. Production schemes like depressurization, hot water and steam injection are tested. Sensitivity analyses using this simulator were carried out to see the effect of each variable on gas recovery.

The major thrust of this work was to model the production of gas from hydrate formations with special emphasis on indirect dissociation of gas hydrates via depressurization of underlain free gas. The primary objective was to determine if declining gas production (from free gas) is indeed controlled by the overlain dissociating gas hydrate. Two different approaches were adopted to model the process; 1) an analytical model, and 2) a commercial reservoir simulator in which a real hydrate phase was not considered but was rather represented as a "pseudo hydrate phase" by a very heavy viscous oil phase.

Production profiles generated from the simulations show that the modification of a commercial simulator was successful. Gas production at the well indicates that an accumulation of methane hydrate in a reservoir will begin to dissociate when the reservoir pressure is lowered. At the end of the simulation, the total cumulative production was 70% of the initial free gas in place. Hydrate dissociation caused by pressure depletion in a hydrate formation will be slowed drastically because of the

endothermic nature of the dissociation reaction and the Joule-Thomson effect. Higher rock thermal conductivity caused higher heat influx from the medium and resulted in more hydrate dissociation. Change in formation permeability can have a significant influence on the reservoir performance.

This work focuses on gas production from a hydrate formation that is underlain by a free water zone and embedded between relatively tight mud/silt formations. This analysis can be applicable to any other hydrate accumulation and initial phase distribution. The CMG STARS simulator is modified to model the gas production by depressurization, heated well and hot water injection schemes. The simulation runs indicated that the production schemes of depressurization and heated well were technically feasible. However, they may not be economical. The heated well method may be used for relatively tight hydrate formations. The hot water injection remarkably improved gas productivity but at the cost of heat loss to the surrounding formations. The energy efficiency ratio for the hot water injection process at 40 °C is high enough to consider it as an appropriate strategy for gas production.

Reservoir temperature decreases below 0 °C because of the endothermic nature of the dissociation reaction and a Joule-Thomson effect. In order to account for low temperatures, the entire system temperature is increased by 10 °C and a complementary shift made in the hydrate reaction parameters from 273.15 to 263.15 K. At the end of simulation, the lowest temperature reached in the reservoir is about –1.6 °C. Based on the above discussion one could probably add as little as 3 °C. The decision to add 10 °C to the system temperature was a result of ease with subtracting. Hydrate dissociation caused by pressure depletion in a hydrate formation will be slowed drastically because of the endothermic nature of the dissociation reaction and a Joule-Thomson effect. An injection well has to be activated to trigger the rate of hydrate dissociation when production declines.

Recognizing the fact that the total recovery of the potential gas volumes from the hydrate over 15 years is low, about 55%, substantial depletion of a reservoir using depressurization alone would be a lengthy process and as such, thermal stimulation methods are employed to increase the rate of dissociation for effectiveness and economic impact. Gas recovery rates were increased to 65% by steam stimulation.

Higher rock thermal conductivity caused higher heat influx from the medium and resulted in additional hydrate dissociation. Change in formation permeability can have a significant influence on the reservoir performance. In this study, reaction frequency factor (*rrf*) had a small effect on gas production until it was reduced by 7 orders of magnitude. The type of well had no effect at that relatively large gas production.

In addition to the simulation study, an analytical model is developed to predict reservoir performance, as gas production by depressurization, of a hydrate reservoir containing excess methane gas and low hydrate saturation. Time evolutions of pressure and temperature in an axisymmetric infinite homogenous hydrate reservoir are analyzed, and the effects of well pressure and reservoir temperature are studied. The sensitivity of natural gas production to permeability is also studied. Motion of the dissociation front under different conditions is analyzed. The following conclusions can be made on the basis of the results obtained:

1. For a semi-infinite axisymmetric homogenous reservoir containing natural gas, the dissociation pressure and temperature are constant and depend only on the reservoir conditions and well pressure.
2. For given reservoir conditions, well pressure controls the rate of natural gas output and the motion of the dissociation front. A lower well pressure leads to a higher natural gas output and a faster movement of the dissociation front.

3. The natural gas output and the motion of the dissociation front are also sensitive functions of reservoir temperature. When the reservoir temperature increases, the natural gas output increases and the dissociation front moves faster.
4. A higher well pressure or higher reservoir temperature lead to a higher dissociation temperature and pressure.
5. In this model, the distance of the moving boundary from the well increases with square root of time and the production rate decreases in inverse proportion.
6. For a homogenous hydrate reservoir, the reservoir permeability significantly affects the production rate of methane gas.
7. For a fixed porosity, the reservoir with higher hydrate zone permeability has higher production rate and the dissociation front penetrates deeper into the reservoir. Variation of permeability has a slight effect on the dissociation pressure and temperature at the front.

In view of the discussion and conclusions stated above, applicability and success of this work can be verified by considering the following facts. First, the production profiles generated from both models clearly indicate that gas production is supported by hydrate dissociation, i.e., it is feasible to produce gas at a constant rate from hydrate formations by a depressurization technique. This is indicative of the fact that the analytical model and the pseudo hydrate phase in a commercial simulator adequately capture the thermodynamics and fluid flow in a hydrate reservoir.

Secondly, the production profiles from these two significantly different approaches were compared for the same geometry but different reservoir parameters (e.g., two orders of magnitude differences in permeability of hydrate layer). The production profiles for the studied reservoir compared reasonably well for the production over a 120 day period. Specifically, the difference between the cumulative gas production for the 120 day cut off using both models was of the order of 13%. Despite the significant differences in

reservoir parameters the similarity in the production profiles by the two approaches is indeed remarkable.

Therefore, if success has to be evaluated or determined in isolation (i.e., purely from a modeling standpoint) the modeling work carried out during the course of this study was certainly successful because 1) the developed models are capable of describing/ simulating the production from a hydrate reservoir associated with a free gas reservoir, 2) additionally, the similarly in the studied production profiles increase the confidence in the modeling approach. Although these are qualitative measures, success cannot be quantified because for comparison purposes, there is not a single case of gas production from hydrate formations on a commercial scale anywhere in the world.

Failure in this work clearly would have been the inadequacy or incapability of the two models to capture the hydrate thermodynamics and the subsequent sustenance of the gas production rates. The very fact that this has been substantially (qualitatively as well as quantitatively) demonstrated in this work is an indicator of success.

6.2 Recommendations for Future Work

Accurate simulation study requires accurate data for methane hydrate's physical properties. Laboratory experiments are needed to determine the relative permeabilities of methane hydrate in porous media.

This model is limited to hydrate saturation values of about 0.3 as the water resulting from the dissociation process is assumed to remain immobile, and is retained within pores of the dissociated zone. Thermo-physical properties are assumed to be constant. Viscous dissipation, inertial effects, and the possibility of mutual or external energy transmission are neglected. Further model developments could be considered to address these factors.

CHAPTER SEVEN
REFERENCES

1. Bayles, G.A., Sawyer, W.K., Anada, H.R., Reddy, S., and Malone, R.D., "A Steam Cyclic Model for Gas Production from a Hydrate Reservoir," Chemical Engineering Communications, Vol. 47, pp. 225 - 245, 1986.

2. Bishnoi, P.R., Gupta, A.K., Englezos, P., and Kalogerakis, N., "Multiphase Equilibrium Flash Calculations for Systems Containing Gas Hydrates", Fluid Phase Equilibrium, Vol. 53, pp. 97 - 104, 1989.

3. Burshears, M., O'Brien, T.J. and Malone, R.D., "A Multi-Phase Multi-Dimensional, Variable Composition Simulation of Gas Production from a Conventional Gas Reservoir in Contact with Hydrates", SPE Paper 15246, presented at the SPE Unconventional Gas Technology Symposium, Louisville, KY, May, 1986.

4. Chu, C., "Current In-Situ Combustion Technology," Journal of Petroleum Technology, Vol. 35, Issue 9, August, pp 1412 - 1418, 1983.

5. "CMG STARS User's Guide", Computer Modeling Group Ltd., Calgary, Alberta, Canada, 2003.

6. Cohen, J.H., Maurer, W.C., and Liu, G., "Down Hole High-Pressure Centrifugal Pump for Jet-Assisted Drilling", Gas Research Institute, GRI - 95/0447, 1995.

7. Collett, T.S., "Detection and Evaluation of Natural Gas Hydrates from Well Logs, Prudhoe Bay, Alaska". M.S. Thesis, University of Alaska Fairbanks, pp.77, 1993.

8. Dillon, W.P., Fehlhaber, K., Coleman, D.F., Lee, M.W., and Hutchinson, D.R., "Maps Showing Gas Hydrate Distribution off the East Coast of the United States", U. S. Geological Survey, Miscellaneous Field Studies Map, MF - 2268, 2 sheets, 1995.

9. Fetkovitch, M.J., "A Simplified Approach to Water Influx Calculations - Finite Aquifer Systems", Journal of Petroleum Technology, July, pp. 814 - 828, 1971.

10. Holder, G.D., Angert, P.F., and Godbole, S.P., "Simulation of Gas Production From a Reservoir Containing Both Gas Hydrates and Free Natural Gas," SPE Paper 11105, Presented at SPE 57th Annual Technical Conference and Exhibition, New Orleans, LA, September 26 - 29, 1982.

11. Hong, M. and Pooladi-Darvish, M., "A Numerical Study on Gas Production from Formations Containing Gas Hydrates", CIMM Paper 2003-060, Presented at the Canadian International Petroleum Conference, Calgary, Alberta, Canada, June 10 – 12, 2003.

12. Howe, S.J., Nanchary, N.R., Patil, S.L., Dandekar, A.Y., Ogbe, D.O., Hunter, R.B., and Wilson, S.J., "Economic Analysis and Feasibility Study of Gas Production from Alaska North Slope Gas Hydrate Resources", Presented at the AAPG Hedberg Research Conference, "Natural Gas Hydrates: Energy Resource Potential and Associated Geologic Hazards" September 12 - 16, 2004, Vancouver, Canada.

13. Iseux, J. C., "The Case of Hot Solvent Hydraulic Fracturing in the Natural Gas Recovery from Gas Hydrate Reservoir," SPE Paper 21889, An Unsolicited Paper Submitted to the Society of Petroleum Engineers, 1990.

14. Islam, M. R., "A New Recovery Technique for Gas Production from Alaskan Gas Hydrates," Journal of Petroleum Science and Engineering, Vol. 11, pp. 267 - 281, 1994.

15. Jamaluddin, A.K.M., Kalogerakis, N., and Bishnoi, P.R., "Modeling of Decomposition of A Synthetic Core of Methane Gas Hydrate By Coupling Intrinsic Kinetics with Heat Transfer Rates," the Canadian Journal of Chemical Engineering, Vol. 67, pp. 948 - 954, December 1989.

16. Ji, C., Ahmadi, G. and Smith, D.H.: "Natural Gas Production from Hydrate Decomposition By Depressurization", Chemical Engineering Science Journal, Vol. 56, pp. 5801 - 5814, 2001.

17. Ji, C., Goodraz, A and Duane, H. S., "Constant Rate Natural Gas Production from a Well in a Hydrate Reservoir", Energy Conversion and Management Journal, Vol. 44, pp. 2403 - 2423, 2003.

18. Kamath, V.A. and Holder, G.D., "Dissociation Heat Transfer Characteristics of Methane Hydrates," American Institute of Chemical Engineers (AIChE) Journal, Vol. 33(2), Feb, pp. 347 - 350, 1987.

19. Kamath, V.A. and Godbole, S.P., "Evaluation of Hot Brine Stimulation Technique for Gas Production from Natural Gas Hydrates," SPE Paper 13596, Presented at the SPE Western Regional Meeting, Bakersfield, CA, 1985.

20. Kamath, V.A., Mutalik, P.N., Sira, J.H., and Patil, S.L., "Experimental Study of Brine Injection and Depressurization Methods for Dissociation of Gas Hydrates," SPE Paper 19810, SPE Formation Evaluation Journal, December, pp. 474 - 484, 1991.

21. Kamath, V.A., Sharma, G.D., and Patil, S.L., "Development of Alaskan Gas Hydrate Resources," A Final report to the U.S. Department of Energy, Grant #DE - FG21 - 86FE61114, June, pp. 497, 1991.

22. Kamath, V.A., and Patil, S.L., "Description of Alaskan Gas Hydrate Resources and Current Field Technology," A Final Report Submitted to Japan Oil Engineering Co., Ltd., Tokyo, Japan, January 1994.

23. Kim, H. C., Bishnoi, P. R., Heidemann, R. A. and Rizvi, S. S. H., "Kinetics of Methane Hydrate Decomposition", Chemical Engineering Science, Vol. 42, pp. 1645 - 1653, 1987.

24. Kuuskraa, V., Hammershaimb, E. and Sawyer, W., "Conceptual Models for Gas Hydrates," Phase I-Technical Directive 6-Final Report, under U.S. Department of Energy Contract DE - AC21 - 82MC19239, June, pp. 59, 1983.

25. Kvenvolden, K.A., "Methane Hydrate - A Major Reservoir of Carbon in the Shallow Geosphere", Chemical Geology, Vol. 71, pp. 41 - 51, 1988.

26. Makogon, Y.F., "Natural Gas Hydrates: The State of Study in the USSR and Perspectives for Its Use," A Paper Presented at the Third Chemical Congress of the North America, Toronto, Canada, June, 1988.

27. Makogon, Y.F., "Hydrates of Hydrocarbons", Pennwell Publishing Company, Tulsa, Oklahoma, pp. 396 - 448, 1997.

28. McGuire, P.L., "Methane Gas Production by Thermal Stimulation," Presented at the Fourth Canadian Permafrost Conference, Alberta, Canada, March, 1981.

29. McIver, R.D, "Long Term Energy Resources", eds. Meyer, R. F. and Olson, H. C., Pitman Boston., Vol.1, pp. 713 - 726, 1981.

30. Moridis, G.J., "Numerical Studies of the Gas Production from Methane Hydrates", SPE Paper 75691, Presented at the SPE Gas Technology Symposium, Calgary, Alberta, Canada, April 30 - May 2, 2002.

31. Patil, S.L. and Nanchary, N., "Potential Techniques for Production of Natural Gas from Hydrate Reservoirs", Presented at the 32nd International Symposium of the Application of Computers and Operations Research in the Mineral Industry (APCOM 2005), Tucson, AZ, March 30 - April 1, 2005.

32. Parker, J.J., Lenhard, R.J., and Kuppusamy, T., "A Parametric Model for Constitutive Properties Governing Multiphase Flow in Porous Media", Water Resources Research, Vol. 23, No. 4, pp. 618 - 624, 1987.

33. Roadifer, R.D., "Numerical Solution of 2-D (r - z) Cylindrical Coordinate Dissociation of Natural Gas Hydrates with Variable Thermal Properties", M.S. Thesis, University of Alaska Fairbanks, Fairbanks, AK, 1988.

34. Sira, J.H., Patil, S.L. and Kamath, V.A., "Study of Hydrate Dissociation by Methanol And Glycol Injection," SPE Paper 20770, Proceedings of the 65th SPE Annual Technical Conference, New Orleans, Louisiana, September 23 - 26, 1989.

35. Sloan, E.D., "Clathrate Hydrates of Natural Gases," Marcel Dekkar Inc., 1991.

36. Sresty, G.C., Dev, H., Snow, R.H., and Bridges, J.E., "Recovery of Bitumen from Tar Sand Deposits with the Radio Frequency Process", SPE Reservoir Engineering, Vol. 1, January, pp. 85 - 94, 1986.

37. Swinkels J.A.M. and Drenth, R.J.J., "Thermal Reservoir Simulation Model of Production from Naturally Occurring Gas Hydrate Accumulations", SPE Reservoir Evaluation and Engineering, Vol. 3, No. 6, pp. 559 - 566, December, 2000.

38. Thomas, D. M., "A Summary of the Chemical Characteristics of the HGPA Well: Puna, Hawaii", Proceedings of the 8th Workshop on Geothermal Reservoir Engineering, Stanford, CA, December, 1982.

39. Tsypkin, G.G., "Effect of Liquid Phase Mobility on Gas Hydrate Dissociation in Reservoirs", Journal of Fluid and Gas Mechanics, Vol. 4, pp. 105 - 114, 1991.

40. Van Genuchten, M.T., "A Closed-Form Equation for Predicting the Hydraulic Conductivity of Unsaturated Soils", Soil Science Society of America Journal, Vol. 44, pp. 892 - 898, 1980.

41. Vinsome, P.K.W. and Westerveld, J.D.,"A Simple Method for Predicting Cap and Base Rock Heat Losses in Thermal Reservoir Simulators", Journal of Canadian Petroleum Technology, Vol.19, 3, July-September, pp. 87 - 90, 1980.

42. Ullerich, J. W., Selim, M. S. and Sloan, E. D., "Theory and Measurement of Hydrate Dissociation", American Institute of Chemical Engineers Journal, Vol. 33, pp. 747 - 752, 1987.

43. Yousif, M.H., Li, P.M., Selim, M.S., and Sloan, E.D., "Depressurization of Natural Gas Hydrates in Berea Sandstone Cores," Journal of Inclusion Phenomena & Molecular Chemistry, Vol. 3, pp. 71 - 88, 1990.

44. Yousif, M. H., Abass, H. H., Selim, M. S. and Sloan, E. D., "Experimental and Theoretical Investigation of Methane Gas Hydrate Dissociation in Porous Media", SPE 18320, SPE Reservoir Engineering Journal, February, pp. 69 - 76, 1991.